



Universidad
de Alcalá

Programa de Doctorado en Electrónica: Sistemas
Electrónicos Avanzados. Sistemas Inteligentes

**Sensor Resource Management with
Evolutionary Algorithms Applied to
Indoor Positioning**

Ph.D. Thesis Presented by
Francisco Domingo Pérez

2016



Universidad
de Alcalá

Programa de Doctorado en Electrónica: Sistemas
Electrónicos Avanzados. Sistemas Inteligentes

**Sensor Resource Management with
Evolutionary Algorithms Applied to
Indoor Positioning**

Ph.D. Thesis Presented by
Francisco Domingo Pérez

Advisors

José Luis Lázaro Galilea

Ignacio Bravo Muñoz

Alcalá de Henares, September 2016

A mi familia

*“If I am to speak ten minutes, I need a week for preparation; if fifteen minutes,
three days; if half an hour, two days; if an hour, I am ready now.”*

Woodrow Wilson

Agradecimientos

Quiero empezar agradeciendo la labor de todos los que han hecho posible este trabajo, empezando por mis directores José Luis y Nacho, sin olvidarme del resto de profesores del grupo GEINTRA de la Universidad de Alcalá, que a través de las numerosas reuniones que hemos tenido desde mi incorporación hace ya más de cuatro años han ayudado a definir lo que estás leyendo ahora mismo.

A los compañeros que he tenido en la Universidad de Alcalá, que desde el principio me han hecho sentir como si hubiera estado toda la vida en esta ciudad.

A David y Esther, por su ayuda con la evaluación y revisión del documento, que seguro ha ayudado a aumentar el nivel de calidad de esta versión final.

A los miembros del grupo Instrumentación y Electrónica Industrial de la Universidad de Córdoba, con los que me inicié en la investigación dentro del ámbito académico.

To Andreas Wieser and the people of the chair of Geosensors and Engineering Geodesy of the Institute of Geodesy and Photogrammetry of ETH Zurich, for their attention during my stay.

To Felix Govaers and the people of the Sensor Data and Information Fusion department of the Fraunhofer Institute for Communication, Information Processing and Ergonomics FKIE, for their orientation and fruitful discussions during my visit at the institute.

Resumen

Esta tesis pretende contribuir a la mejora de la gestión de recursos en sistemas de sensores. Mediante esta gestión pueden abordarse dos temas, la colocación de estos sensores y su uso óptimo una vez colocados, centrándose la tesis en el primero de ellos. Durante la tesis se considera el uso de un sistema de posicionamiento en interiores basado en señales infrarrojas con medida de diferencia de fase. Estas medidas de fase son posteriormente transformadas en distancias, con lo cual nuestro problema es el de trilateración hiperbólica utilizando medidas de diferencia de distancia. Aunque se describe un modelo para el error en diferencia de distancias del enlace infrarrojo, podemos abstraernos de este y simplemente considerar que utilizamos medidas de diferencia de distancia que están normalmente distribuidas con una varianza dada por el modelo usado. De hecho, el trabajo expuesto en esta tesis podría ser usado con cualquier otro sistema del cual obtengamos un modelo de los errores de medida, ya sea empleando además trilateración esférica o angulación.

La gran mayoría de trabajos que mejoran la precisión de un sistema de posicionamiento colocando sensores optimizan funciones de coste basadas en el límite inferior de Cramér-Rao, enfoque que adoptamos también en este trabajo. En el capítulo de la tesis dedicado al estado del arte hacemos un repaso de las diferentes propuestas existentes, que concluye explicando qué pretendemos aportar sobre las contribuciones existentes en la literatura científica. En resumen, podemos clasificar las propuestas actuales en tres clases. La primera de ellas trata de determinar una configuración óptima para localizar un objetivo, normalmente utilizando el determinante de la matriz de información de Fisher o la dilución de la precisión. Estos métodos pueden obtener expresiones analíticas que proporcionan una explicación sobre como intervienen las características de los sensores y su colocación en la precisión obtenida. Sin embargo, carecen de aplicabilidad en situaciones reales. El segundo tipo de propuestas emplea métodos numéricos para optimizar la colocación de sensores considerando varios objetivos o un área entera. Los métodos propuestos en esta tesis encajan dentro de esta categoría. Por último, existen métodos que utilizan técnicas de selección de sensores para obtener configuraciones óptimas. Entre las distintas propuestas encontramos varias deficiencias, como la

simplificación del modelo de error de la medida para obtener expresiones fácilmente tratables, la consideración de un solo criterio de precisión de la localización, colocación de un número determinado y fijo de sensores, o su despliegue en áreas simples que no presenten problemas de oclusiones.

Nuestra primera aportación trata de solucionar la consideración de un único criterio de precisión, que normalmente es el determinante o la traza de la matriz de covarianza o información de la estimación. Cada métrica obtenida de estas matrices tiene un significado práctico distinto, y la consideración de solo una de ellas puede dar lugar a soluciones que presenten deficiencias en las otras, como la obtención de elipses de error muy alargadas. Nuestra propuesta implica el uso de algoritmos evolutivos multifunción que optimicen varias de estas métricas, como el error cuadrático medio en todo el área, la isotropía de la solución, y la máxima desviación que puede aparecer. Esto nos permite tener un conjunto de soluciones dadas en un frente de Pareto, que permitirán al gestor de la red de sensores visualizar las posibles soluciones y elegir entre ellas según las necesidades. También permite obtener colocaciones que mejoren la convergencia de algunos estimadores.

La segunda contribución de la tesis se ocupa de la colocación de sensores en zonas más complejas, donde existan obstáculos que provoquen oclusiones a algunos sensores. De esta manera, podemos introducir el problema de intentar cubrir la mayor cantidad de puntos del espacio con el número mínimo de sensores necesario para calcular la posición de un objetivo. Dicho número influirá en el porcentaje de área cubierto y en la precisión obtenida, además de aumentar el coste del sistema. Debido a esto, también será un objetivo a optimizar junto a la cobertura y la incertidumbre de la posición estimada. Para llevar a cabo esta optimización se propone una mejora sobre el algoritmo utilizado en la aportación anterior basada en el uso de subpoblaciones y añadiendo operadores genéticos que modifiquen el número de sensores según la cobertura y condensación en los distintos puntos de la zona a cubrir.

Cada uno de los capítulos dedicado a las aportaciones descritas contiene resultados y conclusiones que confirman el buen funcionamiento de los métodos propuestos. Finalmente, la tesis concluye con una lista de propuestas que serán estudiadas en un futuro.

Abstract

This thesis contributes to the current research in the field of sensor resource management of indoor positioning systems. Sensor resource management deals with sensor placement and sensor scheduling, although this thesis focuses only on the former. We use an indoor positioning system based on infrared signals with phase-difference of arrival measurements. These phase measurements are subsequently converted to distance-differences; hence, our problem becomes hyperbolic trilateration with range-difference of arrival measurements. We include a model of the error of range-difference measurements with an infrared system, though we can omit the fact that we work with an infrared system and think only on range-difference measurements which have a Gaussian distribution with a variance calculated by the model. As a matter of fact, the work described in this thesis can be applied to other positioning systems using a model of the measurement errors, even when performing spherical trilateration or angulation.

Most of the proposals that place sensors to improve the estimation accuracy optimize metrics of the Cramér-Rao lower bound, as we do in this work. The thesis contains a chapter that reviews the existing contributions on sensor placement for target localization, which concludes stating our own contributions to the current literature. To summarize, we can classify the different approaches in three categories. The first group deals with the determination of an optimal configuration of sensors to locate a target, they usually optimize the determinant of Fisher information matrix or the dilution of precision. These methods obtain analytical expressions that provide explanations of the effect of different elements of the positioning system on the final accuracy. However, they cannot be applied to real situations. To the second group belong the approaches that focus on sensor deployment to cover a whole area or multiple targets. This thesis belongs to this category. Finally, there are methods that use techniques of sensor selection to obtain optimal configurations. Among these three kinds of proposals we can find the following drawbacks: the simplification of the measurement model to obtain mathematically tractable expressions, consideration of a single accuracy performance measure, placement of a fixed amount of sensors, or sensor deployment in simple areas without non-line-of-sight

problems.

Our first contribution aims to overcome the consideration of a single accuracy criterion, which is usually the determinant or trace of the covariance or information matrix of the estimation. Each metric of these matrices has its own practical meaning; hence, considering only one of them provides solutions which are not optimal regarding other metrics. For instance, we can get a solution with a low mean squared error but a high elongation of the error ellipsoids. Our proposal involves the use of multi-objective evolutionary algorithms that optimize several metrics of the covariance of the estimation, such as average mean squared error in the area, isotropy of the solution, or the maximum deviation of a point of the region of interest. This optimization provides a Pareto front with a set of solutions reflecting the trade-off among different metrics. The resource manager can use this set to choose a desired solution according to current needs. This approach also allows us to improve the performance of some estimators.

The second contribution of the thesis involves sensor placement in complex zones, where there are obstacles that cause occlusions to some sensors. Thus, we can introduce the problem of trying to cover as many points of the area as possible with the minimum amount of sensors needed to estimate the position of a target. Not only increases such amount the percentage of covered area and the obtained accuracy, but it also increases the cost of the system. As a consequence, the number of deployed sensors must also be optimized together with the coverage of the area and the uncertainty of the estimated position. In order to achieve this goal, we propose a modification of the previous algorithm based on the use of subpopulations and genetic operators that allow us to place and remove sensors from an existing set according to current coverage and saturation of the region of interest.

Each one of the chapters that describes those contributions provides results and conclusions that confirm the suitability of the proposed methods. Finally, the thesis ends with some proposals about future improvements to the work.

Contents

- Resumen** **ix**

- Abstract** **xi**

- Contents** **xiii**

- List of Figures** **xvii**

- List of Tables** **xix**

- List of Abbreviations** **xxi**

- 1 Preface** **1**
 - 1.1 Introduction 1
 - 1.2 Motivation and objectives 2
 - 1.3 Background 3
 - 1.4 Outline of the document 4

- 2 State of the art** **7**
 - 2.1 Source localization methods 8
 - 2.1.1 TOA 10
 - 2.1.2 TDOA 12
 - 2.1.3 POA/PDOA 13
 - 2.1.4 RSS 14
 - 2.1.5 AOA 15
 - 2.2 Sensor placement techniques 16
 - 2.2.1 Single target localization 18
 - 2.2.2 Multiple targets localization, area coverage 21
 - 2.2.3 Sensor selection techniques 22

2.3	Conclusions	23
3	Problem statement	25
3.1	A simple model of the infrared measurement	25
3.2	Target localization with RDOA	27
3.3	Accuracy of the target localization	30
3.3.1	Position accuracy measures	30
3.3.2	A performance limit on the accuracy of a positioning system: the CRLB	31
3.3.3	Preliminary accuracy studies	32
3.4	Summary and proposed solutions	34
4	Sensor placement determination for target positioning using different performance measures of covariance matrix and multi-objective optimization	37
4.1	Introduction	37
4.2	Performance measures of covariance matrix	39
4.3	Multi-objective optimization	41
4.3.1	Evolutionary multi-objective optimization	43
4.4	Numerical example	45
4.4.1	Single-objective optimization	48
4.4.2	Multi-objective optimization	52
4.5	Obtaining a metric with prior information	56
4.6	Conclusions	57
5	Optimization of the coverage and accuracy of an indoor positioning system with a variable number of sensors	59
5.1	Introduction	59
5.2	Problem statement	61
5.2.1	Accuracy objectives	61
5.2.2	Coverage objective	62
5.3	Proposed algorithm	63
5.4	Numerical example	67
5.4.1	LOS sensors	69
5.4.2	Occluded sensors	69
5.5	Conclusions	73

6	Conclusions and future work	77
6.1	Conclusions	77
6.2	Publications derived from the thesis	78
6.2.1	Peer-reviewed journals	78
6.2.2	International conferences	79
6.2.3	Other contributions	79
6.3	Future work	80
	Bibliography	83

List of Figures

- 2.1 Spherical trilateration 8
- 2.2 Hyperbolic trilateration 9
- 2.3 Angulation 9
- 2.4 2D geometry of target and two anchors 10
- 2.5 Target uncertainty area with good geometry between target and anchors 17
- 2.6 High dilution of precision due to bad geometry 18

- 3.1 Infrared emitter-sensor link 26
- 3.2 Five sensors deployed in the corners of a square and center 32
- 3.3 MLE vs NLS with five sensors 33
- 3.4 MLE vs NLS with four sensors 33
- 3.5 MLE vs NLS with three sensors 33

- 4.1 Symbolic representation of solutions in the space of the objectives of a two-objective optimization problem 42
- 4.2 Noise variance vs distance between sensor and emitter 47
- 4.3 Optimum sensor placement that optimizes the average trace of the CRLB. 48
- 4.4 Optimum sensor placement that optimizes the average determinant of the CRLB. 49
- 4.5 Optimum sensor placement that optimizes the absolute maximum eigenvalues of the CRLB. 49
- 4.6 Optimum sensor placement that optimizes the average isotropy. 50
- 4.7 Optimum sensor placement that optimizes the deviation in a given direction. . . 51
- 4.8 Optimum sensor placement that optimizes the variance of the y coordinate when $x = 1.5$ m. 51
- 4.9 Sensor placement and Pareto front of trace and eigenvalues ratio optimality . . . 52
- 4.10 Sensor placement and Pareto front of trace and maximum eigenvalue optimality 52

4.11	Sensor placement and Pareto front of maximum eigenvalue and eigenvalues ratio optimality	53
4.12	Sensor placement and Pareto front using trace ($x < 1.2 \cup x > 1.8$) and lateral deviation ($1.2 \leq x \leq 1.8$) criteria	53
4.13	Sensor placement and Pareto front of trace, eigenvalues ratio, and maximum eigenvalue	54
4.14	Optimum placement that optimizes the RMSE with NLS.	55
5.1	Pareto fronts of two uncertainty metrics for different numbers of anchor nodes	64
5.2	Proposed GA	68
5.3	Comparison of Pareto fronts with NSGA-II and the proposed algorithm	70
5.4	Some optimal configurations found by the proposed algorithm when deploying 5 to 12 sensors with an obstacle in the center. The whole ROI is at least 3-covered in all cases.	72
5.5	Some optimal configurations found by the proposed algorithm when deploying 5 to 15 sensors with two obstacles. The first three figures show optimum coverage and accuracy deployment, whereas the two objectives are simultaneously optimized in the other cases.	74

List of Tables

- 3.1 System parameters 27
- 4.1 Scalar performance measures referring to individual location 39
- 4.2 Chosen GA parameters 46
- 4.3 Comparison of the 2DRMS attainable by each configuration 55
- 5.1 Probabilities of the genetic operators 69
- 5.2 Extreme values of the Pareto fronts with NSGA-II and the proposed algorithm . 71
- 5.3 Comparison of the Pareto optimal solutions obtained by the proposed algorithm and random deployment for the case with one obstacle. The values for random deployment have been obtained averaging 50 random placed sets of sensors for each amount of sensors. 73
- 5.4 Comparison of the worst Pareto values obtained by the proposed algorithm and random deployment for the case with two obstacles. The values for random deployment have been obtained averaging 50 random placed sets of sensors for each amount of sensors. 75

List of Abbreviations

2DRMS twice the distance root mean square.

AOA angle of arrival.

CEP circular error probability.

CRLB Cramér-Rao lower bound.

DOA direction of arrival.

DOP dilution of precision.

EMO evolutionary multi-objective optimization.

FIM Fisher information matrix.

GA genetic algorithm.

GDOP geometric dilution of precision.

GPU graphics processing unit.

HDOP horizontal dilution of precision.

i.i.d. independent and identically distributed.

IPS indoor positioning system.

KKT Karush-Kuhn-Tucker.

LOS line-of-sight.

MLE maximum likelihood estimator.

MOEA multi-objective evolutionary algorithm.

MOO multi-objective optimization.

MSE mean squared error.

MVUE minimum variance unbiased estimator.

NLOS non-line-of-sight.

NLS nonlinear least squares.

NSGA-II non-dominated sorting genetic algorithm.

PCRLB posterior Cramér-Rao lower bound.

PDF probability density function.

PDOA phase-difference of arrival.

PDOP position dilution of precision.

PF Pareto front.

POA phase of arrival.

RDOA range-difference of arrival.

RMSE root mean square error.

ROI region of interest.

RSS received signal strength.

SNR signal-to-noise ratio.

TDOA time-difference of arrival.

TDOP time dilution of precision.

TOA time of arrival.

VDOP vertical dilution of precision.

WNLS weighted nonlinear least squares.

Chapter 1

Preface

1.1 Introduction

An indoor positioning system (IPS) tries to get the position of a target in an indoor environment, where GPS-based solutions provide poor performance. There are a good deal of applications that require information about the location of people or objects. These applications cover diverse fields such as surveillance systems, ambient assisted living, autonomous vehicle guidance, manufacturing processes, etc. Not only are the methods discussed in this thesis applicable to indoor environments, but they are also useful in other areas where GPS is useless, such as underwater or urban areas where the GPS signal is blocked by buildings or inside tunnels.

As for localization technologies, there is not any clearly dominant technology and its selection is highly dependable on the desired performance and cost of the application. There is currently a wide variety of solutions based on different technologies such as inertial sensors, radiofrequency signals both from established communication networks like wireless local area networks and GSM, or specifically deployed infrastructures like RFID, pseudolites, or ultra-wide band systems. There are also proposals considering systems based on cameras, ultrasound, and optical signals. As we can see, some of these technologies are already deployed in most buildings, hence their low implementation cost.

We address the problem of locating a target using several anchor nodes, which are nodes whose position is fixed and known. The target is located after obtaining information related to the distance or the angle of arrival (AOA) between the target and the anchors. After a process of information fusion of these data we can perform trilateration or angulation to calculate the target position. Thus, the process takes two steps, namely, getting the measurements and estimating the position. Note that the target can be an emitter — source — and the anchors

can be sensors, but the formulation of the problem does not change in the opposite case. However, the specific problem we use to get our results consists of an infrared emitter — the target — and several sensors. From now on we will use sensors and anchors interchangeably, the same goes for emitter and target. Our work focuses on the design stage of an IPS; i.e., where should we deploy sensors so that the performance of the system is optimal. This is an offline process, therefore there are not constraints on the time spent until we have our solution. The performance of an IPS depends on several factors, such as the quality of the measurements, the position of the sensors, and the estimator used to calculate the target position. Sensor resource management comprises the placement of the sensors to optimize the localization and the scheduling of the sensors to use them efficiently once deployed. In this work, we address only the first problem. This thesis contributes to the development of new sensor resource management methods addressing problems never considered before and providing new insights to the field.

1.2 Motivation and objectives

As we will see in Chapter 2, existing sensor placement methods still have some drawbacks that we aim to overcome. The limitations of existing deployment methods are usually the use of a single accuracy criterion, the simplification of the measurement model — such as neglecting the heteroscedasticity and correlations —, or the predefinition of a desired accuracy and positions where the sensors can be deployed. We apply metaheuristics — genetic algorithms — to perform a multi-objective optimization (MOO) of several objectives and obtain sets of Pareto optimal solutions. Our results are not a single solution, but a set of optimal solutions which should be analyzed by the resource manager, which is the human expert that designs the system. This approach is also called decision support system, since we assist the manager by providing the optimal solutions so that he could apply higher level criteria to select a desired solution.

We can summarize our different goals with the following points:

- Obtain a method that automatically finds optimal deployments according to different performance measures.
- Provide a more complete description of the accuracy achievable with our system.
- Check the trade-off among different accuracy performance measures.
- Obtain an algorithm that considers a variable number of anchors and the presence of

obstacles that can cause occlusions to sensors.

1.3 Background

This thesis describes original work developed in the GEINTRA Research Group of the Electronics Department of the University of Alcalá.

GEINTRA is an official group of the University of Alcalá formed by 24 professors and assistant professors, and many grad and undergrad students. The main goal of the group is the development of fundamental and applied research activities in the fields of intelligent spaces and intelligent transport and infrastructure systems. This goal includes research lines related to: mobile robotics, localization systems, human-machine interfaces, embedded digital systems, sensors, sensor networks, sensor fusion, intelligent transport, distributed control and automation, e-health, and independent living.

Within this framework, this thesis is contextualized in the two application fields of the group: intelligent spaces and intelligent transport and infrastructures, being specifically related to the research lines of localization and sensors. This work has been mainly supported by the following research projects:

- ESPIRA (ref. DPI2009-10143) [Spanish Ministry of Science and Innovation]: Contribution to intelligent spaces by developing and integrating positioning sensors (in Spanish). PI: Dr. José Luis Lázaro Galilea. The goal of this project was to develop sensor systems based on discrete infrared sensors and distributed/centralized processing architectures based on reconfigurable systems to increase the sensing and processing capacities of intelligent spaces. The general objective was to locate mobiles such as robots, wheelchairs, or industrial vehicles for future smart spaces built in environments like hospitals, offices, or warehouses. This thesis deals with the management of those developed sensors.
- ALCOR (ref. DPI2013-47347-C2-1-R) [Spanish Ministry of Economy and Competitiveness]: Optimization of wireless sensor network and network control system for the cooperation of mobile units in intelligent spaces (in Spanish). PI: Dr. Felipe Espinosa Zapata, Dr. José Luis Lázaro Galilea. This project is devoted to contributing toward the flexible and cooperative tasking between robot units in extensive indoor industrial scenarios. This goal is addressed with three complementary research lines: remote event-based control techniques for the mobile units to minimize the communication requirements and the complexity of the on-board systems, optical localization sensors and means for their interconnection to provide accurate localization with versatile detection areas, and opti-

mization of the communication network to provide service to the former considering the mobility of some of the nodes (mobile units) and the reconfigurable network topology of others (localization sensors). Within this project, the present thesis addresses part of the tasks of the research line related to localization sensors, specifically the placement of sensors to optimize the performance of the localization.

This thesis has also been supported by the Spanish Ministry of Education, Culture, and Sport through the FPU program (ref. BOE-A-2012-6238) and the UAH mobility program. The latter made possible the attendance to the conferences and research stays for collaboration in the Institute of Geodesy and Photogrammetry of the ETH Zürich (Switzerland) and the Sensor Data Fusion department of the Fraunhofer Institute for Communication, Information Processing and Ergonomics (FKIE) in Wachtberg, Germany.

1.4 Outline of the document

The dissertation is organized as follows:

- Chapter 2: *State of the art*. This chapter starts summarizing and unifying the treatment of different ranging methods for localization. We show the performance bounds of the attainable covariance matrix of time of arrival (TOA), time-difference of arrival (TDOA), AOA, and received signal strength (RSS) before reviewing relevant contributions in the field of sensor placement for target localization. We propose a classification of the existing methods and acknowledge their strengths and weaknesses. Finally, we draw some conclusions where we explain what we could do to overcome the limitations of existing methods.
- Chapter 3: *Problem statement*. We specify the problem for our infrared system in this section. We show a simple model of the ranging error which will be used to get the measurements during simulations. The problem of localization with range-difference measurements is explained in this chapter and the Cramér-Rao lower bound (CRLB) as an indicator of the performance limit is also shown. We show some preliminary results of accuracy studies with two different estimators. These results will help us to introduce some motivations for our contribution, which is detailed in the following chapter.
- Chapter 4: *Sensor placement determination for target positioning using different performance measures of covariance matrix and multi-objective optimization*. The main contribution of this thesis. We optimize several metrics and analyze the trade-offs among them in the Pareto

fronts that we obtain as a result of a MOO. This chapter also includes a proposal to obtain a metric that can be used in a dynamic case where prior information of the target state is available.

- Chapter 5: *Optimization of the coverage and accuracy of an indoor positioning system with a variable number of sensors*. This chapter extends the previous method to situations where the number of sensors is not fixed and the region of interest (ROI) has obstacles that cause occlusions. The occlusions cause that we do not know a priori if we can perform localization in the whole ROI, since we are not sure if all points are covered by the minimum number of sensors. Hence, we add the percentage of covered area as an objective to be maximized.
- Chapter 6: *Conclusions and future work*. The conclusions of each part of the thesis are drawn in their corresponding chapters. This chapter summarizes these conclusions and states our contributions to the state of the art explicitly. Most of the results presented in this work have been published in two journals whose impact factor falls in the top 25 percentile ranking of *Journal Citation Reports* and international conferences. This chapter provides a list of these contributions. Finally, we address some limitations of the current state of the work and comment some possible solutions.

Chapter 2

State of the art

As set out in the introduction, the core of this thesis is the development and use of algorithms to find optimal sensor placements that improve localization performance. The methods can be applied to any system from which we have a model of the error of the estimation, though our results are mainly focused on an infrared IPS [Martin-Gorostiza et al., 2014]. Range-based localization usually involves two steps, namely, obtaining the range measurements and estimating the target position. This work considers the latter step exclusively; thus, this section will not include a comprehensive description of different positioning technologies. The reader can go deeper into that topic in [Mautz, 2012], which analyzes 13 different technologies and provides some comparisons according to user requirements, such as coverage and accuracy. The highly cited paper from [Liu et al., 2007] is also a good starting point to know about positioning techniques and systems. Finally, the book of [Zekavat and Buehrer, 2012] provides an in-depth coverage of position location, from the fundamentals of localization to novel applications.

This section should cover the classic and emerging techniques of sensor placement for target localization. We must find a cost function related to the accuracy and precision of the target position estimation, and it is our idea to develop a framework that can be applied regardless of the localization method. Hence, this section will start reviewing different localization methods that can be used with the proposed framework. Section 2.1 covers the usual localization techniques based on trilateration, multilateration, angulation, etc. It discusses their strengths and weaknesses, as well as the derivation of a function related to the accuracy of the estimation. Sensor placement techniques will be thoroughly analyzed in Section 2.2. Finally, we will draw conclusions on the current deployment techniques in Section 2.3.

Before starting reviewing the localization methods, we would like to make a few comments on mathematical methods for source position estimation. The accuracy metric we use provides a bound on the efficiency of the estimation that can be achieved with an unbiased estimator.

Since we do not restrict ourselves to a specific estimator, they will not be covered in this section. The reader can be referred to [So, 2012] to know the basic iterative and closed-form methods, the book also includes some MATLAB code. [Seco et al., 2009] propose a classification of mathematical methods in four groups and comment the applicability of different methods in non-line-of-sight (NLOS) situations, which may cause a biased solution due to multipath effects. A more comprehensive review of range-based positioning algorithms can be found in [Yan et al., 2013], which compares different estimators in terms of accuracy and complexity.

2.1 Source localization methods

The methods described in the following chapters can be used with any localization method from which we can obtain a model of the accuracy and precision of the estimation. This section describes different positioning methods according to the nature of the observations. When absolute ranges or times are measured, we usually talk about trilateration or spherical trilateration. In case of lack of synchronism between target and anchors we speak of hyperbolic trilateration or just multilateration. Triangulation methods use AOA or direction of arrival (DOA). Finally, some systems based on radio frequency can only use RSS for localization.

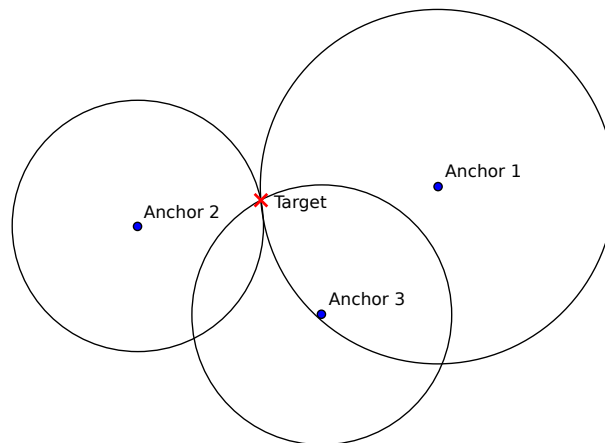


Figure 2.1: Spherical trilateration

Before describing these different kind of measurements we will see a few generalities about their mathematical formulation. The notation for all the measurements will be the same as far as possible. The reader can go deeper into this topic in [So, 2012]. The Fisher information matrix (FIM) and its inverse form, the CRLB, are the usual metrics of uncertainty. [Bishop et al., 2010] find optimal sensor-target geometries and show the FIM of TOA, range-only, and AOA. The work of [Zhao et al., 2013] unifies the problem of sensor placement for AOA, range-only, and RSS. The content of this subsection is mostly based on those studies.

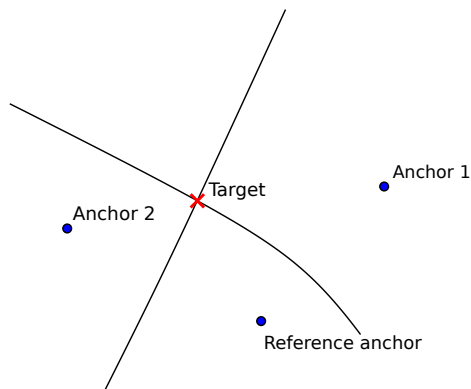


Figure 2.2: Hyperbolic trilateration

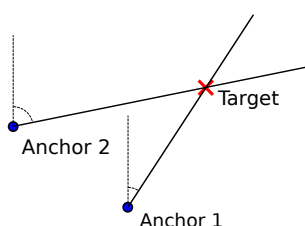


Figure 2.3: Angulation

Assuming additive white Gaussian noise, any set of measurements \mathbf{z} from N sensors can be expressed with the following equation:

$$\mathbf{z} = \mathbf{h}(\mathbf{x}) + \boldsymbol{\epsilon}, \quad (2.1)$$

where \mathbf{x} is the unknown target localization; i.e., a column vector of coordinates with dimension D , where D is usually 2 or 3. The elements h_i of the vector \mathbf{h} are (usually highly nonlinear) functions of the sensor-target distance and i takes integer values from 1 to N , that is to say each h_i maps the coordinates of \mathbf{x} to a scalar value, $h_i : \mathbb{R}^D \rightarrow \mathbb{R}$ and $\mathbf{h} : \mathbb{R}^D \rightarrow \mathbb{R}^N$. Finally, $\boldsymbol{\epsilon} = [\epsilon_1, \epsilon_2, \dots, \epsilon_N]^T$, where $\epsilon_i \sim (0, \sigma_i^2)$ is the deviation of the measurement of sensor i and T is the transpose operator. Expressing it in its vector form: $\boldsymbol{\epsilon} \sim (\mathbf{0}, \boldsymbol{\Sigma})$. The standard deviation of the measurement of the i th sensor is denoted by σ_i , whereas $\boldsymbol{\Sigma}$ represents the $N \times N$ covariance matrix of the set of N observations.

There are many algorithms to solve Eq. (2.1) finding \mathbf{x} and we have already provided some references to know about them. Assuming we use an efficient and unbiased estimator, there is a performance limit on the uncertainty of the estimation known as CRLB. The CRLB is a lower bound of the covariance that can be achieved with an unbiased estimator and it is calculated with the inverse of the FIM. The next chapter will discuss some aspects of the derivation of CRLB, a further insight into it can be found in [Kay, 1993]. Considering additive Gaussian noise, the FIM \mathcal{I} is computed with the Jacobian matrix of $\mathbf{h}(\mathbf{x})$ and the covariance $\boldsymbol{\Sigma}$ of the

observations as in Eq. (2.2).

$$\mathcal{I}(\mathbf{x}) = \left(\frac{\partial \mathbf{h}}{\partial \mathbf{x}^T} \right)^T \boldsymbol{\Sigma}^{-1} \frac{\partial \mathbf{h}}{\partial \mathbf{x}^T} \quad (2.2)$$

When the deviations of different sensors are uncorrelated, the form of the FIM in Eq. (2.3) is very interesting; since each measurement contributes to the FIM as an element of a sum.

$$\mathcal{I}(\mathbf{x}) = \sum_{i=1}^N \frac{1}{\sigma_i^2} \frac{\partial h_i}{\partial \mathbf{x}} \left(\frac{\partial h_i}{\partial \mathbf{x}} \right)^T \quad (2.3)$$

Equation (2.3) and the additive property of FIM can be used to deploy an optimum subset of sensors when the noise of different measurements is uncorrelated. This situation happens when absolute ranges or times are measured; however, in case of differences of times and ranges the equation does not apply.

In the following, we will see how we can obtain Eqs. (2.2) and (2.3) from different localization methods. For the sake of a better understanding of the influence of the relative geometry between target and anchors, the reader can compare Fig. 2.4 with the following equations.

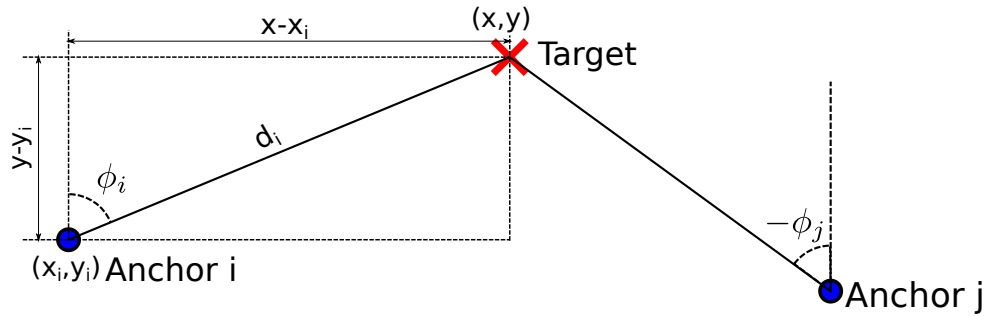


Figure 2.4: 2D geometry of target and two anchors

2.1.1 TOA

TOA is the time that a signal takes to travel from an emitter to a receiver. Multiplying this time t by the known propagation speed c of the signal results in the distance between emitter and receiver, i.e., $d = ct$. Usual values are $c = 340 \text{ m/s}$ or $c = 3 \times 10^8 \text{ m/s}$, which are the speed of sound and light, respectively. In the absence of noise, this distance provides the radius of a circle whose center is the anchor node and that contains the target. As we know from elemental geometry, a 2D point is given by the intersection of three circles, hence we need at least three anchors in order to be able to determine the position of the target. TOAs are usually converted to a set of equations and an optimization algorithm computes the target position. Assuming that a signal emitted by the target at time t_0 reaches the i th anchor at time t_i , the distance

between them is given by:

$$d_i = c (t_i - t_o). \quad (2.4)$$

The target and the anchors must be precisely synchronized to obtain the TOA information.

The distance between the i th anchor and the target d_i is calculated with the ℓ^2 norm ($\|\cdot\|$):

$$d_i = \|\mathbf{x} - \mathbf{x}_i\| = \sqrt{(x - x_i)^2 + (y - y_i)^2}. \quad (2.5)$$

Considering additive Gaussian noise, we can adapt Eq. (2.1) to the TOA measurement \mathbf{z}_{TOA} :

$$\mathbf{z}_{\text{TOA}} = \mathbf{h}_{\text{TOA}}(\mathbf{x}) + \boldsymbol{\epsilon}_{\text{TOA}}. \quad (2.6)$$

Where

$$\mathbf{z}_{\text{TOA}} = [z_{\text{TOA},1}, z_{\text{TOA},2}, \dots, z_{\text{TOA},N}]^T, \quad (2.7)$$

$$\boldsymbol{\epsilon}_{\text{TOA}} = [\epsilon_{\text{TOA},1}, \epsilon_{\text{TOA},2}, \dots, \epsilon_{\text{TOA},N}]^T, \quad (2.8)$$

and

$$\mathbf{h}_{\text{TOA}}(\mathbf{x}) = \mathbf{d} = \begin{bmatrix} \|\mathbf{x} - \mathbf{x}_1\| \\ \|\mathbf{x} - \mathbf{x}_2\| \\ \vdots \\ \|\mathbf{x} - \mathbf{x}_N\| \end{bmatrix}. \quad (2.9)$$

It is assumed that $\epsilon_{\text{TOA},i}$ are zero-mean — under line-of-sight (LOS) transmission — uncorrelated Gaussian noises with variances $\sigma_{\text{TOA},i}^2$. As a consequence, the TOA covariance matrix corresponds to

$$\begin{aligned} \boldsymbol{\Sigma}_{\text{TOA}} &= \text{E} \left[(\mathbf{z}_{\text{TOA}} - \mathbf{d}) (\mathbf{z}_{\text{TOA}} - \mathbf{d})^T \right] \\ &= \text{E} \left[\boldsymbol{\epsilon} \boldsymbol{\epsilon}^T \right] \\ &= \text{diag} \left(\sigma_{\text{TOA},1}^2, \sigma_{\text{TOA},2}^2, \dots, \sigma_{\text{TOA},N}^2 \right), \end{aligned} \quad (2.10)$$

where $\text{E}[\cdot]$ is the expectation operator.

To summarize, $\mathbf{z}_{\text{TOA}} \sim \mathcal{N} \left(\mathbf{d}, \text{diag} \left(\sigma_{\text{TOA},1}^2, \sigma_{\text{TOA},2}^2, \dots, \sigma_{\text{TOA},N}^2 \right) \right)$.

Finally, to obtain the FIM we just need to compute $\frac{\partial \mathbf{h}_{\text{TOA}}(\mathbf{x})}{\partial^T \mathbf{x}}$. Taking into account the fact that the derivative of the norm of a vector with respect to the same vector is its normalized vector, i.e., $\frac{\partial \|\mathbf{x}\|}{\partial \mathbf{x}} = \frac{\mathbf{x}}{\|\mathbf{x}\|}$:

$$\frac{\partial \mathbf{h}_{\text{TOA}}(\mathbf{x})}{\partial^T \mathbf{x}} = \begin{bmatrix} \frac{x-x_1}{\|\mathbf{x}-\mathbf{x}_1\|} & \frac{y-y_1}{\|\mathbf{x}-\mathbf{x}_1\|} \\ \frac{x-x_2}{\|\mathbf{x}-\mathbf{x}_2\|} & \frac{y-y_2}{\|\mathbf{x}-\mathbf{x}_2\|} \\ \vdots & \vdots \\ \frac{x-x_N}{\|\mathbf{x}-\mathbf{x}_N\|} & \frac{y-y_N}{\|\mathbf{x}-\mathbf{x}_N\|} \end{bmatrix} = \begin{bmatrix} \sin(\phi_1) & \cos(\phi_1) \\ \sin(\phi_2) & \cos(\phi_2) \\ \vdots & \vdots \\ \sin(\phi_N) & \cos(\phi_N) \end{bmatrix}. \quad (2.11)$$

We can replace Eq. (2.11) in (2.2) and, since TOA noises are independent and identically distributed (i.i.d.), we can get the expression of (2.3). Moreover, we can consider that $\sigma_{\text{TOA},1} = \sigma_{\text{TOA},2} = \dots = \sigma_{\text{TOA},N} = \sigma_{\text{TOA}}$ to simplify the problem even more.

$$\mathcal{I}_{\text{TOA}}(\mathbf{x}) = \frac{1}{\sigma_{\text{TOA}}^2} \sum_{i=1}^N \frac{\partial h_i}{\partial \mathbf{x}} \left(\frac{\partial h_i}{\partial \mathbf{x}} \right)^T = \frac{1}{\sigma_{\text{TOA}}^2} \sum_{i=1}^N \begin{bmatrix} \sin^2(\phi_i) & \frac{\sin(2\phi_i)}{2} \\ \frac{\sin(2\phi_i)}{2} & \cos^2(\phi_i) \end{bmatrix} \quad (2.12)$$

Inverting Eq. (2.12), we get an expression of CRLB for the TOA problem. Assuming a constant σ_{TOA} we can see that the equation depends only on the relative angles between the target and the sensors; however, we neglect the effect of the distance between sensors and target. Notwithstanding such a naive assumption, some researchers use Eq. (2.12) to compute a theoretical optimum, as we will see in the following section.

2.1.2 TDOA

Calculating TDOA simplifies the TOA method, inasmuch as we do not need that receivers and the emitter source are synchronized, though the synchronization among receivers is a requirement. TDOA is the difference of the time that the signal takes to travel from the source to two different receivers. Again, multiplying this time-difference by the propagation speed of the signal results in the range-difference between the target and two anchors. If the source transmits a signal at time t_o , it reaches the i th sensor at time t_i and the j th sensor at time t_j . Differencing these values: $t_{i,j} = (t_i - t_o) - (t_j - t_o) = t_i - t_j$. If we obtain the TDOAs for all receivers, we get a full TDOA set that contains some redundant information, since $t_{k,j} = t_{k,i} - t_{j,i}$. Because of this reason, we usually pick one anchor as a reference and compute the time-differences regarding the other anchors, obtaining a non-redundant set of $N - 1$ TDOAs. This approach is also known as centralized, there are also authors that look for an optimal pairing instead of selecting a reference, e.g., [Meng et al., 2016]. The differences of distances are obtained with the speed of the signal $d_{i,j} = ct_{i,j}$. If we consider the two anchors as focal points, the target is located in the set of points whose difference of distance to these foci is constant and equal to $d_{i,j}$. This set of points is an hyperbola, knowing the sign of the range-difference allows us to discard one of the branches. Even though two hyperbolae (three anchors) usually intersect in a single point, sometimes they can intersect in two points. We provide again set of equations from which we estimate the position of the target, the 1st anchor is picked as the reference without loss of generality.

$$\mathbf{z}_{\text{TDOA}} = \mathbf{h}_{\text{TDOA}}(\mathbf{x}) + \boldsymbol{\epsilon}_{\text{TDOA}}. \quad (2.13)$$

Where

$$\mathbf{z}_{\text{TDOA}} = [z_{\text{TDOA},2}, z_{\text{TDOA},3}, \dots, z_{\text{TDOA},N}]^T, \quad (2.14)$$

$$\boldsymbol{\epsilon}_{\text{TDOA}} = [\epsilon_{\text{TDOA},2}, \epsilon_{\text{TDOA},3}, \dots, \epsilon_{\text{TDOA},N}]^T, \quad (2.15)$$

and

$$\mathbf{h}_{\text{TDOA}}(\mathbf{x}) = \mathbf{d}_1 = \begin{bmatrix} \|\mathbf{x} - \mathbf{x}_2\| - \|\mathbf{x} - \mathbf{x}_1\| \\ \|\mathbf{x} - \mathbf{x}_3\| - \|\mathbf{x} - \mathbf{x}_1\| \\ \vdots \\ \|\mathbf{x} - \mathbf{x}_N\| - \|\mathbf{x} - \mathbf{x}_1\| \end{bmatrix}. \quad (2.16)$$

The noise of the range-difference measurements is $\epsilon_{\text{TDOA},i} = \epsilon_i - \epsilon_1$. The variance of the difference of two random variables is the sum of the variance of these two variables; thus, $\epsilon_{\text{TDOA},i} \sim \mathcal{N}\left(0, \sigma_{\text{TDOA},i}^2 = \sigma_i^2 + \sigma_1^2\right)$. The fact that every TDOA measurement use the same reference implies that the error of the reference anchor propagates through all of them. Because of this reason, the covariance matrix of \mathbf{z}_{TDOA} is non-diagonal. The element of the i, i entry is $\sigma_{i+1}^2 + \sigma_1^2$, whereas the non-diagonal elements are σ_1^2 . Finally, the Jacobian matrix of the TDOA function is

$$\begin{aligned} \frac{\partial \mathbf{h}_{\text{TDOA}}(\mathbf{x})}{\partial^T \mathbf{x}} &= \begin{bmatrix} \frac{x-x_2}{\|\mathbf{x}-\mathbf{x}_2\|} - \frac{x-x_1}{\|\mathbf{x}-\mathbf{x}_1\|} & \frac{y-y_2}{\|\mathbf{x}-\mathbf{x}_1\|} - \frac{y-y_1}{\|\mathbf{x}-\mathbf{x}_1\|} \\ \frac{x-x_3}{\|\mathbf{x}-\mathbf{x}_3\|} - \frac{x-x_1}{\|\mathbf{x}-\mathbf{x}_1\|} & \frac{y-y_3}{\|\mathbf{x}-\mathbf{x}_2\|} - \frac{y-y_1}{\|\mathbf{x}-\mathbf{x}_1\|} \\ \vdots & \vdots \\ \frac{x-x_N}{\|\mathbf{x}-\mathbf{x}_N\|} - \frac{x-x_1}{\|\mathbf{x}-\mathbf{x}_1\|} & \frac{y-y_N}{\|\mathbf{x}-\mathbf{x}_N\|} - \frac{y-y_1}{\|\mathbf{x}-\mathbf{x}_1\|} \end{bmatrix} \\ &= \begin{bmatrix} \sin(\phi_2) - \sin(\phi_1) & \cos(\phi_2) - \cos(\phi_1) \\ \sin(\phi_3) - \sin(\phi_1) & \cos(\phi_3) - \cos(\phi_1) \\ \vdots & \vdots \\ \sin(\phi_N) - \sin(\phi_1) & \cos(\phi_N) - \cos(\phi_1) \end{bmatrix}. \end{aligned} \quad (2.17)$$

Because of the full population of the covariance matrix, we cannot use Eq. (2.3) as we did with TOA. We can calculate the FIM with Eq. (2.2), which has a more complex form than (2.12).

2.1.3 POA/PDOA

Both phase of arrival (POA) [Povalac and Sebesta, 2010] and phase-difference of arrival (PDOA) [Povalac and Sebesta, 2011] estimate the distances between source and receivers by measuring the phase added to the signal during its propagation. Multiplying the phase φ by the speed of the signal and dividing by its frequency provides the distance $d = \frac{c}{2\pi f} \varphi$. Once the distance is calculated, the position is estimated the same way as TOA or TDOA.

2.1.4 RSS

The average power that reaches a receiver when it is emitted by a source is the RSS. The received power at sensor i $P_{r,i}$ is usually a function of the originally transmitted power P_t , path loss constant α , and the distance between source and receiver, among other factors K_i : $P_{r,i} = K_i P_t \|\mathbf{x} - \mathbf{x}_i\|^{-\alpha}$. Taking logarithms and simplifying, we model the RSS signal as

$$z_{\text{RSS},i} = -\alpha \ln(\|\mathbf{x} - \mathbf{x}_i\|) + \epsilon_{\text{RSS},i}. \quad (2.18)$$

Putting Eq. (2.18) in vector form:

$$\mathbf{z}_{\text{RSS}} = \mathbf{h}_{\text{RSS}}(\mathbf{x}) + \boldsymbol{\epsilon}_{\text{RSS}}. \quad (2.19)$$

Where

$$\mathbf{z}_{\text{RSS}} = [z_{\text{RSS},1}, z_{\text{RSS},2}, \dots, z_{\text{RSS},N}]^T, \quad (2.20)$$

$$\boldsymbol{\epsilon}_{\text{RSS}} = [\epsilon_{\text{RSS},1}, \epsilon_{\text{RSS},2}, \dots, \epsilon_{\text{RSS},N}]^T, \quad (2.21)$$

and

$$\mathbf{h}_{\text{RSS}}(\mathbf{x}) = \mathbf{p} = -\alpha \begin{bmatrix} \ln(\|\mathbf{x} - \mathbf{x}_1\|) \\ \ln(\|\mathbf{x} - \mathbf{x}_2\|) \\ \vdots \\ \ln(\|\mathbf{x} - \mathbf{x}_N\|) \end{bmatrix}. \quad (2.22)$$

As we did with TOA, we can assume that ϵ_{RSS} is a zero-mean Gaussian distributed random variable; hence, $\mathbf{z}_{\text{RSS}} \sim \mathcal{N}(\mathbf{p}, \text{diag}(\sigma_{\text{RSS},1}^2, \sigma_{\text{RSS},2}^2, \dots, \sigma_{\text{RSS},N}^2))$.

Finally, after obtaining the Jacobian matrix of $\mathbf{h}_{\text{RSS}}(\mathbf{x})$ in Eq. (2.23), we can calculate the FIM in Eq. (2.24). We make again the simplification of considering that all variances are equal:

$$\sigma_{\text{RSS},1} = \sigma_{\text{RSS},2} = \dots = \sigma_{\text{RSS},N} = \sigma_{\text{RSS}}.$$

$$\frac{\partial \mathbf{h}_{\text{RSS}}(\mathbf{x})}{\partial^T \mathbf{x}} = -\alpha \begin{bmatrix} \frac{x-x_1}{\|\mathbf{x}-\mathbf{x}_1\|^2} & \frac{y-y_1}{\|\mathbf{x}-\mathbf{x}_1\|^2} \\ \frac{x-x_2}{\|\mathbf{x}-\mathbf{x}_2\|^2} & \frac{y-y_2}{\|\mathbf{x}-\mathbf{x}_2\|^2} \\ \vdots & \vdots \\ \frac{x-x_N}{\|\mathbf{x}-\mathbf{x}_N\|^2} & \frac{y-y_N}{\|\mathbf{x}-\mathbf{x}_N\|^2} \end{bmatrix} = -\alpha \begin{bmatrix} \frac{\sin(\phi_1)}{d_1} & \frac{\cos(\phi_1)}{d_1} \\ \frac{\sin(\phi_2)}{d_2} & \frac{\cos(\phi_2)}{d_2} \\ \vdots & \vdots \\ \frac{\sin(\phi_N)}{d_N} & \frac{\cos(\phi_N)}{d_N} \end{bmatrix}. \quad (2.23)$$

$$\mathcal{I}_{\text{RSS}}(\mathbf{x}) = \frac{1}{\sigma_{\text{RSS}}^2} \sum_{i=1}^N \frac{\partial h_i}{\partial \mathbf{x}} \left(\frac{\partial h_i}{\partial \mathbf{x}} \right)^T = \frac{\alpha^2}{\sigma_{\text{RSS}}^2} \sum_{i=1}^N \frac{1}{d_i^2} \begin{bmatrix} \sin^2(\phi_i) & \frac{\sin(2\phi_i)}{2} \\ \frac{\sin(2\phi_i)}{2} & \cos^2(\phi_i) \end{bmatrix} \quad (2.24)$$

As can be seen in Eq. (2.24), each measurement contributes again as an element of a sum.

2.1.5 AOA

AOA also appears in literature as DOA [Elkachouchi and Mofeed, 2005] and bearing [Eren et al., 2006]. The angle of the emitted source signal observed at a receiver is the AOA. We can draw a line of bearing from this angle for every receiver, the intersection of these lines of bearing provides the position of the target. As can be seen in Fig. 2.4, the arrival angle at the i th sensor can be expressed as $\tan(\phi_i) = \frac{x-x_i}{y-y_i}$. When measurement errors are present, we can model the AOA measurements as

$$\mathbf{z}_{\text{AOA}} = \mathbf{h}_{\text{AOA}}(\mathbf{x}) + \boldsymbol{\epsilon}_{\text{AOA}}. \quad (2.25)$$

Where

$$\mathbf{z}_{\text{AOA}} = [z_{\text{AOA},1}, z_{\text{AOA},2}, \dots, z_{\text{AOA},N}]^T, \quad (2.26)$$

$$\boldsymbol{\epsilon}_{\text{AOA}} = [\epsilon_{\text{AOA},1}, \epsilon_{\text{AOA},2}, \dots, \epsilon_{\text{AOA},N}]^T, \quad (2.27)$$

and

$$\mathbf{h}_{\text{AOA}}(\mathbf{x}) = \boldsymbol{\phi} = \begin{bmatrix} \tan^{-1}\left(\frac{x-x_1}{y-y_1}\right) \\ \tan^{-1}\left(\frac{x-x_2}{y-y_2}\right) \\ \vdots \\ \tan^{-1}\left(\frac{x-x_N}{y-y_N}\right) \end{bmatrix}. \quad (2.28)$$

We assume once again that the deviations are independent zero-mean Gaussian distributed random variables, so we have $\mathbf{z}_{\text{AOA}} \sim \mathcal{N}\left(\boldsymbol{\phi}, \text{diag}\left(\sigma_{\text{AOA},1}^2, \sigma_{\text{AOA},2}^2, \dots, \sigma_{\text{AOA},N}^2\right)\right)$.

Finally, we calculate the Jacobian matrix and the FIM as usual:

$$\frac{\partial \mathbf{h}_{\text{AOA}}(\mathbf{x})}{\partial^T \mathbf{x}} = \begin{bmatrix} \frac{y-y_1}{\|\mathbf{x}-\mathbf{x}_1\|^2} & -\frac{x-x_1}{\|\mathbf{x}-\mathbf{x}_1\|^2} \\ \frac{y-y_2}{\|\mathbf{x}-\mathbf{x}_2\|^2} & -\frac{x-x_2}{\|\mathbf{x}-\mathbf{x}_2\|^2} \\ \vdots & \vdots \\ \frac{y-y_N}{\|\mathbf{x}-\mathbf{x}_N\|^2} & -\frac{x-x_N}{\|\mathbf{x}-\mathbf{x}_N\|^2} \end{bmatrix} = \begin{bmatrix} \frac{\cos(\phi_1)}{d_1} & -\frac{\sin(\phi_1)}{d_1} \\ \frac{\cos(\phi_2)}{d_2} & -\frac{\sin(\phi_2)}{d_2} \\ \vdots & \vdots \\ \frac{\cos(\phi_N)}{d_N} & -\frac{\sin(\phi_N)}{d_N} \end{bmatrix}. \quad (2.29)$$

$$\mathcal{I}_{\text{AOA}}(\mathbf{x}) = \frac{1}{\sigma_{\text{AOA}}^2} \sum_{i=1}^N \frac{\partial h_i}{\partial \mathbf{x}} \left(\frac{\partial h_i}{\partial \mathbf{x}} \right)^T = \frac{1}{\sigma_{\text{AOA}}^2} \sum_{i=1}^N \frac{1}{d_i^2} \begin{bmatrix} \cos^2(\phi_i) & -\frac{\sin(2\phi_i)}{2} \\ -\frac{\sin(2\phi_i)}{2} & \sin^2(\phi_i) \end{bmatrix} \quad (2.30)$$

We have again assumed that the variances of different measurements are equal.

RSS usually provides the lowest accuracy, but its implementation is simple and cheaper, since LOS and synchronization are not a requirement. AOA requires smart antennas, but it does not require synchronization and only two receivers are needed to locate a source. Both TDOA and TOA require LOS conditions, but the accuracy is high. However, a full synchronization is required with TOA, whereas TDOA does not need that the source is synchronized with the receivers.

To summarize, we can unify the expressions of the FIM of TOA, RSS, and AOA as it was done in [Zhao et al., 2013]. Even without the assumption that the variances of the measurements are not equal, the FIM can be written as a sum of the products of a coefficient and a matrix for each sensor: $\mathcal{I} = \sum_{i=1}^N \gamma_i \mathbf{G}_i$, where

$$\mathbf{G}_{\text{TOA},i} = \mathbf{G}_{\text{RSS},i} = \begin{bmatrix} \sin^2(\phi_i) & \frac{\sin(2\phi_i)}{2} \\ \frac{\sin(2\phi_i)}{2} & \cos^2(\phi_i) \end{bmatrix}, \quad (2.31)$$

$$\mathbf{G}_{\text{AOA},i} = \begin{bmatrix} \cos^2(\phi_i) & -\frac{\sin(2\phi_i)}{2} \\ -\frac{\sin(2\phi_i)}{2} & \sin^2(\phi_i) \end{bmatrix}, \quad (2.32)$$

$$\gamma_{\text{TOA},i} = \frac{1}{\sigma_{\text{TOA},i}^2}, \quad (2.33)$$

$$\gamma_{\text{RSS},i} = \frac{\alpha^2}{\sigma_{\text{RSS},i}^2 d_i^2}, \quad (2.34)$$

and

$$\gamma_{\text{AOA},i} = \frac{1}{\sigma_{\text{AOA},i}^2 d_i^2}. \quad (2.35)$$

Some contributions reviewed in the next section leverage this expression of the FIM. However, we cannot apply it to range-difference methods and we just calculate the FIM with Eq. (2.2).

2.2 Sensor placement techniques

Sensor placement is an important task in the design of indoor positioning systems, since the amount of sensors and their location affect the accuracy and the cost of the whole system. The major contributions to the accuracy of a range-based positioning system are the quality of the measurements, the target-anchor geometry, and the estimation algorithm. We assume that we will use an efficient estimator — i.e., the estimator attains the CRLB — for computing the estimated position; hence, we can optimize the performance limit of the system without restricting ourselves to a single algorithm. We can easily see the effect of the uncertainty of the measurements and the geometry when we look at the intersection of the circles, hyperbolae, or lines of bearing. A good geometry provides an orthogonal intersection that minimizes the propagation of the measurement uncertainties to the position estimation error [Kaune, 2012]. This propagation of the uncertainty is known as dilution of precision (DOP) [Langley, 1999]. DOP is usually split in other metrics like horizontal dilution of precision (HDOP), vertical dilution of precision (VDOP), position dilution of precision (PDOP), time dilution of precision (TDOP),

and geometric dilution of precision (GDOP). They share the following relations:

$$\text{PDOP} = \sqrt{\text{HDOP}^2 + \text{VDOP}^2}, \quad (2.36)$$

$$\text{GDOP} = \sqrt{\text{PDOP}^2 + \text{TDOP}^2}. \quad (2.37)$$

When we are performing 2D positioning, VDOP does not exist. Hence, HDOP and PDOP have the same value. Even though GDOP also contains time information, it is frequently used in literature as PDOP in both 2D and 3D positioning systems. Informally speaking, DOP is a dimensionless number defined as the ratio between the uncertainty of the position and the uncertainty of the measurements:

$$\text{DOP} = \frac{\Delta(\text{Target position})}{\Delta(\text{Measurement})}. \quad (2.38)$$

The following figures make it simple to appreciate the effect of DOP in hyperbolic trilateration. The red solid lines intersect in the true position of the target, whereas the grey dashed lines represent the effect of the noise in the range-difference measurements. The green area is the zone where the system can detect the target position due to the presence of noise. In the absence of noise, both configurations of Figs. 2.5 and 2.6 provide the true solution. We can see

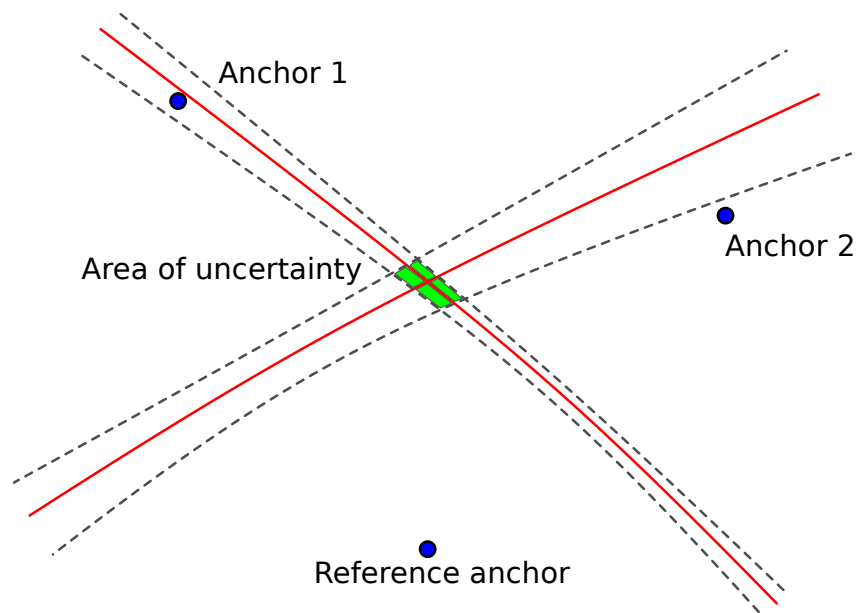


Figure 2.5: Target uncertainty area with good geometry between target and anchors

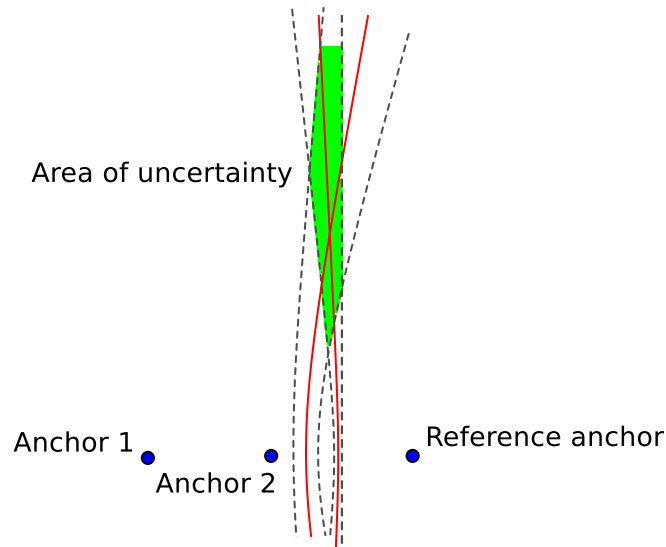


Figure 2.6: High dilution of precision due to bad geometry

that the area of uncertainty when the noise is present in a good sensor deployment is still very small. However, in the bad configuration of Fig. 2.6 even the slight deviation produces a big area where the position of the target can be estimated.

[Bronk and Stefanski, 2007] show the influence of geometric configuration in TDOA systems. They also propose two ways of overcoming such a situation. Placing another measurement unit in a good position reduces the GDOP considerably. In case we cannot afford to deploy a new sensor, their proposal involves the use of a hybrid positioning system with the current sensors such as the combination of TDOA and AOA. Even though the CRLB is usually used to find good configurations of sensors for localization, we will see in the next paragraphs that there are researchers who consider the GDOP as well.

2.2.1 Single target localization

The CRLB, which is computed with the inverse of the FIM, is the minimum variance attainable with an unbiased estimator — in this case the estimator is said to be efficient. Much has been written on the subject of finding geometries that optimize a metric of the CRLB or FIM. [Abel, 1990] uses a geometric interpretation of the CRLB to place sensors along a linear array. This work was able to replicate the results achieved in [Carter, 1977] without extensive algebraic manipulation, computer-aided maximization, or the consideration of a particular estimator. [Levanon, 2000] finds the lowest GDOP considering absolute ranges, pseudo-ranges, and bearing. He simplifies the problem assuming constant variances in the error of the measurements. In this case the GDOP is proportional to the CRLB obtained with Gaussian measurements [Chaffee and Abel, 1994]. Assuming a constant variance σ^2 of the measurements, $\Sigma = \sigma^2 \mathbf{I}$, where \mathbf{I}

is the identity matrix. The CRLB is given by the inverse of Eq. (2.2):

$$(\mathcal{I}(\mathbf{x}))^{-1} = \left(\left(\frac{\partial \mathbf{h}}{\partial \mathbf{x}^T} \right)^T \boldsymbol{\Sigma}^{-1} \frac{\partial \mathbf{h}}{\partial \mathbf{x}^T} \right)^{-1} = \sigma^2 \left(\left(\frac{\partial \mathbf{h}}{\partial \mathbf{x}^T} \right)^T \frac{\partial \mathbf{h}}{\partial \mathbf{x}^T} \right)^{-1}. \quad (2.39)$$

If we use this expression as the uncertainty of the target position estimation, we can calculate the DOP from Eq. (2.38) using σ^2 as the uncertainty of the measurements:

$$\text{DOP} = \frac{\sigma^2 \left(\left(\frac{\partial \mathbf{h}}{\partial \mathbf{x}^T} \right)^T \frac{\partial \mathbf{h}}{\partial \mathbf{x}^T} \right)^{-1}}{\sigma^2} = \left(\left(\frac{\partial \mathbf{h}}{\partial \mathbf{x}^T} \right)^T \frac{\partial \mathbf{h}}{\partial \mathbf{x}^T} \right)^{-1}. \quad (2.40)$$

We can also write it as $\text{DOP} = \frac{1}{\sigma^2} \text{CRLB}$. The assumption of the constant variances implies that the CRLB depends only on the anchors-target geometry. Then, he determines the lowest GDOP using N anchors and shows that it is found in the center of the corresponding regular polygon whose vertices are the anchors. [Zhang, 1995] minimizes the joint covariance matrix, which is the same than minimizing the CRLB. Each measurement provides an uncertainty ellipse, and the combination of N ellipses results in another ellipse, which should be as small as possible. He proposes an iterative method that solves the problem in $N - 3$ iterations. Even though he considers that the covariance of different sensors can be different, the ellipses are only sensitive to the orientation of the sensors with respect to the object been observed. Another work [Yang and Scheuing, 2005] deals with optimum sensor arrays for TDOA localization and derives sufficient conditions to achieve a minimum CRLB. Again, the system is oversimplified with constant and even uncorrelated noise variances. [Lui and So, 2009] reach to the same conclusions considering correlated variances; i.e., uniform angular arrays provide the best geometry. [Martínez and Bullo, 2006] provide closed-form expressions for the determinant of the FIM in 2D and 3D scenarios and analyze the set of points that yields global optima in the 2D case. They use the Extended Kalman Filter to track a moving target and consider moving sensors as well. The equation for updating the covariance matrix in Kalman Filter can be written as

$$P_{k+1,k+1}^{-1} = P_{k+1,k}^{-1} + \left(\frac{\partial \mathbf{h}(\mathbf{x}_{k+1})}{\partial \mathbf{x}_{k+1}^T} \right)^T \boldsymbol{\Sigma}^{-1} \frac{\partial \mathbf{h}(\mathbf{x}_{k+1})}{\partial \mathbf{x}_{k+1}^T}. \quad (2.41)$$

The prior and posterior covariances are denoted by $P_{k+1,k}$ and $P_{k+1,k+1}$, respectively. The term of the right is the usual FIM. They show that, as expected, maximizing the FIM improves the performance of the filter. They optimize only the non-random static parameter, instead of considering the previous states as well. The same metric is considered in [Bishop et al., 2010] to minimize the volume of the uncertainty ellipsoid for range, TOA [Bishop et al., 2007b], and bearing [Bishop et al., 2007a] localization under the assumption of a constant noise variance which is equal for all the sensors. An interesting result of this work and the previous one is the

upper bound of the determinant of FIM for 2D range-only positioning with N anchors whose variances are equal and constant σ :

$$\max |\mathcal{I}| = \frac{N^2}{4\sigma^4}. \quad (2.42)$$

A similar approach is discussed in [Dogancay and Hmam, 2009] for TDOA considering both equal and unequal variances, though constant. They conclude that considering unequal variances requires numerical methods for solving the problem. They also prove that, considering constant and equal variances, the upper bound of the determinant of the FIM is the same that appears in Eq. (2.42). [Meng et al., 2013] study the same problem when using combinations of different types of sensors. Recently, the same authors study in [Meng et al., 2016] optimal sensor geometries for TDOA positioning considering both a single reference and individual pairs of sensors. They also deal with the prior uncertainty of the location of the target. The metrics they use are the traces of CRLB and posterior covariance matrix. Most of these approaches consider sensor placement to improve the localization of a known source. On the other hand, [Isaacs et al., 2009] consider an uncertain target location in a TDOA problem. They conclude that the sensor-target range affects the localization performance and they find that arrays of sensors with the same angular separation provide the best geometries. [Ho and Vicente, 2008] study the problem when the target is distant and find good geometries with the shape of rings and sensors in the center. [Zhao et al., 2013] apply frame theory to sensor placement in 2D and 3D spaces and get necessary and sufficient conditions for optimal sensor placement. The results they get for 2D sensor placement are similar to those obtained by previous authors. Additionally, they unify the treatment of range-only, RSS, and AOA methods. Frame theory should be applied in systems where redundancy is a must. In sensor placement we talk about redundancy when we are using more sensors than those that are needed for localization, i.e., a higher number of sensors than the dimension of the problem. To know more about Frame theory the reader is referred to [Kovacevic and Chebira, 2007a] and [Kovacevic and Chebira, 2007b]. To deal with measurements whose noises are distance-dependent such as in underwater positioning, [Fang et al., 2016] introduce a parameter in the measurement model. They maximize the determinant of the full FIM and they also consider the case where the distances between sensors and target are fixed. Finally, [Liang and Jia, 2016] place a heterogeneous sensor network — at least two sensors of a different type — in a constrained space and consider that the noises of RSS, range-only, and AOA measurements are distance-dependent. They maximize the determinant of the FIM.

2.2.2 Multiple targets localization, area coverage

The studies described above focus on the localization of a single source, whereas in a more realistic situation we are interested in placing the sensors to cover an area. [Moreno-Salinas et al., 2013] extend the work of [Martínez and Bullo, 2006; Bishop et al., 2010; Isaacs et al., 2009] to multiple targets. They use numerical methods to maximize the sum of the logarithms of the FIMs of each target and obtain values very close to the theoretical optimum. [Chen et al., 2006] derive an upper bound of the localization error of the linear least squares algorithm and propose an iterative search algorithm to determine the optimum sensor placement. They apply their proposal to simple, regular areas and find that simple geometries like triangles and squares which enclosed other simple geometries are the optimum deployments. They focus on RSS and TOA. [Neering et al., 2007] compute the CRLB of several grid points of the ROI as candidates for the target position and minimize a weighted sum using a gradient descent method. The weights allow us to give priorities to some positions of the area. [Jourdan and Roy, 2008] present an iterative coordinate descent method that places sensors to minimize the position error bound, which is a metric introduced in [Jourdan et al., 2008] computing the square root of the trace of the CRLB. They consider very realistic scenarios but the amount of sensors is fixed and their positions are constrained to lie on boundaries. In addition, they only optimize one criterion. [Perez-Ramirez et al., 2013] find the optimization of an averaged metric over a grid to have the problem of hiding spots with poor localization performance. Their proposal involves the minimization of the minimum Fisher information matrix — the worst case — with an iterative method. The error model under consideration is distance-dependent and they deal with a 3D scenario. Additionally, they consider the use of heterogeneous sensors and the placement of sensors in an area where there are other fixed sensors. However, they minimize a single objective such as the volume of the error ellipsoid, which does not provide information about the shape of the error ellipsoids. Their approach deals only with a fixed number of sensors.

Some researchers have also applied a genetic algorithm (GA) to the sensor placement problem. [Ray and Mahajan, 2002] use a GA to get deployment patterns of a TDOA system that avoid singularities. They formulate the problem and linearize it, their goal is to avoid situations where a matrix that must be inverted is singular. This situation happens when there are two observations that provide the same information. [Roa et al., 2005] also use a GA, which was later improved in [Roa et al., 2006], to solve the sensor placement problem. They build an utility function that evaluates DOP, cost, and areas of poor precision or with singularities. The DOP and the unavailable areas can be weighted to change priorities in the function, whereas

the cost of the system is determined by the number of anchors. This algorithm is then outperformed by some of the same authors using a diversified local search [Laguna et al., 2009]. This work considers a variation of the weights of the cost function in order to generate a Pareto front (PF). In addition, they start optimizing the deployment of a given number of sensors until they find an optimum solution. From this solution, they remove the sensor whose contribution is the lowest and perform the optimization process again so that the optimum placement for different number of sensors is obtained. Another work [Roa et al., 2007] shows the improvement of the solutions attainable by this algorithm over the placement of regular lattices with the shapes of squares and triangles. The study is carried out considering spherical and hyperbolic trilateration. Other authors [Leune et al., 2013] place sensors in complex environments considering obstacles with a GA that optimizes the DOP. He includes mutation operations that can add or remove a sensor from a set. The trace of the covariance of the estimation is used in [Burke and Bos, 2011] for range-only sensor deployment with a simplex method [Nelder and Mead, 1965]. This work considers obstacles that can cause NLOS conditions. They also propose to use the uncertainty map that results from the evaluation of the objective over the ROI for path planning, defining low uncertainty routes. Penalties for uncovered and overcovered zones are introduced to a cost function that evaluates the DOP of an RSS system in [Kammoun et al., 2014]. They use simulated annealing [Kirkpatrick et al., 1983] to find the optimal placement.

2.2.3 Sensor selection techniques

Recent approaches solve the sensor placement problem with sensor selection and convex optimization. [Joshi and Boyd, 2009] propose an heuristic for selecting a subset of sensors out of a higher number of candidates for linear measurement models. [Chepuri and Leus, 2015] deal with the same problem considering non-linear measurement models with independent observations. They use the additive property of FIM for independent measurements and place sensors so that a predefined accuracy is achieved with a given probability. Their approach involves sparse sensing, introducing a boolean vector \mathbf{w} of size N whose elements $w_i = \{0, 1\}$ multiply the contribution of each sensor to the FIM. Using the expression we provided at the end of section 2.1 with this new selection vector:

$$\mathcal{I} = \sum_{i=1}^N w_i \gamma_i \mathbf{G}_i = \sum_{i=1}^N w_i \mathcal{I}_i, \quad (2.43)$$

where only the sensors whose corresponding weight in the selection vector \mathbf{w} is 1 will be active. The goal is to keep the number of one elements of \mathbf{w} , which is the ℓ_0 norm, as low as possible while keeping the amount of information of the resulting FIM above a predefined threshold. This problem is not convex and the ℓ_0 norm is relaxed to the ℓ_1 norm, which is a sum of the

absolute values of the elements of the vector. The constraint $w_i = \{0, 1\}$ is also relaxed to $w_i = [0, 1]$.

Another approach involves leveraging the submodular property of some performance metrics [Krause et al., 2008]. The concept of submodularity means that when adding an element e to a subset S of a given set \mathcal{U} , we obtain a higher increment over a function Φ when this function is evaluated for the smaller set S than for the bigger \mathcal{U} . This function Φ is said to be submodular.

$$\forall S, \mathcal{U}; S \subseteq \mathcal{U}; \forall e \notin \mathcal{U}; (\Phi(S \cup e) - \Phi(S)) \geq (\Phi(\mathcal{U} \cup e) - \Phi(\mathcal{U})) \quad (2.44)$$

The advantage of optimizing a submodular function is the availability of simple algorithms which are near-optimal. On the other hand, we must find metrics related to the accuracy of the position estimation that are submodular, some of them are presented in [Ranieri et al., 2014], whereas [Jawaid and Smith, 2015] show that usual metrics such as the trace, determinant, or maximum eigenvalue of the covariance matrix are not generally submodular. They also provide sufficient conditions so that the estimation error is a submodular function. [Shamaiah et al., 2010] use a greedy algorithm for solving the sensor placement problem in a linear dynamical system. Their work shows that the greedy algorithm outperforms convex relaxation in both accuracy and computation time. As for non-linear models, [Rao et al., 2015] linearize the range-only problem and use a greedy algorithm to optimize two submodular functions.

2.3 Conclusions

According to the number of reviewed contributions, especially since the beginning of the last decade, sensor placement for localization is currently a trending topic. It has been studied in different fields like signal processing, control theory, communication theory, expert systems, etc. Even in the past year, there are articles in top journals that just compare random deployment with regular patterns to highlight the importance of sensor placement [Han et al., 2015]. Hence, we consider that the timeliness of this thesis is quite good.

First, we have reviewed some algebraic methods that have a strong importance, both theoretical and practical. They allow us to determine which aspects and how they can influence in the accuracy of the estimation regarding sensor deployment. However, such a study requires many simplifications that make it useless in practical applications. Additionally, if we read those papers in a chronological order we can see that they reach the same conclusion over and over again, repeating the classic solution of a regular polygon enclosing the target throughout different approaches with minor contributions.

The latest proposals that can be found in literature still have some shortcomings that we aim to solve in this thesis. For example, to the best of our knowledge, there is not any author that exploits different metrics from the estimation error. All of them optimize a single metric of the error ellipsoids that does not provide any hint about the actual confidence ellipsoids and their shape or orientation. Moreover, these metrics can hide some undesired characteristics like an elongation along the major axis. Another aspect barely addressed is the use of placements with a given number of anchors to determine other deployment schemes with more or less anchors. This approach was taken by [Laguna et al., 2009]; however, they only deal with it when decreasing the number of sensors of an optimum solution. [Leune et al., 2013] use mutations in a GA that can add or remove a sensor to a given set randomly. This random addition or deletion means that we will obtain a solution far from the optimum most of the time. On the contrary, we propose to place or remove a sensor after analyzing the coverage and saturation of the ROI. These two issues will be discussed in the following chapters.

Finally, we would like to conclude this chapter highlighting that none of the contributions on sensor placement for localization in a ROI address the same problem. Most of them consider range-only measurements and use numerical methods. Since we must use numerical methods and we want to perform MOO, we have chosen to use the (arguably) most used algorithm, which is non-dominated sorting genetic algorithm (NSGA-II) [Deb et al., 2002]. We will use it during Chapter 4 without modifications and we will just include our evaluation functions. However, we will propose some modifications in Chapter 5.

Chapter 3

Problem statement

After having acknowledged the strengths and weaknesses of different sensor placement techniques existing in literature, this section focuses on an exposition of our particular problem of hyperbolic trilateration with infrared measurements. This thesis started from previous work of the research group whose major concerns for the present work are recalled here. As the reader can probably guess from the previous chapter, we need a model of the error of the range-difference distances to compute the final error of the position estimation. We show a simple calculation of the distance measurement error based on the computation of the signal-to-noise ratio (SNR) at the output of the sensors in Section 3.1. Two estimators based on nonlinear least squares (NLS) are shown on Section 3.2 for solving the range-difference of arrival (RDOA) problem. The most important part of this chapter involves obtaining an expression of the accuracy of the estimation, which is the content of Section 3.3. Finally, Section 3.4 provides a summary of the problems we aim to overcome and gives a short description of our proposal, which is detailed in the following chapters.

3.1 A simple model of the infrared measurement

The final distance measurement is mostly affected by the parameters of the emitter, receiver, and subsequent conditioning stages. Modeling the infrared signal is out of the scope of this work; hence, this section provides a simple calculation of the SNR at the output of the conditioning stage. A description of the system can be found in a PhD thesis from our research group [Martin-Gorostiza, 2011]. [Gorostiza et al., 2011] describe the hardware, whereas an overview of the whole system is also given in [Martin-Gorostiza et al., 2014].

The system achieves the RDOA principle by measuring phase differences of a modulated infrared signal emitted by a mobile target and recorded continuously by receivers (anchors) at

fixed and known positions. The infrared emitter uses a wide angle IR-LED at 940 nm, intensity modulated at 8 MHz, in order to generate the measurement signal. The receivers, placed at the ceiling of the coverage area, are formed by a low level conditioning stage adapting the photocurrent generated by a wide angle silicon PIN photodiode. The outputs of the receivers are simultaneously digitized and RDOA measurements are estimated from the resulting sequences.

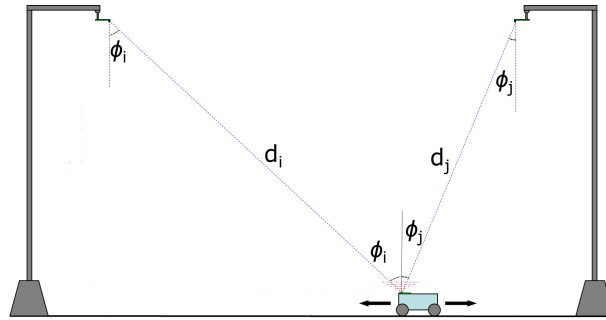


Figure 3.1: Infrared emitter-sensor link

The optical power P_o reaching an arbitrary receiver is given by the emitted power and the solid angle of the emission covered by the receiver photodiode sensitive area as expressed in Eq. (3.1):

$$P_o = \frac{I_e}{d^2} \pi \left(\frac{D}{2} \right)^2 \cos^2(\phi), \quad (3.1)$$

where I_e is the emitted optical power per solid angle in the direction normal to the emitter surface, D is the receiver photodiode sensitive area diameter, d is the Euclidean distance between emitter and receiver and ϕ is the line-of-sight angle to the vertical direction representing the decay on both emitter and receiver effective areas due to disorientation (see Fig. 3.1). The received optical power generates a proportional photocurrent which is converted into a voltage and conditioned in the receivers. The output voltage V_o of an arbitrary receiver is defined as:

$$V_o = P_o \mathcal{R} G_{V/I} G_{VV}, \quad (3.2)$$

where \mathcal{R} is the responsivity of the photodiode, $G_{V/I}$ is the transimpedance amplifier gain at the modulation frequency and G_{VV} is the total voltage gain of subsequent conditioning stages.

The output SNR of a receiver, shown in Eq. (3.3), is defined by the output signal power and the total noise contributions of the infrared link, dominated by the noise added in the transimpedance amplifier, hence uncorrelated between different receivers.

$$\text{SNR} = \frac{\frac{V_o^2}{2}}{N_0 B_n}. \quad (3.3)$$

N_0 is the total noise spectral density around the modulation frequency, considered to be flat given the narrow band where the final estimation is carried out, and B_n is the noise equivalent bandwidth defined by the final filtering stage around the band of interest.

The variance of each receiver single-phase estimation is inversely proportional to its output SNR, yielding a typical standard deviation σ_ϕ of the single-phase measurement:

$$\sigma_\phi \simeq \frac{\gamma}{\sqrt{\text{SNR}}}, \quad (3.4)$$

where γ is a scale factor and during simulations $\gamma = 1$. σ_ϕ can easily be converted into a distance standard deviation (σ_d) considering the emitted signal modulation wavelength which can be expressed with sufficient accuracy for the current purpose using the modulation frequency f_m and the approximate propagation speed $c = 3 \cdot 10^8$ m/s.

$$\sigma_d = \sigma_\phi \frac{c}{2\pi f_m}. \quad (3.5)$$

Table 3.1 shows the numerical values of our real IR-based positioning system, as needed for Eqs. (3.1) to (3.5).

Table 3.1: System parameters

	Parameter	Symbol	Value	Units
Emitter	Intensity	I_e	50	$\frac{\text{W}}{\text{sr}}$
	Frequency	f_m	8	MHz
Receiver	Diameter	D	5.08	mm
	Responsivity	\mathcal{R}	0.64	$\frac{\text{A}}{\text{W}}$
	I to V gain	$G_{V/I}$	$\frac{33}{\sqrt{2}}$	k Ω
	Total voltage gain	G_{VV}	100	–
	Noise equivalent bandwidth	B_n	$30 \cdot \frac{\pi}{2}$	Hz
	Noise spectral density	N_0	$1.34 \cdot 10^{-11}$	$\frac{\text{W}}{\text{Hz}}$

Finally, we can calculate σ_d for each sensor with Eq. (3.5) to determine the covariance matrix of the RDOA observations.

3.2 Target localization with RDOA

In this section, we formulate again the hyperbolic trilateration problem as an RDOA problem. This time, we specify our infrared system in 3D in a more rigorously way.

Let $\mathbf{x} \in \mathbb{R}^3$ be the unknown position of the target and $\mathbf{x}_i \in \mathbb{R}^3$ the coordinates of the i th sensor, where i takes values from 1 to N . Without loss of generality, we assume that the first sensor is the reference. Pairing the first sensor with the other $N - 1$ sensors and differencing their measurements provide us with $N - 1$ RDOA observations \mathbf{z} . The function $h_{i,1} : \mathbb{R}^3 \rightarrow \mathbb{R}$ takes as input the coordinates of the target and produces as output the difference of distances of target-sensor and target-reference. Assuming additive Gaussian noise, we model the RDOA measurement of the i th, where i cannot be 1, and reference sensors as

$$z_{i,1} = h_{i,1}(\mathbf{x}) + \epsilon_{i,1} = \|\mathbf{x} - \mathbf{x}_i\| - \|\mathbf{x} - \mathbf{x}_1\| + \epsilon_{i,1}, \quad (3.6)$$

where $\epsilon_{i,1} \sim \mathcal{N}(0, \sigma_i^2 + \sigma_1^2)$. Equation (3.5) is used to calculate the two variances. After acquiring the non-redundant set of $N - 1$ measurements we can put the equation in its vector form:

$$\mathbf{h}_1 = [h_{2,1}(\mathbf{x}), h_{3,1}(\mathbf{x}), \dots, h_{N,1}(\mathbf{x})]^T, \quad (3.7)$$

$$\boldsymbol{\epsilon}_1 = [\epsilon_{2,1}, \epsilon_{3,1}, \dots, \epsilon_{N,1}]^T, \quad (3.8)$$

and

$$\mathbf{z}_1 = [z_{2,1}, z_{3,1}, \dots, z_{N,1}]^T. \quad (3.9)$$

The problem can be solved with NLS as in chapter five of [Martin-Gorostiza, 2011]. We have a data fitting problem where we try to minimize the difference between the observed values \mathbf{z}_1 and the computed values \mathbf{h}_1 to get an estimate $\hat{\mathbf{x}}$ of \mathbf{x} .

$$\arg \min_{\mathbf{x}} \left(\frac{1}{2} (\mathbf{z}_1 - \mathbf{h}_1(\mathbf{x}))^T (\mathbf{z}_1 - \mathbf{h}_1(\mathbf{x})) \right). \quad (3.10)$$

As we can see in Eq. (3.10), we optimize an euclidean distance. We can solve it using non-linear least squares algorithms or we can also linearize the problem. We will apply one of the former methods, which is the Gauss-Newton iterative algorithm. It does not require the computation of second derivatives, but we must provide a first estimated solution before iterating, which can lead to local minima. Equation (3.11) is the iterative Gauss-Newton algorithm for solving (3.10).

$$\hat{\mathbf{x}}^{k+1} = \hat{\mathbf{x}}^k + \left(\mathbf{J}_1^T \mathbf{J}_1 \right)^{-1} \mathbf{J}_1^T \left(\mathbf{z}_1 - \mathbf{h}_1(\hat{\mathbf{x}}^k) \right). \quad (3.11)$$

The iteration instant is denoted by k , \mathbf{J}_1 is the Jacobian matrix $\frac{\partial \mathbf{h}_1(\mathbf{x})}{\partial \mathbf{x}^T}$, and $\hat{\mathbf{x}}$ is the estimated solution. The algorithm takes usually two or three iterations to converge. We simplify the problem assuming that the height of the target is constant; hence the third element of \mathbf{x} is Z . This assumption implies that the dimension of \mathbf{J}_1 is $(N - 1) \times 2$:

$$\mathbf{J}_1 = \begin{bmatrix} \frac{x-x_2}{\|\mathbf{x}-\mathbf{x}_2\|} - \frac{x-x_1}{\|\mathbf{x}-\mathbf{x}_1\|} & \frac{y-y_2}{\|\mathbf{x}-\mathbf{x}_2\|} - \frac{y-y_1}{\|\mathbf{x}-\mathbf{x}_1\|} \\ \frac{x-x_3}{\|\mathbf{x}-\mathbf{x}_3\|} - \frac{x-x_1}{\|\mathbf{x}-\mathbf{x}_1\|} & \frac{y-y_3}{\|\mathbf{x}-\mathbf{x}_3\|} - \frac{y-y_1}{\|\mathbf{x}-\mathbf{x}_1\|} \\ \vdots & \vdots \\ \frac{x-x_N}{\|\mathbf{x}-\mathbf{x}_N\|} - \frac{x-x_1}{\|\mathbf{x}-\mathbf{x}_1\|} & \frac{y-y_N}{\|\mathbf{x}-\mathbf{x}_N\|} - \frac{y-y_1}{\|\mathbf{x}-\mathbf{x}_1\|} \end{bmatrix}. \quad (3.12)$$

As was expressed in Eq. (2.17), this function depends only on anchor-target geometry. Solving the problem with Eq. (3.11) provides a solution without considering the noise of the measurements. We can multiply the cost function of Eq. (3.10) by a weight matrix \mathbf{W} to take the reliability of each measurement into account, formulating the problem with weighted nonlinear least squares (WNLS):

$$\arg \min_{\mathbf{x}} \left(\frac{1}{2} (\mathbf{z}_1 - \mathbf{h}_1(\mathbf{x}))^T \mathbf{W} (\mathbf{z}_1 - \mathbf{h}_1(\mathbf{x})) \right). \quad (3.13)$$

When $\mathbf{W} = \boldsymbol{\Sigma}_1^{-1}$, the cost function of Eq. (3.13) is called a Mahalanobis distance. The covariance matrix $\boldsymbol{\Sigma}$ of RDOA is fully populated and takes the form:

$$\boldsymbol{\Sigma}_1 = \begin{bmatrix} \sigma_2^2 + \sigma_1^2 & \sigma_1^2 & \cdots & \sigma_1^2 \\ \sigma_1^2 & \sigma_3^2 + \sigma_1^2 & \ddots & \vdots \\ \vdots & \ddots & \ddots & \vdots \\ \sigma_1^2 & \cdots & \cdots & \sigma_N^2 + \sigma_1^2 \end{bmatrix}. \quad (3.14)$$

Finally, solving (3.13) with Gauss-Newton:

$$\hat{\mathbf{x}}^{k+1} = \hat{\mathbf{x}}^k + \left(\mathbf{J}_1^T \boldsymbol{\Sigma}_1^{-1} \mathbf{J}_1 \right)^{-1} \mathbf{J}_1^T \boldsymbol{\Sigma}_1^{-1} (\mathbf{z}_1 - \mathbf{h}_1(\hat{\mathbf{x}}^k)). \quad (3.15)$$

This method clearly relies on good observations, since measurement with a high error will not contribute to the estimation.

Estimating the target position with Eq. (3.15) is equivalent to the maximum likelihood estimator (MLE). As we have already assumed, $\mathbf{z}_1 \sim \mathcal{N}(\mathbf{h}_1, \boldsymbol{\Sigma}_1)$. Thus, the probability density function (PDF) of \mathbf{z}_1 given the unknown target position \mathbf{x} is [Torrieri, 1984]

$$p(\mathbf{z}_1 | \mathbf{x}) = \frac{1}{(2\pi)^{N-1} \sqrt{|\boldsymbol{\Sigma}_1|}} e^{-\frac{1}{2} (\mathbf{z}_1 - \mathbf{h}_1(\mathbf{x}))^T \boldsymbol{\Sigma}_1^{-1} (\mathbf{z}_1 - \mathbf{h}_1(\mathbf{x}))}. \quad (3.16)$$

The expression of the log-likelihood is

$$\ln(p(\mathbf{z}_1 | \mathbf{x})) = \ln \left(\frac{1}{(2\pi)^{N-1} \sqrt{|\boldsymbol{\Sigma}_1|}} \right) - \frac{1}{2} (\mathbf{z}_1 - \mathbf{h}_1(\mathbf{x}))^T \boldsymbol{\Sigma}_1^{-1} (\mathbf{z}_1 - \mathbf{h}_1(\mathbf{x})). \quad (3.17)$$

As can be seen, the first term is constant, whereas the second term is a function of \mathbf{x} . MLE maximizes Eq. (3.17), which is the same as minimizing the term of the right

$\frac{1}{2} (\mathbf{z}_1 - \mathbf{h}_1(\mathbf{x}))^T \boldsymbol{\Sigma}_1^{-1} (\mathbf{z}_1 - \mathbf{h}_1(\mathbf{x}))$. This expression is the same as Eq. (3.13). Thus, when the weight matrix of WNLS is the covariance, WNLS is equivalent to MLE.

A few remarks on these iterative estimation methods before specifying how we can evaluate the performance of target localization. The selection of the sensor which acts as the reference does not change the MLE solution. The proof can be found in Section 4.4.1 of [Wieser, 2001]. As we have already mentioned, these methods require an initial guess \mathbf{x}^0 . This initial solution can lead to local minima. This situation can be avoided if we use a close-form method that provides an initial solution whose accuracy is lower but it is near the actual value enough, such as the well known closed-form estimator given in [Chan and Ho, 1994].

3.3 Accuracy of the target localization

3.3.1 Position accuracy measures

We can evaluate the performance of target localization with a given configuration by running Monte Carlo iterations and analyzing the resulting set of solutions. In Chapter 5 of [Martin-Gorostiza, 2011], two metrics were used, namely, the root mean square error (RMSE) and the elliptical errors. The former is a circle that contains between the 63 and 68 % of the estimated solutions, whereas the latter are the standard deviations of the major and minor axes of the error ellipsoid. After getting the Monte Carlo solutions, a covariance matrix can be determined — not to be confused with the covariance matrix of the noise of the measurements $\boldsymbol{\Sigma}$. This covariance matrix represents an ellipse that encloses the estimated solutions [Smith and Cheeseman, 1986]. Applying singular value decomposition to the covariance matrix provides the singular values, which are proportional to the deviations of each axis of the ellipse. Such a study carried out in [Martin-Gorostiza, 2011] is not necessary; since the covariance matrix is symmetric and positive definite, its singular values and eigenvalues will be exactly the same.

There are many metrics related to the RMSE that can be used to show the accuracy of a positioning system. The reader can find a description and the relation between these measures in [Van Diggelen, 1998]. Some of the most common include the circular error probability (CEP), RMSE, and twice the distance root mean square (2DRMS). The RMSE is computed with the square root of the mean squared error (MSE). After having obtained M estimations $\hat{\mathbf{x}}_i$, where $i = 1, 2, \dots, M$, of a target position \mathbf{x} , we can compute the RMSE as

$$\text{RMSE} = \sqrt{\frac{1}{M} \sum_{i=1}^M ((\hat{\mathbf{x}}_i - \mathbf{x})^T (\hat{\mathbf{x}}_i - \mathbf{x}))}. \quad (3.18)$$

The CEP is a circle that encloses 50% of the estimates, whereas the 2DRMS contains between

95 and 98%. The latter is given by multiplying Eq. (3.18) by two:

$$2\text{DRMS} = 2\sqrt{\frac{1}{M} \sum_{i=1}^M \left((\hat{\mathbf{x}}_i - \mathbf{x})^T (\hat{\mathbf{x}}_i - \mathbf{x}) \right)}. \quad (3.19)$$

The elliptical form of the scatter graph of the M estimates determines the 95 – 98% variability of the 2DRMS.

3.3.2 A performance limit on the accuracy of a positioning system: the Cramér-Rao lower bound

The metrics we have shown in Section 3.3.1 are not useful to evaluate the performance of a given distribution of sensors. They depend on the estimator in use and we must evaluate a candidate target position several times — usually between 100 and 1000 times — to get a significant value of the accuracy. If we represent Eq. (3.16) as a function of the unknown parameter \mathbf{x} instead of \mathbf{z}_1 we have the likelihood function. Since this likelihood function is exponential we take the natural logarithm to remove the exponential function. The graphical representation of this likelihood function is the well known *bell curve* of a Gaussian distribution centered in the true value of \mathbf{x} . The *sharper* the curve is, the more accurate we can estimate the unknown parameter. To study the *sharpness* of the log-likelihood function, we use second derivatives. The minimum variance that any unbiased estimator can attain is given by the CRLB [Kay, 1993], which has already been mentioned, but not formally introduced:

$$\text{var}(\hat{\mathbf{x}}) \geq \frac{1}{-E \left[\frac{\partial^2 \ln p(\mathbf{z}_1; \mathbf{x})}{\partial \mathbf{x}^2} \right]} \quad (3.20)$$

If an estimator attains the CRLB, then it is of course a minimum variance unbiased estimator (MVUE). It is known that if the CRLB is attained, the MLE generally attains it. The denominator of Eq. (3.20) is the FIM $\mathcal{I}(\mathbf{x})$. Information has two important properties; namely, it is nonnegative and it is additive for independent observations. The latter means that additional observations may carry no information, so the CRLB will not decrease by adding more measurements.

The CRLB for the hyperbolic trilateration problem is given in [Chan and Ho, 1994]:

$$\mathcal{I}^{-1}(\mathbf{x}) = \left(\mathbf{J}_1^T \boldsymbol{\Sigma}_1^{-1} \mathbf{J}_1 \right)^{-1}. \quad (3.21)$$

As mentioned during the state of the art description, the CRLB depends only on the covariance of the noise of the measurements and the target-sensors geometry. It is expected that a set of sensors that yields a low CRLB will generally get a low MSE [Chepuri and Leus, 2015].

In the following chapters, we will obtain several metrics from Eq. (3.21) that will be used as objective functions to determine optimal sensor placements.

3.3.3 Preliminary accuracy studies

[Martin-Gorostiza, 2011] analyzes the performance of the infrared PDOA based IPS considering a 9 m^2 square room. Five sensors are deployed in the area, four of them in the corners and another one in the center. He tried NLS with Eq. (3.11) considering three kinds of subsets; namely, the full set, four sensors, and three sensors. As it was pointed out in [Burke and Bos, 2011], the addition of sensors reduce the performance of the unweighted least squares solution. The author of this thesis published some results of the study of this subset selection comparing NLS, MLE, and the CRLB in [Domingo-Perez et al., 2013]. Having deployed five sensors in the aforementioned configuration, we divide the ROI and choose a grid of points which are separated by 3 cm. We consider a small subset of points due to the symmetry of both room and deployment. Obviously, MLE provides the best results and almost attains CRLB. However, the statistic of the noise may not be available. Additionally, the computation cost of MLE is higher than that of NLS. Using an estimator that does not need to use the covariance of the noise could be desirable sometimes. Figure 3.2 shows some subset selection for NLS estimation without a great loss of performance.

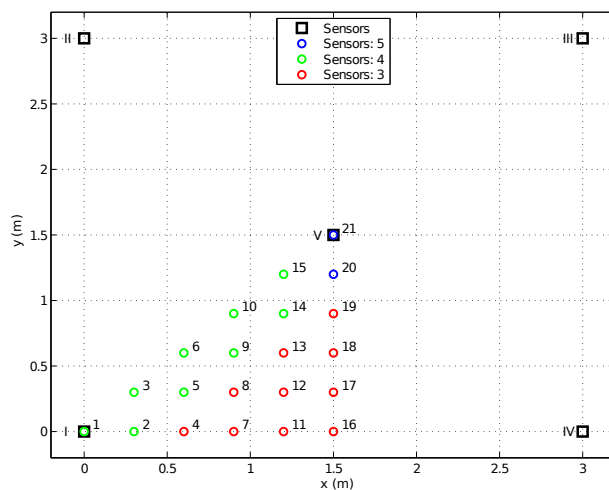


Figure 3.2: Five sensors deployed in the corners of a square and center. When using only four sensors — green dots —, sensor III is removed. The points estimated with three sensors do not consider sensor II neither. Sensor V is always the reference.

The following figures show the RMSE obtained with MLE and NLS computed with Eq. (3.18) after 5000 Monte Carlo runs. They are also compared with the square root of the trace of the CRLB, computed with Eq. (3.21). To have an indicator of the best accuracy any time, we always show the CRLB of the full set.

The test points in the x -axis must be checked with the corresponding point of Fig. 3.2. Figure 3.3 shows the location performance with five sensors. As can be seen, MLE almost

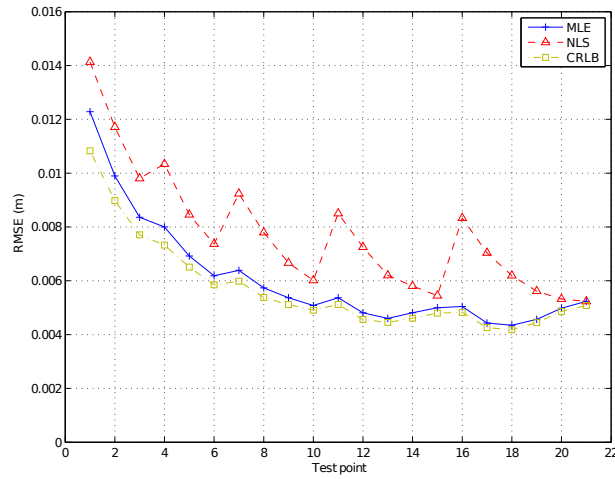


Figure 3.3: MLE vs NLS with five sensors.

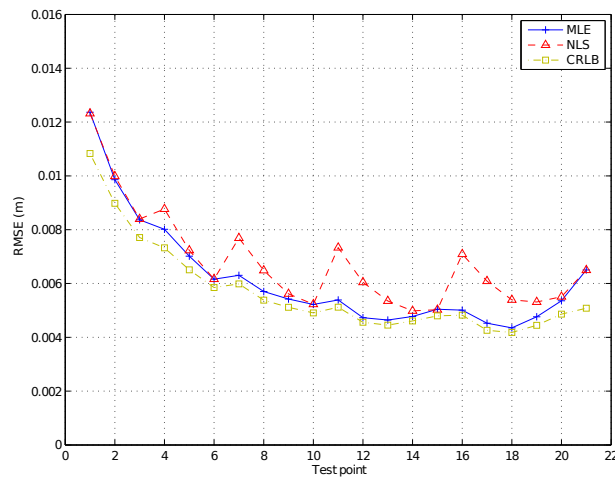


Figure 3.4: MLE vs NLS with four sensors. Sensor III unused.

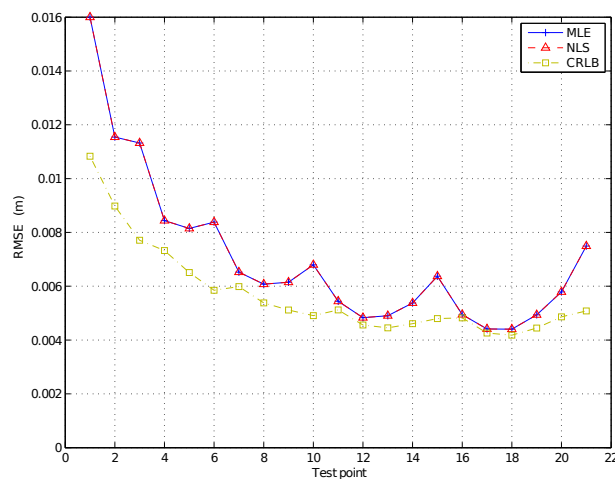


Figure 3.5: MLE vs NLS with three sensors. Sensors II and III unused.

attains CRLB, whereas the performance of NLS is significantly lower and it only attains CRLB in the central points.

Figure 3.4 shows the RMSE of both estimators after removing the furthest sensor (III). We can see that MLE stays almost the same as before. However, its performance has decreased in the central points. As for NLS, its RMSE values equal those of MLE in some points. The points that are still far from MLE results are those that are further from sensor II.

The last figure, Fig. 3.5, shows the accuracy of both estimators after removing sensors II and III. We can see that MLE matches NLS. This is obvious, since there are only two observations and both of them are taken equally into account regardless their weights. The estimation of the points which are further from sensors II and III still attains CRLB.

The point we want to make clear here is that we could place sensors so that the accuracy with NLS is improved. NLS considers that each observation has the same importance; i.e., it neglects the heteroscedasticity and the correlations. The covariance matrix of the measurements turns to be the identity matrix. If we represent the error ellipsoid we can see that in those positions whose CRLB is attained by NLS they are almost a circle — see chapter V of [Martin-Gorostiza, 2011]. We can try to deploy sensors so that the observations have the same variance and the correlations should be as small as possible, while keeping a high accuracy.

3.4 Summary and proposed solutions

We have introduced the positioning problem with an infrared PDOA IPS. After presenting two methods which differ in the consideration of the noise statistic, we have provided some preliminary results of accuracy with a given configuration. NLS has a lower computational cost than MLE, since the covariance matrix is not needed we do not compute, invert, and multiply it. Even though time can be critical in some positioning applications such as surveillance systems, this is not the only reason to avoid using the covariance matrix of the measurements. The statistic of the noise may not be available at all, and at the time of acquiring the measurements and performing localization we do not have information about the actual position of the target. Hence, we cannot remove any sensor before estimating.

Apart from the aforementioned problem, we have seen that current state-of-the-art placement methods consider only a single metric of the covariance matrix of the estimate. They usually maximize the determinant of the FIM or minimize the trace of the CRLB. These metrics do not provide any information about the error ellipsoids, and they can hide huge deviations in case of an elongation of the ellipsoids.

The first contribution of this thesis is a proposal of sensor placement with MOO considering several metrics related to the error ellipsoids simultaneously. It is presented in chapter 4. Some metrics are discussed and we use the well known multi-objective evolutionary algorithm

(MOEA) NSGA-II to determine the optimal sensor placement, which is a set of Pareto optimal solutions instead of a single solution. We show an application of these Pareto solutions to the problem discussed in the previous section. Additionally, we also provide a metric for the dynamic case that leverages the prior information of the position of the target. In this chapter we only consider the room that we have already exposed with a fixed number of sensors. Chapter 5 extends those results to a variable number of sensors. Instead of using NSGA-II directly as we do in Chapter 4, we propose some modifications to overcome some limitations of the algorithm. This chapter also considers room shapes with obstacles that cause occlusions due to NLOS situations. Hence, not only do we optimize the accuracy, but we also include the coverage as objective. Our results are shown along these two chapters, they are satisfactory and confirm the suitability of our methods for sensor placement.

Chapter 4

Sensor placement determination for target positioning using different performance measures of covariance matrix and multi-objective optimization

This chapter describes the first and main contribution of this thesis, which is the consideration of several metrics of the covariance of the estimation as objectives for sensor placement. Most important results were published in [Domingo-Perez et al., 2016b]. The chapter is organized as follows. Section 4.1 introduces the topic and details the contributions and differences with previous approaches. The performance measures of the covariance matrix we use are described in Section 4.2. Fundamentals of MOO and the MOEA we use to obtain our results are provided in Section 4.3. Some results are shown in Section 4.4. Section 4.5 obtains a metric for the dynamic case, where prior information of the state of the target is taken into account. Part of this study was published in [Domingo-Perez et al., 2015]. Finally, we draw conclusions in Section 4.6.

4.1 Introduction

Multi-objective optimization to provide the sensor resource manager with a decision support system has been used before in localization applications. This method obtains Pareto efficient solutions of the sensor placement problem for target localization. This proposal was also suggested by [Grasso et al., 2013], but they focus on area and tracking coverage instead of accuracy. [Laguna et al., 2009] apply Pareto optimality as well; however, they only use a very simple ac-

curacy metric — the DOP — that does not provide much information of the final accuracy. When we know more details — such as the noise statistics — about the positioning system, we can do better taking them into account.

We present an optimization of the positions of the sensors that involves dealing with several conflicting objectives, which are performance measures obtained from the covariance matrix of the estimate. Our approach includes the possibility of specifying different localization priorities for different zones. Another application presented in [Chiu and Lin, 2011] proposed the division of the ROI in zones with different priorities. However, their approach involves binary localization and the solutions they obtain are restricted to a grid. The solutions that we obtain are not restricted and they can be placed in any position of the ROI.

Our work presents a framework for sensor placement that avoid assuming the simplifications discussed in this section. Such simplifications involve:

- restricting the positions of the sensors to grid points,
- using simplified and easy to derive models of noise,
- focusing on a single target instead of optimizing the performance metrics for a whole area,
- applying a single optimization criterion.

The benefits of properly using a genetic algorithm allow us to overcome those issues. The chromosomes are the positions of the sensors represented as real numbers; therefore, we obtain a sensor placement in a continuous domain. We do not need to deal with derivatives of the objective functions, thus the objectives are only evaluated and they can be complex functions. By using such intractable functions we can consider fairly complex models, obtaining solutions that relate better to a real situation. We also propose two scalar metrics to consider a ROI instead of focusing on a single target. These scalar values are the average error in the ROI and the maximum error, i.e., the worst case. We apply them to the performance measures that are obtained from CRLB to compute different metrics that provide different interpretations of the accuracy that we will obtain in the localization process after having deployed the sensors.

The optimization of different performance metrics is the main contribution of our approach. To the best of our knowledge, there is not any work in literature focusing on this topic. The importance of considering several metrics relies on the fact that each one of them has a different practical interpretation. The optimization of the determinant of the FIM minimizes the volume of the error ellipsoid. However, an elongated ellipse may have a low volume that masks a high error in the major axis direction. In the same way, focusing only on the worst case may lead

to solutions that deteriorate the performance on a great part of the ROI but achieve good performance in small or less important zones. We propose to assist the expert human that serves as the sensor resource manager with a decision support system based on multi-objective evolutionary optimization. After performing the optimization, the resource manager receives the Pareto efficient solutions that optimize several performance metrics, as we show in Section 4.4. The task of the manager consists in analyzing the Pareto front and selecting an appropriate solution according to his own criteria. Obtaining a complete overview of the Pareto efficient solutions is the advantage of this method, since the resource manager does not need to decide a priori parameters that affect the obtained solution. The next section shows and discusses the performance measures that we consider in this work.

4.2 Performance measures of covariance matrix

We propose five scalar performance measures derived from the covariance matrix of the estimated position $\Sigma_{\hat{x}\hat{x}}$. Each measure is originally defined and evaluated for a single point — i.e., an assumed, stationary target position. We can derive a related scalar performance measure for the whole ROI by repeating the evaluation of the measure for all points of a sufficiently dense grid covering the entire ROI and condensing those evaluations into a single scalar value. We will focus on the transition from individual points to a whole ROI later in this section. Table 4.1 shows the proposed scalar performance measures, where \hat{x} is the estimated position of the target, $\Sigma_{\hat{x}\hat{x}}$ represents its covariance matrix, and λ is the vector of eigenvalues of $\Sigma_{\hat{x}\hat{x}}$.

Table 4.1: Scalar performance measures referring to individual location

Performance measure	Expression	Practical meaning related to
Trace	$\text{tr}(\Sigma_{\hat{x}\hat{x}}) = \sum \lambda$	MSE
Determinant	$\det(\Sigma_{\hat{x}\hat{x}}) = \prod \lambda$	Volume of the error ellipsoid
Maximum eigenvalue	$\max(\lambda)$	Largest axis of the ellipsoid
Ratio of maximum to minimum eigenvalue	$\frac{\max(\lambda)}{\min(\lambda)}$	Isometry of uncertainty
Uncertainty in spatial direction \mathbf{a}	$\mathbf{a}^T \Sigma_{\hat{x}\hat{x}} \mathbf{a}$	Uncertainty in the direction given by the unit vector \mathbf{a}

Assuming normally distributed measurements and a correct functional and stochastic model, the covariance matrix represents an ellipsoid about the estimated position, containing the true position with a certain probability. The covariance matrix is symmetric, hence its

eigenvectors are orthogonal and represent the direction of the major and minor axes. The eigenvalues of the covariance matrix are the variances of the data in the direction of the eigenvectors [Chan et al., 2015].

The trace, determinant, and maximum eigenvalue have been widely used as optimization criteria in the theory of design of experiments, and the designs minimizing these criteria are known as A-, D-, and E-optimal, respectively. Most researchers use D-optimality because of its advantages, in particular its invariance under scale changes in the parameters [Ucinski, 2004]. It is also noteworthy the fact that the minimization of the determinant of the covariance matrix is dual to the maximization of the determinant of the information. The eigenvalues of the covariance matrix are the inverse of the eigenvalues of the information matrix, and the inverse of the product is the product of the inverse. This result is not true in the case of the trace, since the inverse of a sum of values is not the sum of the inverted values. E-optimality can lead to more than a single optimum solution when the number of dimensions of the problem is greater than 2 [Yang et al., 2012]. We also propose the ratio of the maximum and minimum eigenvalues as a criterion because it indicates the elongation of the error ellipsoid. It is to be observed that the ratio of eigenvalues of a symmetric matrix is the condition number of that matrix. When optimizing for this criterion, the resulting error ellipsoid is as spherical as possible indicating that the uncertainty is almost independent of the direction. Finally, including a measure of the uncertainty in a predefined spatial direction is useful for problems where the uncertainty is more critical in a certain direction — e.g., when targets are to be kept at a safe distance from walls along a narrow hallway. These last two metrics are usually used in optimal design [Banks et al., 2010], but they have rarely been considered in sensor placement for localization. The condition number of a matrix was used by [Neering et al., 2008] for two estimators of the least squares solution of TDOA.

For a given sensor configuration, any scalar from Table 4.1 can be interpreted as a function $\mathcal{O}(x, y, z)$ of the target position coordinates, i.e., an individual evaluation at a specific point of an ROI. We can get the scalar measure referring to a whole ROI as mean value over the whole ROI by dividing the respective volume integral by the volume V_{ROI} of the ROI:

$$\mathcal{O}(\text{ROI}) = \frac{1}{V_{\text{ROI}}} \iiint_V \mathcal{O}(x, y, z) dx dy dz. \quad (4.1)$$

We can solve Eq. (4.1) numerically by evaluating the function \mathcal{O} at P grid points, i.e. by calculating $\mathcal{O}(p_j)$, $j = 1, 2, \dots, P$, where p_j is the j point of the grid. This also enables us to derive other representative values for the entire ROI by choosing suitable functions of $\mathcal{O}(p_j)$. Some examples of useful functions are the mean (Eq. (4.2)) or the maximum (i.e., the worst case, Eq. (4.3)). Additionally, the evaluated function can be weighted by location dependent weights

$w_j = [0, 1]$. This location dependent weighting is useful to define areas within the ROI where we are predominantly and exclusively interested in a specific measure, e.g., minimum lateral error in an elongated narrow path and minimum MSE elsewhere. Generally, we propose the following functions for the transition from the individual points p_j to the whole ROI, represented by $\{p_1, p_2, \dots, p_P\}$:

$$\mathcal{O}_{\text{mean}}(\text{ROI}) = \frac{\sum_{j=1}^P (w_j \mathcal{O}(p_j))}{\sum_{j=1}^P w_j}, \quad (4.2)$$

$$\mathcal{O}_{\text{max}}(\text{ROI}) = \max \left(\bigcup_{j=1}^P (w_j \mathcal{O}(p_j)) \right). \quad (4.3)$$

According to the conclusion provided by [Yang et al., 2012], for stationary target localization applications (individual point), the trace, determinant, and maximum eigenvalue measures lead to the same goal of placing the sensors as close to the target as possible to achieve the best positioning quality and to surround the target for most isometric uncertainty. Since each measure corresponds to a different aspect of the uncertainty, there could be multiple objectives to satisfy instead of focusing on a single measure. [Yang et al., 2012] left the multi-objective case open for future work. The present work focuses on getting the Pareto front as the result of a multi-objective optimization problem.

4.3 Multi-objective optimization

Multi-objective optimization involves minimizing or maximizing multiple objective functions subject to a set of constraints. The M objectives are functions of N decision variables. We need to distinguish between the space of the decision variables ($\mathbb{D} \subseteq \mathbb{R}^N$) and that one of the objectives ($\mathbb{O} \subseteq \mathbb{R}^M$). It is usual that these objectives are in conflict with each other and the final solution requires a trade-off between the objectives. In this case, there is no single optimum solution but a set of solutions representing the respective optimum of one objective constrained on fixed values of the other objectives. This set, expressed in the objective domain, is the Pareto front. For each point on this Pareto front it is impossible to find a vector in the space of the decision variables improving on any of the objectives without deteriorating at least one of the others. A qualitative example (for two objectives) is shown in Fig. 4.1. The solutions inside the feasible region \mathcal{F} are dominated by those of the Pareto front \mathcal{P} . A solution is said to dominate another one if each of its objective values is better - or at least none is worse - than those of the other solution. The end points of the Pareto front correspond to decision variables which globally optimize the respective objective. A solution whose objective values are both

additional knowledge or criteria. Common techniques of preferred solution selection include the computation of a single scalar objective function from the M different objectives (utility function approach) so that a single solution is obtained using a single-objective optimization. Another approach consists of assigning weights to the objectives along the Pareto front and selecting the proper solution according to the situation. The weights range from 0 to 1 for each objective, it is up to the designer to select appropriate weights. Finally, we could also select the point on the Pareto front which is next to the ideal optimum, i.e., has the shortest distance from $\mathcal{O}(\mathbf{x}^I)$ as of Fig. 4.1 [Deb, 2001]. The main disadvantage of the utility function approach is that the design of the utility function may be arbitrary - and therefore the finally selected optimum. Basing the decision on an analysis of the Pareto front allows to better understand the trade-offs involved. The shortest distance from the ideal optimum allows to automatically and objectively select a solution, whereas the weights approach can be useful for having a representation of the solutions with their percentage of objective fulfillment and selecting a value according to current priorities.

4.3.1 Evolutionary multi-objective optimization

Evolutionary algorithms are among the most popular metaheuristic algorithms for solving multi-objective optimization problems. One of the main reasons is that they can evaluate a whole population (a population is made of individuals, each representing a decision variable vector $\mathbf{x} \in \mathbb{D}$) in a single run of the algorithm, so that it is possible to find several members of the Pareto optimal set in a single run. Additionally, they are less sensitive to the shape and continuity of the Pareto front [Coello Coello, 2006]. In the sensor placement problem, a single individual consists of three coordinates (3D case) per anchor, i.e., $3n$ variables with n anchors. Given a population size of 100 individuals and five sensors a single run of the algorithm evaluates the fitness of 100 candidates, each consisting of 15 variables.

We have chosen to use the modified version of the NSGA-II algorithm [Deb et al., 2002] as implemented in the Global Optimization Toolbox™ of Matlab®. The algorithm is briefly explained in this section for convenience. The algorithm is based on the computation of how many individuals dominate each other and identifying the set of individuals which each one dominates, assigning a nondomination rank to each individual. The nondomination rank and a measure of the density of individuals surrounding a particular one (crowding distance) are used to compare individuals with respect to fitness.

The initial population (of size s_p) is randomly generated in the decision variable space and the objective functions are evaluated for each individual $\mathbf{x}_i^{(0)}$, where the superscript (0) denotes

the initial generation and i takes integer values from 1 to s_p . Then the nondomination rank is assigned to each individual. Any individual whose vector of evaluated objectives is not greater than any other objective vector (in the sense of the above product order) has rank = 1. The ranked individuals are then removed and the product order comparison is performed again to assign rank = 2. The assignment continues until the whole population is ranked. Each rank number corresponds to a front and a front of individuals with a given rank will dominate all fronts associated with a greater rank. The individuals belonging to the same front are assigned a crowding distance. For each one of the objectives $\mathcal{O}_j, j = 1, 2, \dots, M$, the values of all individuals i within the front are normalized according to $\mathcal{O}'_{j,i} = \frac{\mathcal{O}_{j,i}}{1 + \max_{i=1, \dots, s_f} |\mathcal{O}_{j,i}|}$, where s_f is the number of individuals of the front and j and i are as above. The objectives are then sorted such that $\mathcal{O}'_{j,1} \leq \mathcal{O}'_{j,2} \leq \dots \leq \mathcal{O}'_{j,s_f}$. The best and the worst individuals are given an infinite distance value. The distance of remaining individuals is $d_{c_{j,i}} = \mathcal{O}'_{j,i+1} - \mathcal{O}'_{j,i-1}$, where $d_{c_{j,i}}$ is the crowding distance of the i individual of a front for the objective j . This process is done for each objective and the $d_{c_{j,i}}$ values for each individuals are added to compute the final crowding distance $d_{c_i} = \sum_{j=1}^M d_{c_{j,i}}$ of individual i .

At the end of the above step we have the ranks and the crowding distances of the initial population. The first genetic algorithm step where a new population of size s_p is created with crossover and mutated children now takes place. The number of crossover children is $n_x = r_x s_p$, where r_x is a predefined ratio. The number of mutated children is $n_m = s_p - n_x$. We need two parents for each crossover child and only one parent for each mutated child, making the number of parents $n_p = 2n_x + n_m$. A tournament selection process chooses n_p parents making n_p tournaments among four randomly picked individuals chosen from the current population. In case that two chosen individuals have equal rank the one with greater crowding distance is preferred to keep diversity. Crossover children are generated as weighted average of their respective parents, evaluated in the decision variable domain: $\mathbf{x}_{*i}^{(l)} = \mathbf{x}_{i_1}^{(l)} + \boldsymbol{\rho} \circ (\mathbf{x}_{i_2}^{(l)} - \mathbf{x}_{i_1}^{(l)})$, where $\boldsymbol{\rho}$ is a vector whose elements are random numbers between 0 and 1, acting as weights in the crossover process, $\mathbf{x}_{*i}^{(l)}$ is the i^{th} child emerging from the l^{th} generation, $\mathbf{x}_{i_k}^{(l)}$ is the k^{th} parent of the i^{th} child, and \circ denotes the entry-wise product. Expressed in the decision variables domain, each crossover child will be inside the hypercube defined by its two parents.

The adaptive feasible mutation method is used for generating n_m further children. This method uses a set of randomly generated directions together with directions parallel to the boundaries in case the decision variable is near any boundary constraint. This set is randomly permuted and the variables are moved in the first direction an initial step size, i.e., the step size is the module of the displacement vector. The feasibility of the movement is checked

with the constraints. In case of feasibility the new variable is the mutated child, otherwise the individual keeps its previous value and the next direction is checked. Subsequent calls to the mutation function will test the improvement of the current generation in order to decrease the step size in case there is no improvement. A more detailed explanation of adaptive feasible mutation can be found in [Kumar, 2010].

At this point we have the old population (l^{th} generation) extended by the newly created crossover and mutated children. The algorithm will now create the $(l + 1)^{\text{th}}$ generation by selecting s_p individuals from this extended population of the l^{th} generation. Therefore, the fitness of the children is calculated, the old population and the children are merged and the ranks and crowding distances are computed within this extended population. From the first front we extract $r_{\mathcal{P}}s_p$ individuals, where $r_{\mathcal{P}}$ indicates the fraction of individuals from the Pareto front and takes values between 0 and 1. The number of individuals to keep from remaining fronts (when existing) is chosen with a geometric progression of ratio 0.8, decreasing as long as the rank increases. The number of individuals to be retained from each front is adjusted in case there are less individuals than individuals to be retained. The individuals from each front are sorted by crowding distance and those with the smaller values are removed from being part of the next population. Since both parents and children are merged before computing rank and distance and creating the next generation, elitism is present in the sense that parents can also be part of the population of the following generation.

The steps of evaluation of objectives, ranking, and derivation of a new generation are now carried out iteratively for several generations. The loop is aborted when the generation number reaches a predefined threshold G . Finally, the algorithm returns the individuals of the best front of the last generation. They are the estimate of the Pareto front.

4.4 Numerical example

This section shows simulation results of the sensor placement problem solved with the aforementioned MOEA. First, a single-objective optimization is shown using each of the five scalar measures introduced in Section 4.2. We show the error ellipses to check the practical meaning mentioned at Table 4.1. Then, the MOO simulation shows the point cloud of the sensor placement corresponding to a Pareto front for different combinations of two of the five objectives. We have chosen to show combinations of two objectives so that the Pareto front could be clearly represented. However, an example with three objectives has been included as well.

We have run simulations for placing five sensors over a squared area of side 3 m. We have considered an empty area without LOS obstructions so that any sensor can cover almost the

whole area. Thus, we do not need to take into account neither the number of sensors to deploy nor the necessity of each point in the area to be 3-covered, we will deal with both issues in the next chapter. We have evaluated a total of uniformly spaced 121 points which have been equally considered ($w_j = 1$), we have also included an example with location dependent weights in the multi-objective optimization. The GA has been run for 1000 generations, the values of the different parameters that were mentioned in Section 4.3.1 appear in Table 4.2. The population size is 15 times the number of decision variables (five sensors with three coordinates, i.e. 15 variables). We have created an initial population placing the five sensors all over the area dividing the square in five squares of side 1.5 m. One of the squares is centered inside the original square and the remaining squares are those left by dividing the first area horizontally and vertically, the former square overlaps the other. The first individuals are generated by randomly placing each of the five sensors in a square of side 1.5 m. This constraint on the initial population has been made so that we can initially have a deployment layout approaching the optimum.

Table 4.2: Chosen GA parameters

Parameter	Symbol	Value
Maximum number of generations	G	1000
Population size	s_p	225
Pareto fraction	r_p	0.35
Crossover fraction	r_x	0.8

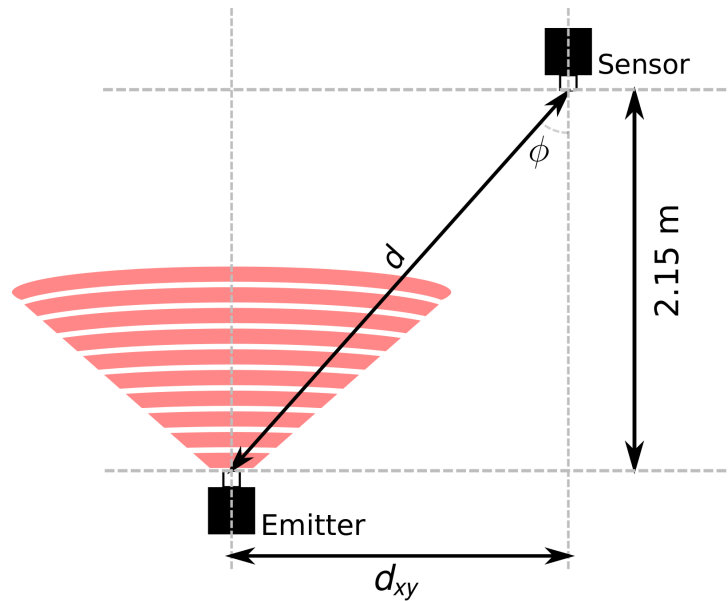
Restricting the height of the sensors to 2.80 m — since the height of the emitter was fixed to 0.65 m, the difference of the height of the sensors and the emitter is 2.15 m —, the optimization problem takes the form:

$$\begin{aligned}
& \text{Minimize} && \mathcal{O}(\mathbf{x}_s); \\
& \text{subject to} && 0 \leq x_i \leq 3, \quad i = 1, 2, \dots, 5; \\
& && 0 \leq y_i \leq 3, \quad i = 1, 2, \dots, 5; \\
& && z_i = 2.80, \quad i = 1, 2, \dots, 5,
\end{aligned} \tag{4.5}$$

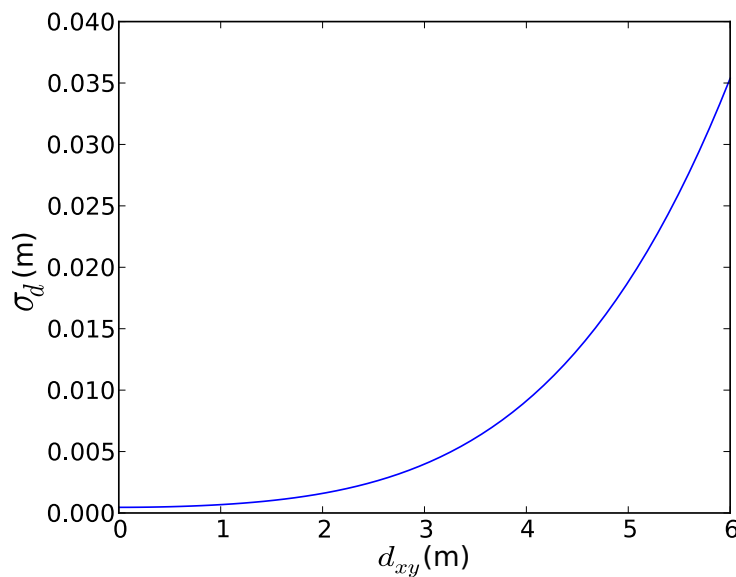
where the decision variable \mathbf{x}_s is a vector of the sensor positions $\mathbf{x}_s = [x_1 \ y_1 \ z_1 \ \dots \ x_5 \ y_5 \ z_5]$ and the objective vector \mathcal{O} will change according to the objective(s) to be minimized, see Table 4.1 and Eqs. (4.2) and (4.3).

We will not formulate again the RDOA position estimation in this chapter, it has already been detailed in Chapter 3. The simulations we show are based on the infrared system de-

scribed in that chapter as well. We use the same parameters for the emitter and receivers that appear in Table 3.1. In this chapter we will just show how the distance in the xy -plane affects the deviation of the measurements.



(a) Infrared emitter-sensor link



(b) Distance measurement deviation vs distance in the xy -plane

Figure 4.2: Noise variance vs distance between sensor and emitter

Figure 4.2a shows a simplified infrared emitter-sensor link. As seen in Eq. (3.1), the power that reaches the sensor is a function of the distance d and the angle ϕ . Fixing the height of both emitter and sensors makes d and ϕ to be a function of the distance in the xy -plane d_{xy} , since $d = \sqrt{2.15^2 + d_{xy}^2}$ and $\tan(\phi) = \frac{d_{xy}}{2.15}$. The parameters of emitter and receivers are constant;

hence we can express the deviation of the distance measurement σ_d as a function of d_{xy} in Fig. 4.2b.

In Section 4.2 we talked about the covariance matrix of the estimation $\Sigma_{\hat{x}\hat{x}}$, which should not be confused with the covariance matrix of the measurements Σ . The latter is built with the deviations calculated with the infrared model presented in the corresponding section of the problem statement chapter 3.1. These deviations are the same that are shown in Fig. 4.2b as σ_d . As for the covariance matrix of the estimation which is used to compute the objectives, we already know that it is bounded by the CRLB when an unbiased estimator is used. We use the CRLB as the covariance matrix of the estimation to optimize the performance limit of our system in terms of accuracy. It is computed with the inverse of the FIM using the Jacobian matrix of the RDOA equations and the covariance matrix of the measurements, as shown in Eq. (3.21). As stated in Section 3.2, the sensor selected as the reference has not any influence on the MLE solution, nor does it have on the CRLB. Thus, we still consider that the first sensor x_1 is the reference.

4.4.1 Single-objective optimization

The following figures show optimum sensor placement according to different single optimality criteria. The average trace and determinant solutions are almost the same keeping in mind the symmetry of the considered area as can be seen in Figs. 4.3 and 4.4.

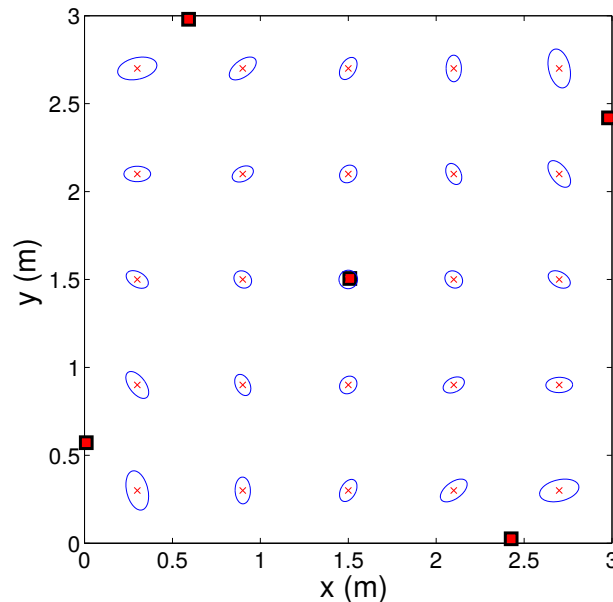


Figure 4.3: Optimum sensor placement that optimizes the average trace of the CRLB.

Red squares represent the sensors, whereas blue ellipses are the shape of the error ellipsoid defined by the CRLB. They are centered in the true values — red cross — of the evaluated

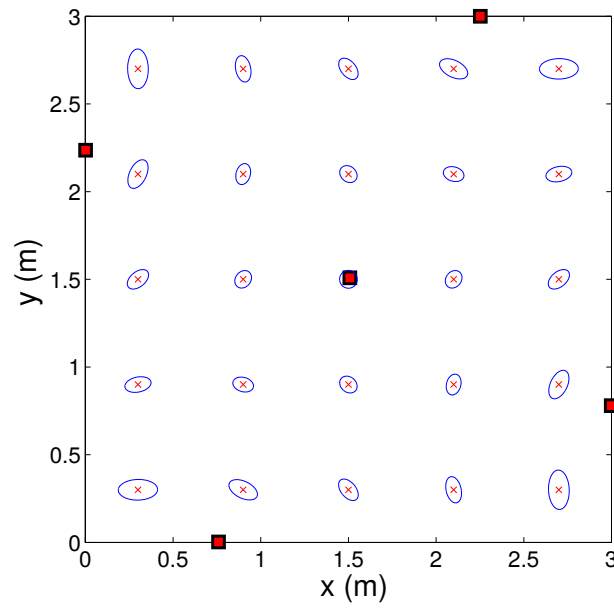


Figure 4.4: Optimum sensor placement that optimizes the average determinant of the CRLB.

position. For the sake of clarity, we only represent a subset of the evaluated points.

Figure 4.5 shows the solution that optimizes the maximum direction of error that can be found in the whole ROI; i.e., we do not optimize an averaged value, but an absolute maximum as in Eq. (4.3). This solution may have a more practical interest when we do not want to focus

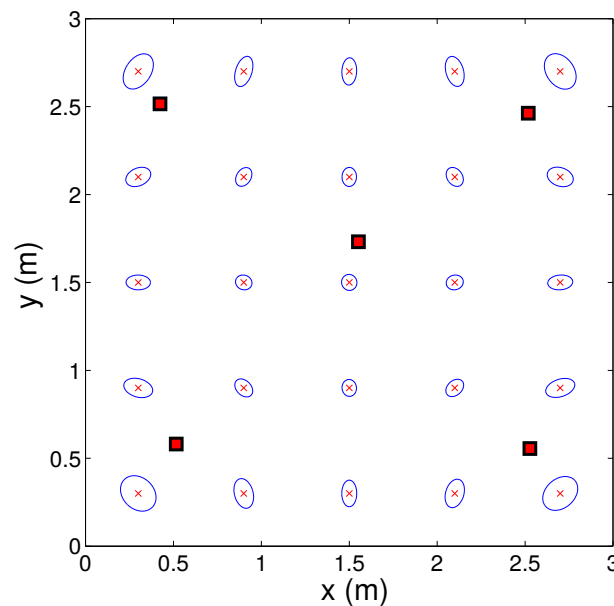


Figure 4.5: Optimum sensor placement that optimizes the absolute maximum eigenvalues of the CRLB.

on an average accuracy, but we just want to assure that we will not have a deviation above a given value.

Figure 4.6 shows the solution that minimizes the maximum-minimum eigenvalue ratio, also known as the condition number of the CRLB. The figure clearly shows that we should not use

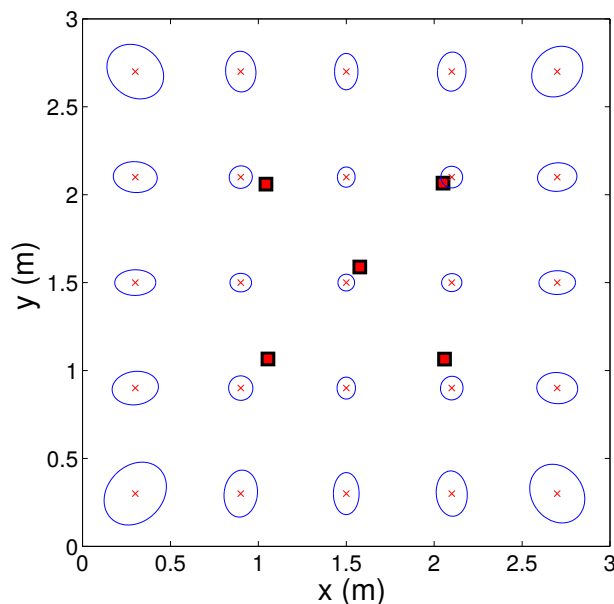


Figure 4.6: Optimum sensor placement that optimizes the average isotropy.

this metric by itself, since the solution is more isotropic, yet the uncertainty areas are higher than those of previous solutions. In the next section we will see that the metric is useful when combined with another in a MOO.

Finally, we show the last of the performance measures in Fig. 4.7. The two parameters we estimate in the localization problem are the x and y coordinates of the target position. Hence, when we consider that the vector \mathbf{a} of Table 4.1 is any of the vector of the standard basis, we are optimizing the variance of one of the parameters. We have set $\mathbf{a} = [1, 0]^T$ in Fig. 4.7a and $\mathbf{a} = [0, 1]^T$ in Fig. 4.7b. With this metric we can optimize the error in a given direction, which is useful in case we know something about the trajectory of the target. Figure 4.8 shows the optimum sensor placement when the target follows a straight vertical line ($x = 1.5$). This example considers different weights for the points that are the candidates of the position of the target. The points whose x coordinate is 1.5 use a weight of 1 ($w_j = 1$), whereas ($w_j = 0$) for all the other points. With this placement we could estimate the position of the target and discard the estimate of the x coordinate, since we already know its value. In case the trajectory is not a straight line but known, we can use a tangent vector to the trajectory, which will not be the same for each point of the grid.

It can be seen that the sensor distribution follows a square distribution plus center of mass (as showed in [Chen et al., 2006]) for the five cases but the distance from the center is different in each case. It is a good sign the fact that we are getting solutions that resemble those on

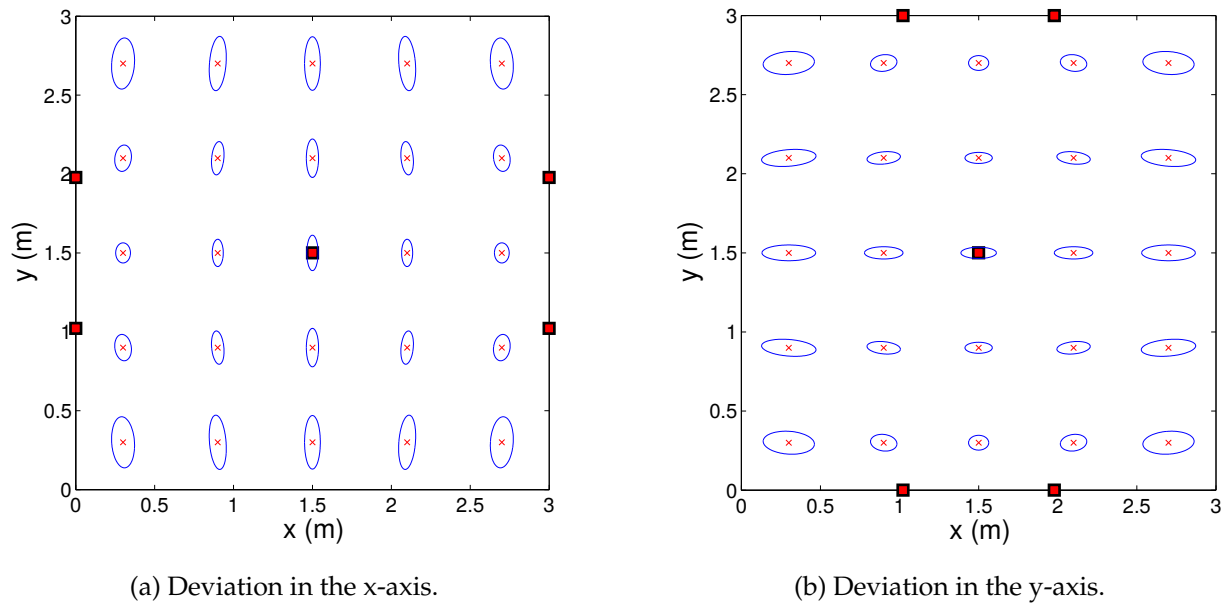


Figure 4.7: Optimum sensor placement that optimizes the deviation in a given direction.

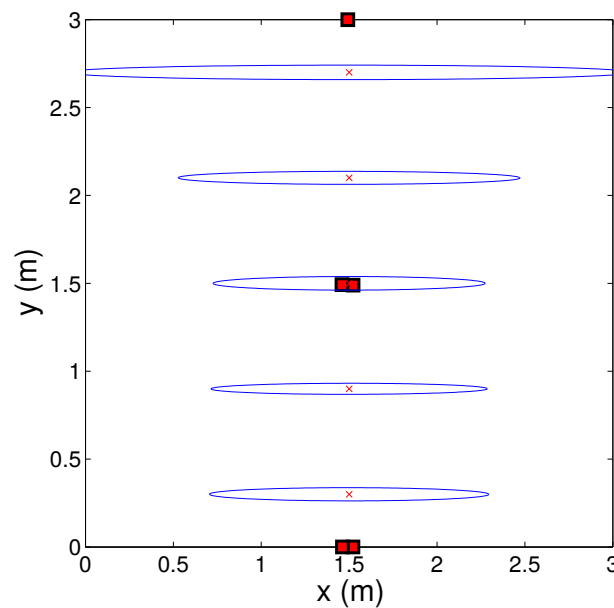


Figure 4.8: Optimum sensor placement that optimizes the variance of the y coordinate when $x = 1.5$ m.

the state-of-the-art. Increasing the proximity to the center of the area improves the average circularity throughout the whole area, but it decreases the MSE and the volume of the error ellipsoid. The maximum eigenvalue has been evaluated for the worst case of the whole area (Eq. (4.3)), whereas the other objectives were evaluated as an average (Eq. (4.2)) over the ROI.

4.4.2 Multi-objective optimization

The results of various MOO processes on pairs of criteria are shown and discussed below. Each of the figures shows potential optimum locations of the sensors on the left and the corresponding points of the Pareto front in the objective domain on the right. Figs. 4.9 to 4.13 should be read following the color in the Pareto front and locating the five points of the same color in the point cloud. We have not shown simulation results for the determinant criterion because they are similar to the ones using the trace.

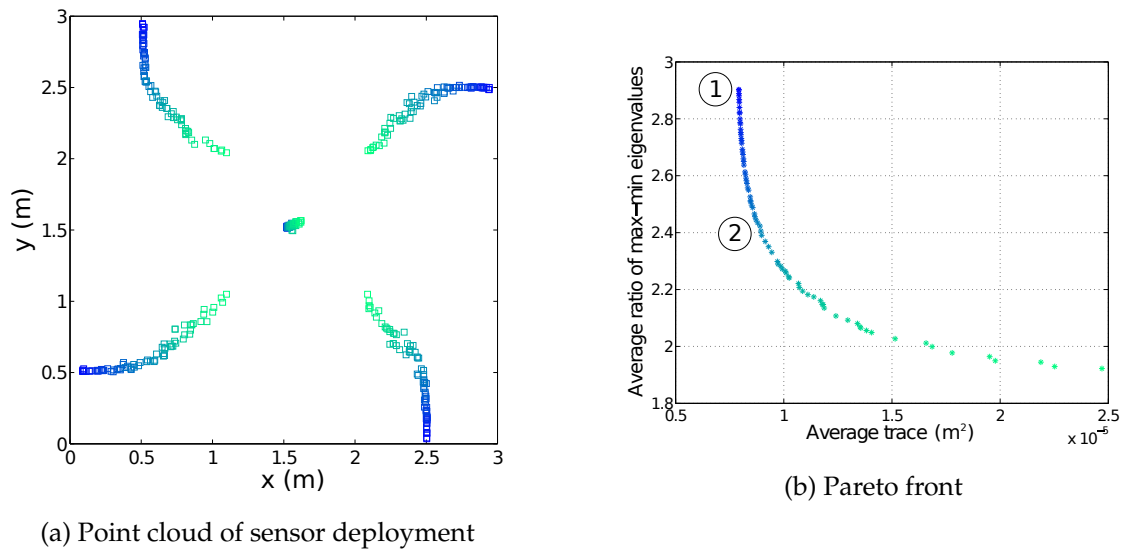


Figure 4.9: Sensor placement and Pareto front of trace and eigenvalues ratio optimality

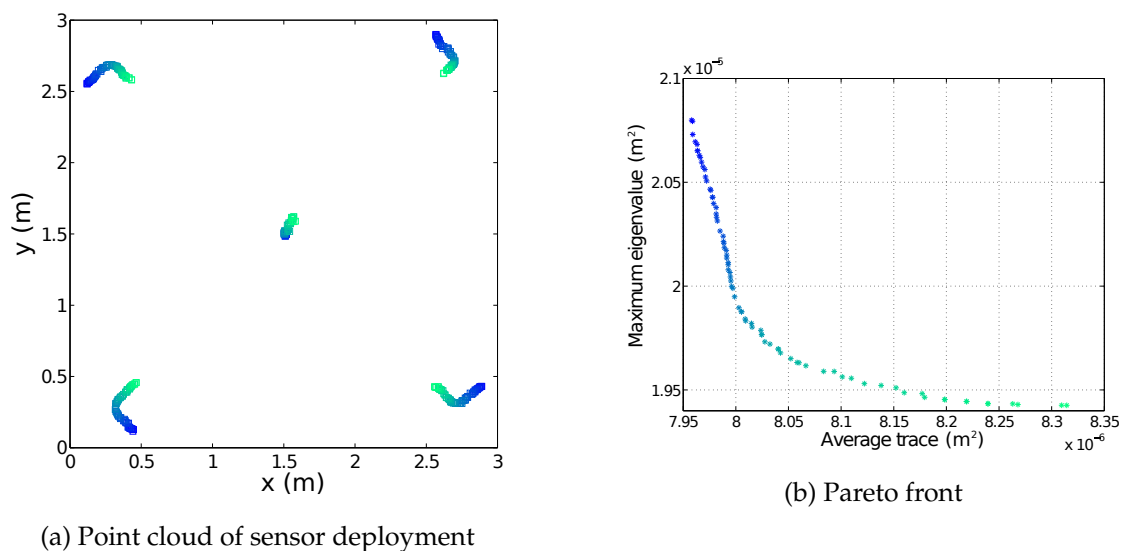


Figure 4.10: Sensor placement and Pareto front of trace and maximum eigenvalue optimality

The example of Fig. 4.12 has been obtained using location dependent weights. The lateral deviation objective is evaluated in a small corridor in the center, where the weights w_{lat} take

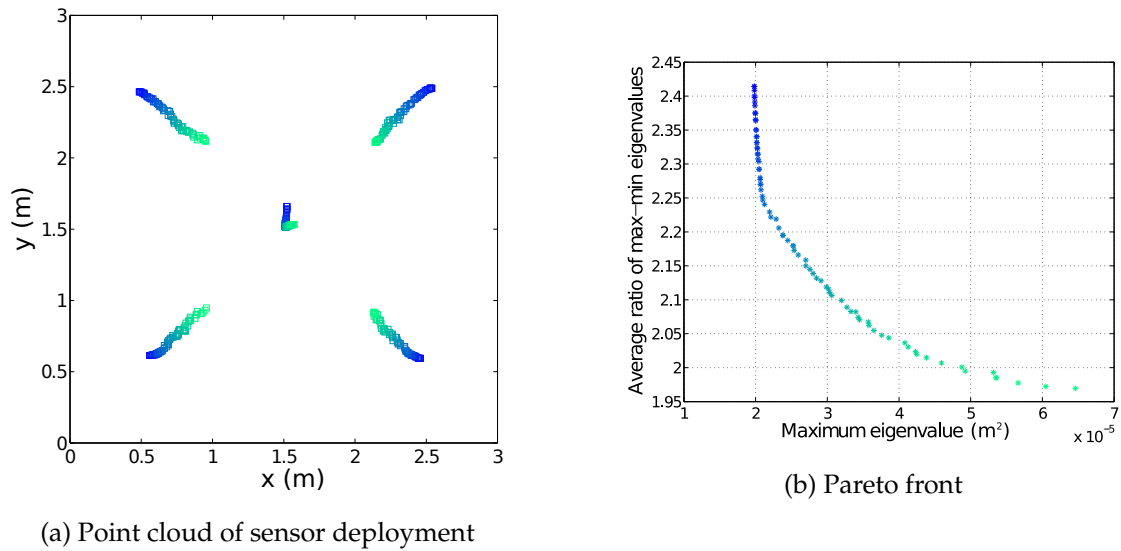


Figure 4.11: Sensor placement and Pareto front of maximum eigenvalue and eigenvalues ratio optimality

the value 1 for $1.2 \leq x \leq 1.8$ and 0 otherwise. The trace is evaluated with the opposite weights, i.e. $w_{tr} = 1 - w_{lat}$.

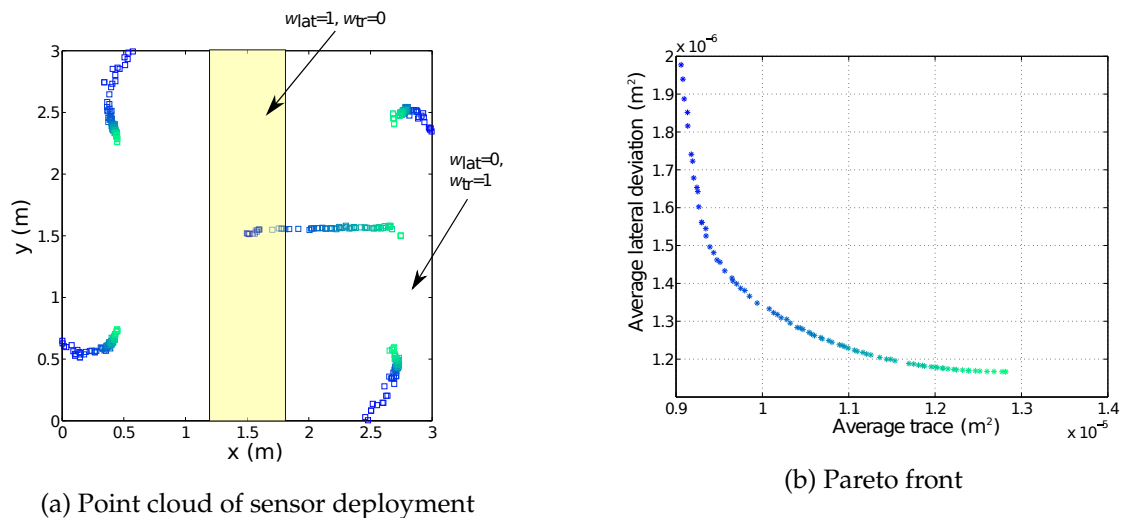


Figure 4.12: Sensor placement and Pareto front using trace ($x < 1.2 \cup x > 1.8$) and lateral deviation ($1.2 \leq x \leq 1.8$) criteria

Studying the Pareto front allows the selection of a configuration that provides the different performance measures throughout the covered area. The selection of the desired solution should be made by considering the specific case under study, e.g. if we are trying to locate a mobile in a tunnel or corridor we might not be interested in getting a circular error bound but the minimum uncertainty in a specific direction. Fig. 4.9 shows that when minimizing the MSE over the entire area we would obtain a sensor distribution that provides highly anisotropic un-

certainties (variance is three times larger in direction of maximum uncertainty than in direction of minimum uncertainty, see point 1 in Fig. 4.9b). However, descending along the Pareto front from the position of minimum MSE or determinant we reach with only a small deterioration of MSE a sensor distribution yielding a ratio of maximum and minimum eigenvalues of 2.4, (point 2 in Fig. 4.9b), i.e. we find a solution which is only very slightly less optimum with respect to MSE but much better in terms of isotropy. Figs. 4.10 and 4.11 use the maximum eigenvalue for optimization, trying to reduce the maximum uncertainty in any point of the cell (the worst case). This measure avoids the potential problem of low errors in some parts of the ROI masking greater errors in other parts of the region. Fig. 4.11 shows that the spread of the eigenvalues can be reduced from 2.4 to 2.25 while keeping the maximum eigenvalue almost constant.

The last simulation shows a case with three objectives in Fig. 4.13.

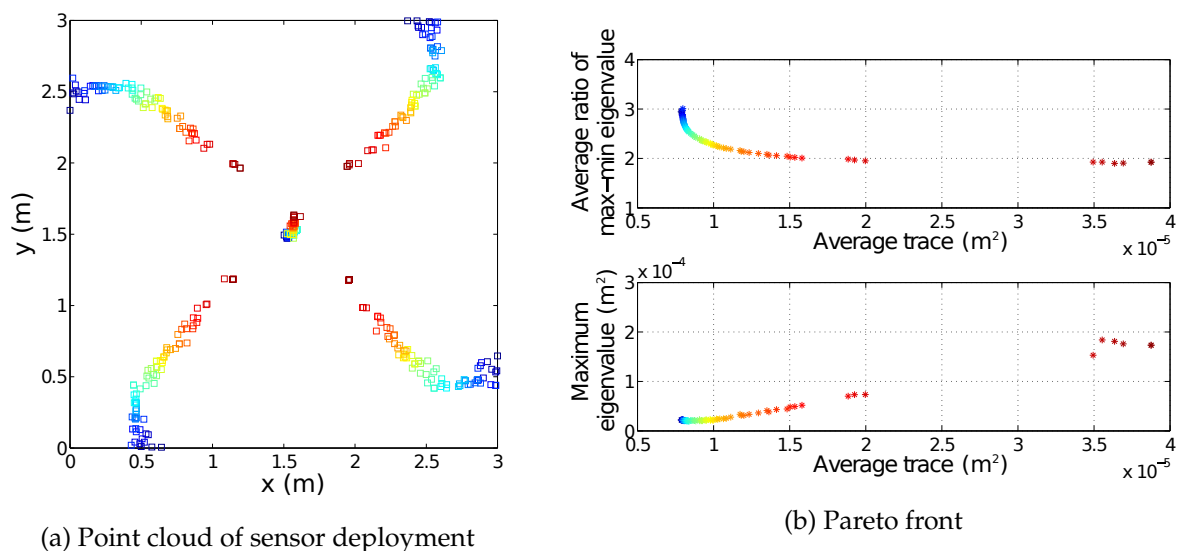


Figure 4.13: Sensor placement and Pareto front of trace, eigenvalues ratio, and maximum eigenvalue

Finally, after obtaining the Pareto front and its corresponding sensor distributions we have to make the final decision and pick a single solution. This decision requires a high level knowledge of the final application and is left to the localization infrastructure designer.

Before concluding this section, we would like to comment a possible application of this approach apart from providing more information about the error ellipsoids. As we concluded in Section 3.3.3 of Chapter 3, we can deploy sensors so that the solution provided by NLS without using the noise of the measurements is improved. As we said, NLS considers that each observation has the same importance. We can reach this situation if we deploy the sensors so that each observation has the same standard deviation and the noise of the reference is low.

Intuitively, we can get this situation using the results of Fig. 4.9, where we optimized the MSE and the ratio of eigenvalues of the CRLB. The observations of RDOA are hyperbolae, and they contribute almost equally to the estimated position when the error ellipsoid is almost circular. The results of Fig. 4.9 allow us to select sets of sensors that improve the circularity of the error ellipsoid while keeping the MSE to a minimum. Testing these results with NLS using Eq. (3.11) and 1000 Monte Carlo runs, considering the placement proposed in [Martin-Gorostiza, 2011] and [Chen et al., 2006] as well, we find the results of Fig. 4.14.

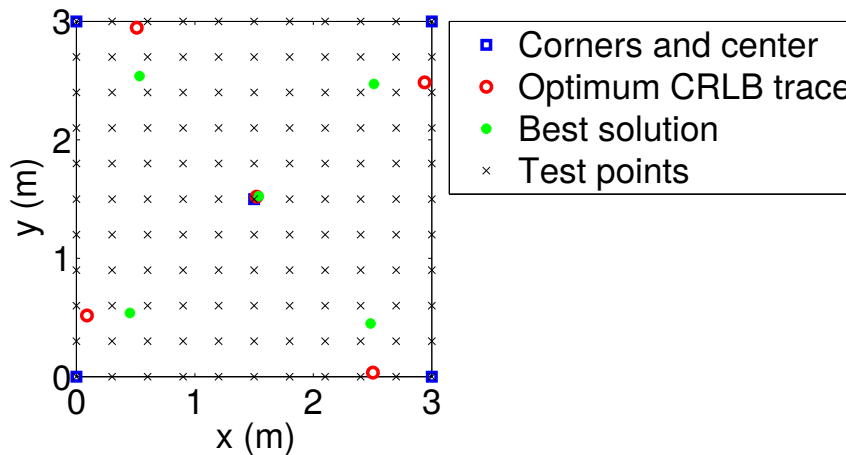


Figure 4.14: Optimum placement that optimizes the RMSE with NLS.

Table 4.3 shows the 2DRMS values of each configuration. The improvement of the best solution over the usual configuration of four sensors in the corners and one in the center is significant. We can improve the localization performance by almost 16 %. The improvement over the solution that optimizes the trace of the CRLB is about 6 %.

Table 4.3: Comparison of the 2DRMS attainable by each configuration

Configuration	Averaged 2DRMS (m)
Corners and center	0.0081
Optimum trace of CRLB	0.0072
Best solution	0.0068

The low values — though within the expected range — of Table 4.3 are caused by the values of the infrared system parameters of Table 3.1, which provide the standard deviation of the distance measurement presented in Fig. 4.2b. We have run the same test lowering the intensity of the emitter to $10 \frac{\text{mW}}{\text{Sr}}$ and the modulation frequency to 4 MHz. The results obtained are 10 times higher than those that are given in Table 4.3; hence, we have an improvement of more than a centimeter.

4.5 Obtaining a metric with prior information

We consider the case of a target moving in a 2D Cartesian coordinate system with a dynamic white noise acceleration model, where the velocity is constant except for a noise term [Zuo et al., 2007]. The next state at time t_{k+1} is evolved from the state at t_k according to

$$\mathbf{x}_{k+1} = \mathbf{F}\mathbf{x}_k + \mathbf{v}_k, \quad (4.6)$$

where $\mathbf{x}_k = [x_k \ \dot{x}_k \ y_k \ \dot{y}_k]^T$ and $\mathbf{v}_k \sim \mathcal{N}(0, \mathbf{Q})$, which denotes a normal distribution with zero mean and covariance matrix \mathbf{Q} . x_k and y_k are the target positions and \dot{x}_k and \dot{y}_k denote its velocities at instant t_k . Using a sampling time T , \mathbf{F} and \mathbf{Q} take the form:

$$\mathbf{F} = \begin{bmatrix} 1 & T & 0 & 0 \\ 0 & 1 & 0 & 0 \\ 0 & 0 & 1 & T \\ 0 & 0 & 0 & 1 \end{bmatrix}, \quad (4.7)$$

$$\mathbf{Q} = q_0 \begin{bmatrix} \frac{T^3}{3} & \frac{T^2}{2} & 0 & 0 \\ \frac{T^2}{2} & T & 0 & 0 \\ 0 & 0 & \frac{T^3}{3} & \frac{T^2}{2} \\ 0 & 0 & \frac{T^2}{2} & T \end{bmatrix}, \quad (4.8)$$

where q_0 is the power spectral density of the process noise.

The measurement model of range-difference of arrival (RDOA) estimation for a pair of sensors i and j is

$$r_k^{i,j} = h(\mathbf{x}_k) + w_k^{i,j} = \|\mathbf{x}_k^P - \mathbf{s}^i\| - \|\mathbf{x}_k^P - \mathbf{s}^j\| + w_k^{i,j}. \quad (4.9)$$

\mathbf{x}_k^P is the position vector of the target. Only the x and y components are part of the target state \mathbf{x}_k , whereas the z coordinate is assumed to be constant, i.e. $z_k = Z, \forall k$: $\mathbf{x}_k^P = [x_k \ y_k \ Z]^T \cdot \mathbf{s}$ is the position vector of a sensor, $w_k^{i,j} \sim \mathcal{N}\left(0, (\sigma_k^i)^2 + (\sigma_k^j)^2\right)$, and σ is the standard deviation of the measurement of a sensor. Having N sensors we can use one of them as a reference (sensor r). Pairing it with the remaining $N - 1$ sensors we obtain the RDOA measurement vector $\mathbf{r}_k = [r_k^{1,r}, r_k^{2,r}, \dots, r_k^{N-1,r}]^T$.

The posterior Cramér-Rao lower bound (PCRLB) [Tichavský et al., 1998] is recursively computed for the following state with the inverse of the posterior Fisher information matrix $\mathbf{M}_{k+1,k+1}$ [Trees et al., 2006] as in Eq. (4.10). The latter consists of a data matrix, which is the standard Fisher information matrix evaluated at t_{k+1} , and a prior matrix $\mathbf{M}_{k+1,k}$ (4.11).

$$\mathbf{M}_{k+1,k+1} = \mathbf{M}_{k+1,k} + \mathbf{J}_{k+1}^T \boldsymbol{\Sigma}_{k+1}^{-1} \mathbf{J}_{k+1} \quad (4.10)$$

$$\mathbf{M}_{k+1,k} = \left(\mathbf{F}\mathbf{M}_{k,k}^{-1}\mathbf{F}^T + \mathbf{Q} \right)^{-1} \quad (4.11)$$

$\mathbf{P}_{0,0} = \mathbf{M}_{0,0}^{-1}$ must be known based on prior target information. Eqs. (4.12) and (4.13) show, respectively, the Jacobian matrix \mathbf{J}_k of \mathbf{r}_k and the covariance of the RDOA measurements Σ_k .

$$\mathbf{J}_k \triangleq \frac{\partial \mathbf{r}_k}{\partial \mathbf{x}_k^T} = \begin{bmatrix} \frac{x_k - x^1}{d_k^1} - \frac{x_k - x^r}{d_k^r} & 0 & \frac{y_k - y^1}{d_k^1} - \frac{y_k - y^r}{d_k^r} & 0 \\ \frac{x_k - x^2}{d_k^2} - \frac{x_k - x^r}{d_k^r} & 0 & \frac{y_k - y^2}{d_k^2} - \frac{y_k - y^r}{d_k^r} & 0 \\ \vdots & \vdots & \vdots & \vdots \\ \frac{x_k - x^{N-1}}{d_k^{N-1}} - \frac{x_k - x^r}{d_k^r} & 0 & \frac{y_k - y^{N-1}}{d_k^{N-1}} - \frac{y_k - y^r}{d_k^r} & 0 \end{bmatrix} \quad (4.12)$$

d_k^i is the 3D euclidean distance between the target at t_k and sensor i , i.e. $d_k^i = \|\mathbf{x}_k^P - \mathbf{s}^i\|$.

$$\Sigma_k = \begin{bmatrix} (\sigma_k^1)^2 + (\sigma_k^r)^2 & (\sigma_k^r)^2 & \cdots & (\sigma_k^r)^2 \\ (\sigma_k^r)^2 & (\sigma_k^2)^2 + (\sigma_k^r)^2 & \cdots & \vdots \\ \vdots & \ddots & \ddots & \vdots \\ (\sigma_k^r)^2 & \cdots & \cdots & (\sigma_k^{N-1})^2 + (\sigma_k^r)^2 \end{bmatrix} \quad (4.13)$$

The objective of our study is to minimize a scalar value related to the inaccuracy of the estimate of the position of the moving target. We can get the MSE of the estimate using $P_{k,k} = \mathbf{M}_{k,k}^{-1}$ and adding the components for the x and y coordinates. Finally, we obtain an accuracy metric for the state estimation of a single trajectory averaging for the whole set of instants T_{MSE}

$$T_{\text{MSE}} = \frac{\sum_{k=1}^K \left((P_{k,k})_{1,1} + (P_{k,k})_{3,3} \right)}{K}, \quad (4.14)$$

where K is the last instant.

4.6 Conclusions

We have presented an optimization of the placement of sensors for target localization considering several performance measures of the CRLB. We have seen that there is a trade-off between most of these metrics for our particular case. The performance of the unweighted least squares solution has also been improved by optimizing the obtainable RMSE and the isotropy of the solution of the localization problem as well. Our results are sets of Pareto optimal solutions that can be checked by the resource manager to select a desire performance according to the current needs. We can also use the deployment patterns that we obtained — the point clouds — for different values of the objective functions to generate trajectories for the sensors — in case they can be in motion. This approach results in a mobile positioning system whose sensors can be rearranged according to the desired criteria and the estimated position of the target.

The optimization of these metrics was suggested as future work by [Yang et al., 2012], but the effect that a solution that optimizes only one criterion can have on the other was never shown. Analyzing the Pareto front in both spaces (decision variables and objectives) we have a total overview of the solutions together with the values of the objectives, as we can see in the figures of Section 4.4. The other approaches that obtain a single solution would have needed to apply some weights to compute a single objective function, losing all the information that we have with the Pareto front. Regarding the application field of this proposal, it can be applied to any localization system based on range-difference measurements. Adapting the method to other kind of measurements should be easy. The strengths of the proposed methods can be summarized as follows: We have proposed a sensor placement method that is based on a well known multi-objective optimization algorithm, hence it can be easily implemented since it is included in most open and commercial software for numerical analysis. We have already stated how optimizing a single accuracy criterion may lead to sub-optimal solutions, e.g. minimizing the volume of the error ellipsoids may lead to elongated ellipsoids with an unacceptable error in the major axis direction. On the other hand, focusing only on finding solutions whose error ellipsoids axes are equal may lead to a higher MSE than optimizing the length of the axis. Combining the two objectives and obtaining the Pareto front we can get a full set of Pareto efficient solutions. The human expert can check these solutions and select one of them according to the current needs of the system. We avoid computing derivatives of the objective functions by using a genetic algorithm, thus we do not need to simplify the problem finding tractable mathematical expressions. Finally, we do not limit our final solutions to a subset of grid points that were decided before solving the problem.

The next steps of this work are presented in the next chapter and involve its extension to sensor placement in complex zones. These new ROIs may have obstacles that cause occlusions on some sensors so that we have to take care of the coverage. At first, we do not know how many sensors should we use to properly cover a complex ROI. We will include mutation operators that alter the number of sensors of a set. Using more sensors will increase the accuracy and coverage in the area, or at least it will not reduce it. In order to look for an optimum number of deployed sensors we need to define a metric that evaluates the difference of the objective functions as well as the drawbacks of including more sensors, i.e. the increase of computational cost, energy consumption, and cost of the whole system. For the time being we will just consider the amount of sensors as another objective to be minimized.

Chapter 5

Optimization of the coverage and accuracy of an indoor positioning system with a variable number of sensors

This chapter describes the second contribution of this thesis, which extends the methods applied in Chapter 4 to situations where the number of sensors is not fixed and there are obstacles in the ROI that cause occlusions. Main results were published in [Domingo-Perez et al., 2016a], whereas prior work appeared in [Domingo-Perez et al., 2014]. The chapter is organized as follows. We introduce the topic in Section 5.1. The problem of sensor placement considering accuracy and coverage objectives is introduced in Section 5.2. Section 5.3 explains our proposed algorithm to deal with the problem after highlighting the drawbacks of the algorithm previously used. Results are shown in Section 5.4. Finally, we draw conclusions in Section 5.5.

5.1 Introduction

We apply again evolutionary multi-objective optimization (EMO) to obtain the optimum sensor placement in this chapter. Inspired by [Chaudhry et al., 2011], we have adapted the well known NSGA-II [Deb et al., 2002] to solve the sensor placement problem for target localization. This chapter continues our work of Chapter 4, where we used a standard multi-objective genetic algorithm to place sensors considering multiple criteria. In that chapter, we placed a fixed number of sensors for localization with range-difference measurements while considering several criteria related to accuracy. However, the shape of the ROI was very simple and

each sensor could almost cover the whole area. When introducing obstacles that cause occlusions to the sensors, we do not know a priori how many sensors should we deploy. Hence, it would be a good idea to obtain Pareto fronts with the trade-off between accuracy, coverage, and amount of sensors.

This contribution introduces the problems that appear when applying the algorithm without modifications considering a variable number of sensors. When the number of sensors of different sets is not fixed to a single constant, the population has individuals with different sizes. The amount of sensors is now an objective to be minimized, but we also have the problem of performing genetic operators that involve individuals of different size. We will also see that the obtained Pareto front is biased toward the solutions with lower number of sensors. Because of these reasons, we opt to modify the original NSGA-II adding speciation and evolving subpopulations according to the size of different sensor sets. Results show a considerable improvement over standard NSGA-II. Overall, we can summarize the global advantages of our work compared to those contributions in optimum sensor placement for target localization:

- The multi-objective optimization of different metrics from the CRLB. Most of the related proposals deal with the determinant of the FIM. This metric is related to the volume of the error ellipsoid. However, an elongated ellipsoid may result in a small volume, whereas the error in the major axis is high.
- We do not constrain the position of the sensors.
- The consideration of obstacles that can cause occlusions to NLOS sensors. We must therefore maximize the coverage of the ROI.
- The number of sensors can vary within an interval. Searching solutions with high accuracy but a low amount of sensors is also an objective.
- Since we optimize conflicting objectives, we obtain a set of Pareto optimal solutions. We find this to be the greatest advantage of multi-objective optimization, since we obtain every optimal solution and know the values of the objectives. This information can be used by the resource manager according to the current needs and availability. To the best of our knowledge, there are not any other researchers that address the sensor placement problem for localization this way. A comprehensive review of multi-objective optimization applied to sensor networks was recently published [Iqbal et al., 2015]. Most of the approaches referenced in the survey focus on sensor deployment for optimizing coverage and energy management, and those that deal with target tracking just address the sensor scheduling problem [Cao et al., 2013; Hu et al., 2013]. MOO was used in [Laguna et al.,

2009] to obtain the optimal layout of beacons in an IPS. However, the accuracy metric was very simple — DOP — and does not provide much information about the position error. The other objectives are mostly similar to ours, namely, the amount of sensors and the amount of area which is not covered by the IPS.

5.2 Problem statement

In order to obtain an optimum sensor deployment scheme, we focus on three design criteria, namely, number of sensors, accuracy, and coverage. We aim to develop an algorithm that automatically finds optimal deployment patterns that minimize the number of sensors in use and the uncertainty of the target position estimation while maximizing the coverage. There is obviously a trade-off among these criteria, since the accuracy and coverage improve as long as the number of sensors increases. Different accuracy measures are also in conflict with each other. Thus, we do not obtain a single optimum solution, but a set of optimal solutions, the so-called PF. Selecting one of these Pareto-optimal solutions involves the application of high-level criteria. The advantage of finding the Pareto front of the sensor deployment problem is the fact that the resource manager knows every possible solution; therefore, he can select one of them according to the current needs or the availability of resources. To summarize, we will use the algorithm presented in Section 5.3 to solve a multi-objective optimization problem. The objectives under consideration are described in this section. The decision variables are the coordinates of the sensors. The amount of decision variables changes according to the number of sensors. Since the sensors cannot be deployed out of the ROI or within obstacles, our constraints are these boundaries. The last constraint is the amount of sensors, which is given by two values representing the minimum and the maximum number. We detail the actual parameters of the problem at the beginning of each example of Section 5.4.

5.2.1 Accuracy objectives

We use again performance metrics of the CRLB as described in Section 4.2, so we will not repeat them again. In order to keep it simple, we consider in this chapter only the trace — MSE — and the circularity measure of the CRLB. The two metrics are denoted by f_{MSE} and f_{circ} , respectively. Equations (5.1) and (5.2) show their computation, where operator $\text{eig}(\cdot)$ is the vector of eigenvalues of its argument.

$$f_{\text{MSE}} = \sum \text{eig}(\mathcal{I}^{-1}) \quad (5.1)$$

$$f_{\text{circ}} = \frac{\max(\text{eig}(\mathcal{I}^{-1}))}{\min(\text{eig}(\mathcal{I}^{-1}))} \quad (5.2)$$

The eigenvalues of a covariance matrix are proportional to the length of the axes of the ellipsoid. Equation (5.1) is equivalent to the trace of \mathcal{I}^{-1} , which is the MSE. Dividing the maximum eigenvalue by the minimum provides a measure of the circularity — see Equation (5.2). The goal is to keep f_{circ} as close to one as possible, without incrementing the value given by f_{MSE} .

After defining the ROI where the localization of the target takes place, we select P test points as candidates for the true localization of the target. A regular square or cubic grid is considered for obtaining these points. After obtaining the P evaluations of the performance measures, we need a scalar value related to the evaluation of the metric for the whole region. According to the requirements of the resource manager, it could be interesting to focus on the worst case or on the average uncertainty of the region. In the previous chapter we considered both metrics; however, in these examples we will only optimize the average uncertainty f_{avg} in a ROI as expressed in Eq. (5.3).

$$f_{\text{avg}} = \frac{\sum_{j=1}^P (w_j f_{\text{metric}})}{\sum_{j=1}^P w_j} \quad (5.3)$$

The function f_{metric} could be any of Eqs. (5.1) and (5.2). The weights w_j $j = 1, 2, \dots, P$, take real values between 0 and 1 to vary the priority given to different zones. Note that when NLOS conditions are present, we replace P with the amount of points which are covered. Hence, non-covered positions do not affect the accuracy metrics.

5.2.2 Coverage objective

The indoor positioning system should be able to provide the localization of a target in any part of the ROI. When estimating a 2D position with RDOA, it is necessary to acquire at least two range-difference measurements that provide two intersecting hyperbolae. Thus, we need at least three distance measurements to perform localization. The target must therefore be within the scope of at least three sensors, only when this condition is satisfied the target is considered to be 3-covered. To ensure a high degree of coverage for localization we need to optimize the k -coverage of the ROI, where $k = 3$ in 2D localization and $k = 4$ in a 3D scenario. We consider that a point of the ROI is covered by a sensor if the point has a LOS connection with the sensor, and we denote with P_k the number of points of the grid that are k -covered. Maximizing the division of this number by the total amount of test points P increases the percentage of the ROI which is k -covered:

$$f_{k\text{-cov}} = \frac{P_k}{P} \quad (5.4)$$

We should clarify that we only consider that a point is covered by a sensor if there is a LOS connection between the point and the sensor. Of course, the sensor will not detect anything if its distance to the target is sufficiently high. In our prior work published in [Domingo-Perez et al., 2014], we considered a coverage radius after selecting a desired deviation of the distance measurement from Fig. 4.2b. For the sake of simplicity, we will not do it here. However, it will not have any influence on the solution since sensors which are far from the target will not contribute to the MLE solution as seen in Chapter 3. The coverage radius can also be used to calculate the minimum number of sensors so that the area is covered. In [Domingo-Perez et al., 2014] we used the approach described in [Li and Kao, 2010]. A fraction of the coverage radius r_c is used to reduce the k -coverage problem to $k = 1$. Finally, the minimum number of sensors that cover a surface of area A is given by $N_{\min}^k = \frac{4Ak}{3\pi r_c^2}$. This approach considers that the area covered by a sensor is a circle of radius r_c and approximate it to an hexagon. This method can be useful to determine the range of the number of sensors that it considered by our algorithm in case we want to assure a full coverage.

5.3 Proposed algorithm

At the beginning of this section we describe the problems that we have encountered when applying NSGA-II to the sensor placement problem. Then we introduce and justify the modifications that we propose for NSGA-II. We have used the DEAP framework available for Python [Fortin et al., 2012] to implement an evolutionary algorithm based on NSGA-II and to obtain the results that we present in Section 5.4.

NSGA-II starts ranking the population and assigning the crowding distance to the individuals. The algorithm compares the values that the individuals achieve after evaluating the objectives. An individual dominates another individual if all the evaluated objectives of the former are better than those of the latter. Individuals that are not dominated by any other individual belong to the first front, which is called the PF. Individuals that are only dominated by those individuals of the PF are assigned to the second front, and so on. Once the population is ranked, the crowding distance is computed for each individual of a same front. The crowding distance is an estimation of the perimeter of the cuboid formed by an individual and its immediate neighbours of the front in the objective space. Among the individuals of the same front, NSGA-II prefers those with a higher crowding distance so as to keep diversity within the population. After the assignation of non-dominance and crowding distance, the algorithm

continues with the usual steps of a genetic algorithm (GA), namely, selection, crossover, and mutation. When selecting the parents, the individuals compete in a tournament selection. The algorithm selects the individual of the lowest front. In case they belong to the same front, the individual whose crowding distance has a higher value is preferred. Crossover and mutation operators create a new offspring population, which is merged with the original population. Finally, this bigger population is reduced to the size of the original population after reassigning non-dominance and crowding distance. The reader can go deeper into NSGA-II through the aforementioned work [Deb et al., 2002].

In [Domingo-Perez et al., 2016b] we used the algorithm out-of-the-box as it is implemented in MATLAB for deploying a fixed number of anchor nodes. The obtained results were satisfactory; however, when applying the algorithm for deploying a variable number of anchor nodes we do not obtain a full PF. We should be able to obtain the same solutions that we would get running the algorithm for different fixed numbers of anchor nodes independently. Of course, the algorithm must discard those solutions that achieve a lower accuracy even though their number of sensors is higher. After running NSGA-II for deploying 3 to 8 sensors in a regular square, the obtained solutions are biased towards the lowest number of sensors. Figure 5.1 is useful for explaining this tendency.

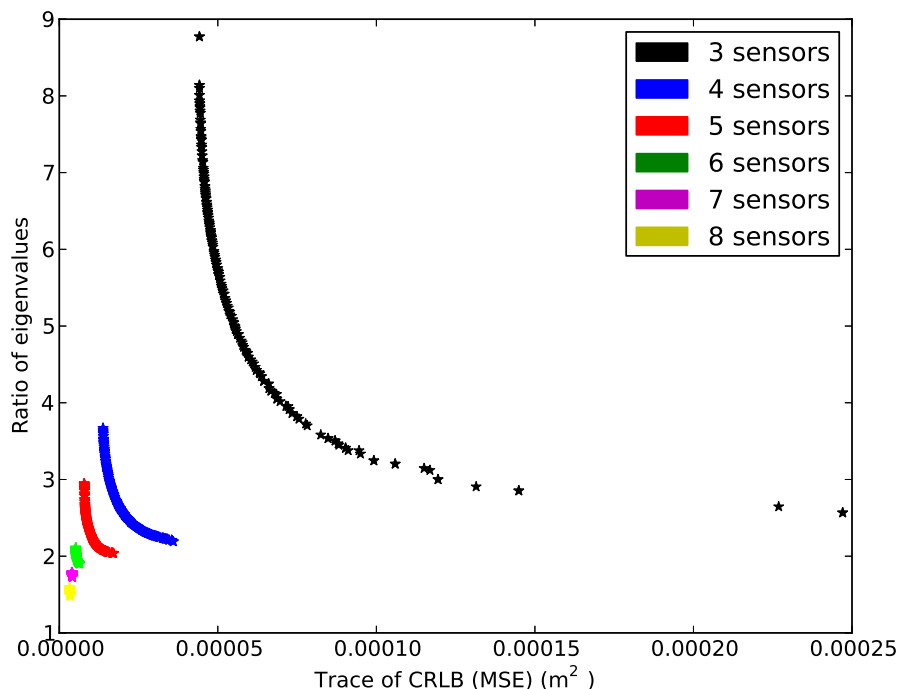


Figure 5.1: Pareto fronts of two uncertainty metrics for different numbers of anchor nodes

Figure 5.1 shows the PFs for different number of sensors after optimizing the MSE and the spread of the error ellipsoids. The solutions have been obtained with independent runs of

NSGA-II varying the number of sensors. Since each PF has the same number of points, it can be seen that the crowding distance of solutions with 3 sensors will be higher. The tournament selection of NSGA-II uses the crowding distance as a mechanism to keep the variety of the individuals within the population. It is well known that for many-objective optimization the solution's convergence of NSGA-II is usually biased and some researchers have proposed some mechanisms for diversity management [Adra and Fleming, 2011; Deb and Jain, 2014]. Among those mechanisms, evolving multiple subpopulations independently allows keeping diversity and improves the performance of the evolutionary algorithm [Garza-Fabre et al., 2011], this process is known as speciation or niching. After analyzing Fig. 5.1, it is evident that there is a wide gap in the fitness landscape according to the number of sensors. Taking this issue into account, it seems to be a good idea to consider that those topologies with the same number of sensors belong to the same species. Additionally, we use the coordinates of the anchors with real numbers as chromosomes; hence, crossover operations between individuals with different number of sensors become cumbersome and that is another reason for speciation. We also have the benefit of being able to generate new topologies using structural mutation and migration, so that a topology formed after adding or removing a sensor competes with other topologies of the same number of sensors. We took this idea from [Chaudhry et al., 2011], where authors deploy a wireless sensor network optimizing coverage, connectivity, and energy. However, they do not focus on accuracy.

Figure 5.2 provides a general overview of the proposed GA. The algorithm starts creating S subpopulations SP_k with the same size S_p . The index k of the subpopulations takes values in the range $[1, S]$. The minimum and maximum number of sensors are constant and belong to SP_1 and SP_S , respectively. The individuals of SP_2 have exactly one more sensor than SP_1 , and so on. The independent evolution of species also allows us to parallelize the creation and evolution processes. To summarize, the proposed GA is a basic NSGA-II where the population is split by the number of sensors. The subpopulations evolve concurrently, and it is possible that the amount of sensors varies due to the mutation operator. A structural mutation involves the addition or removal of a sensor. In case this happens to an individual of SP_k , a migration process moves the individual to SP_{k+1} if addition, or to SP_{k-1} when a sensor is removed. Each subpopulation undergoes four states during an iteration of the GA:

- SP_k : initial population. Population size: S_p .
- SP_k^* : evolved population, the initial population and its offspring. It can contain individuals with different number of sensors. Population size: $2S_p$.
- SP_k^{**} : evolved population without individuals with different number of sensors. Popula-

tion size varies among subpopulations.

- Trimmed SP_k^{**} : best individuals of SP_k^{**} according to NSGA-II selection; *i.e.*, non-dominance rank and crowding distance. It becomes the initial population in the next GA iteration. The size of the population is S_p .

We only evaluate the objectives — and assign ranks and crowding distances — of the individuals after creating the initial population and at the beginning of the trimming step. Once the algorithm has iterated over G generations, the resulting subpopulations are merged and the algorithm returns the PF. We do not consider the number of sensors as an objective during the GA iterations. However, after merging all the subpopulations we perform another NSGA-II selection operation including the number of sensors as a function to be minimized. This allows the algorithm to discard those solutions that achieve lower accuracy and coverage with more sensors; since they can be dominated by some individuals of species with a lower index.

Finally, we describe the genetic operators that we use to create the offspring population. The remaining aspects of the GA are common or should have already been clarified. Since the beginning of the evolution step and just before the migration process we apply a sequence of four genetic operators to the individuals of each subpopulation:

- Selection: tournament selection of two individuals. It selects S_p individuals, which will be the parents of the offspring subpopulation. Two individuals are picked randomly among the initial subpopulation. The method checks first the non-dominance rank of each individual and selects the best one, in case they belong to the same front it chooses the one with the higher crowding distance.
- Crossover: blend crossover. For each consecutive pair of two parents (\mathbf{p}_i and \mathbf{p}_{i+1}) of the list given by the previous step there is an r_x chance of generating two new individuals (\mathbf{c}_i and \mathbf{c}_{i+1}) that replace the parents, otherwise they remain unchanged. Equation (5.5) gives the new individuals:

$$\begin{aligned}\mathbf{c}_i &= (1 - \alpha) \circ \mathbf{p}_i + \alpha \circ \mathbf{p}_{i+1} \\ \mathbf{c}_{i+1} &= \alpha \circ \mathbf{p}_i + (1 - \alpha) \circ \mathbf{p}_{i+1}\end{aligned}\tag{5.5}$$

In our case, \mathbf{c} and \mathbf{p} are the coordinates of each sensor of the individual in a consecutive array. The variable α is a vector of random elements with the same length of \mathbf{p} and it takes random values in the range $[-1, 2]$. The operator \circ is the Hadamard (element-wise) product. The offspring can therefore be in the expanded cuboid formed by the parents. In case any sensor falls into any obstacle the algorithm sends them to the nearer corner so that they cover a bigger space without altering their position too much.

- Mutation: Gaussian mutation. There is an r_m chance that an individual undergoes mutation. If mutated, a random variable $v \sim (\mu_m, \sigma_m)$ is added to each gene of the individual; *i.e.*, to a coordinate. We perform again the same procedure if the sensor falls into an obstacle.
- Structural mutation: at a given chance r_s a sensor can be added to or removed from the individual. If the individual belongs to the first or last subpopulation we can only add or delete a sensor, respectively; otherwise the operation is randomly selected. When deleting, we compute the number of sensors that are LOS with each other and delete the sensor with the higher value. When there are two or more sensors with the same number of LOS sensors we compute the sum of the distance from each one of these sensors to its LOS neighbors. The sensor with the lower value is then removed. The sensor which is nearer to the others should be the sensor that adds less information, since very close sensors result in almost overlapping hyperboloids. This deletion mutation allows us to obtain a sensor placement scheme with less sensors without sacrificing a good deal of accuracy and coverage. On the other hand, when adding a new sensor we compute the k-coverage level for each grid point. We place the sensor in the point of the grid with the lowest k-coverage level; in case two or more grid points share the same value, we choose the one with the higher sum of the distances from the grid point to its LOS sensors.

5.4 Numerical example

We use the distance measurement model of an infrared system to get the covariance matrix of the observations. As was shown in Figure 4.2a, the emitter moves along the xy-plane, while the height between emitter and sensor is constant. The distance error is a function of the distance between emitter and sensor $d = \sqrt{d_{xy}^2 + 2.15^2}$ as well as the angle of incidence $\phi = \text{atan}\left(\frac{d_{xy}}{2.15}\right)$. We will not repeat the other constant parameters that model the system, which can be found in the papers that describe it [Martin-Gorostiza, 2011; Martin-Gorostiza et al., 2014]. Finally, Fig. 4.2b showed the evolution of the standard deviation of the distance measurement error σ_d versus the distance in the xy-plane d_{xy} . Since we know the height of the emitter, we perform 2D localization in the horizontal plane.

We use the same probabilities for the genetic operators during the simulations that appear in the following subsections. Table 5.1 shows these values.

After each test, we provide the average execution time of each iteration of the algorithm. The code has been run in an Intel® Core™ i7-4712MQ mobile processor with 8GB RAM DDR3

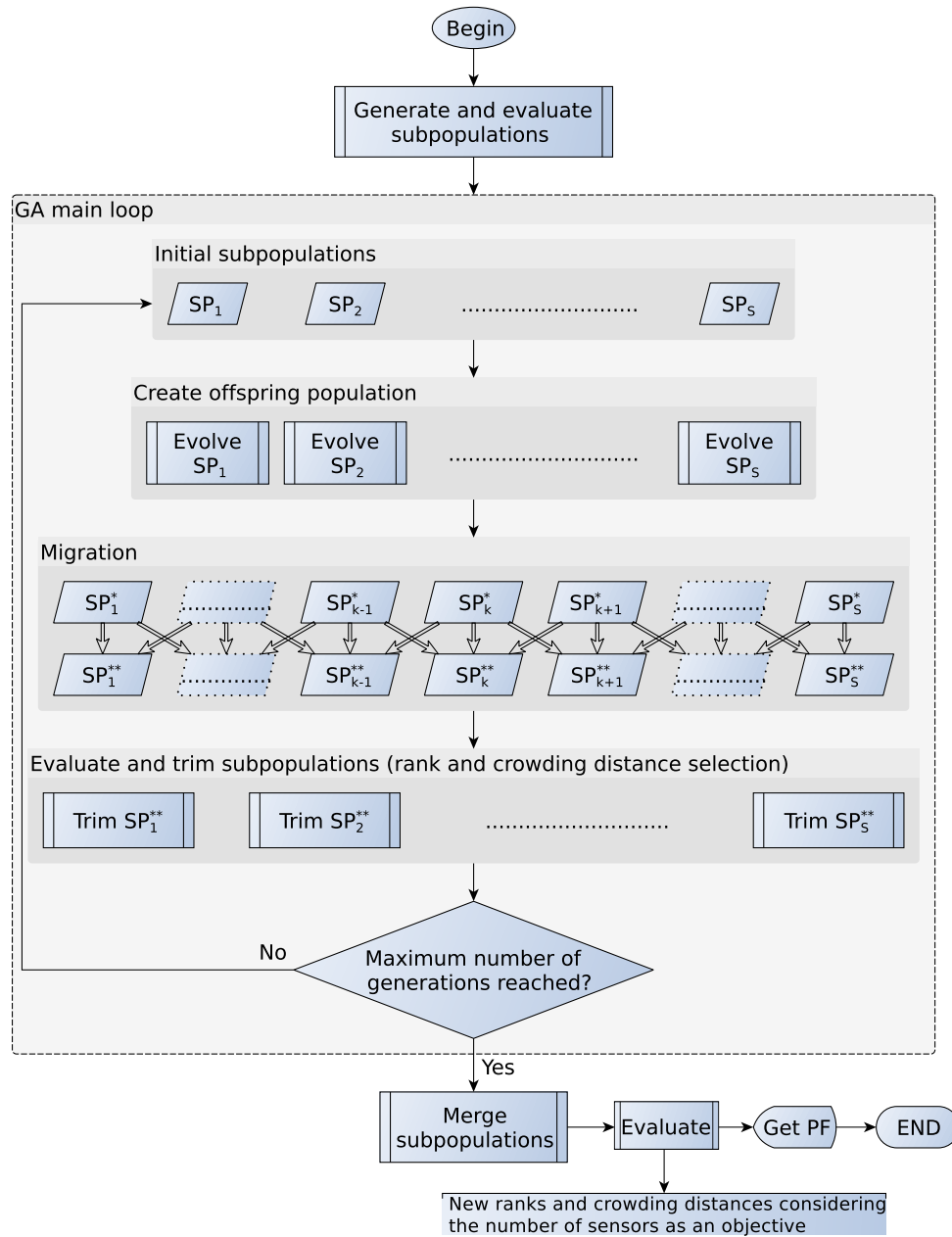


Figure 5.2: Proposed GA

1333 MHz.

Putting it all together, we define a model of the ROI and a grid of points, which are the candidates for the location of the target. Our approach evaluates the objectives using these points as the position of the target and then it obtains a metric related to the whole area (e.g., the average accuracy). The algorithm starts generating a random population — sets of sensors placed in the ROI — and evaluating the objective functions for each individual. To compute the accuracy metrics, which are based on CRLB, we use the infrared model to obtain the covariance of the distance measurements and get the value of CRLB. After evaluating the population, the algorithm starts iterating until a given number of generations is reached. Finally, it returns the PF.

Table 5.1: Probabilities of the genetic operators

operator	Symbol	Probability
Crossover	r_x	0.80
Mutation	r_m	0.10
Structural mutation	r_s	0.05

5.4.1 LOS sensors

These results show the Pareto front for a sensor placement case when there is always a LOS path between the emitter and the sensors. It is the same case studied in [Domingo-Perez et al., 2016b] without fixing the number of sensors to a scalar constant. We consider six subpopulations and the amount of sensors varies in the range 3–8. Each subpopulation contains 100 individuals. The ROI is a 9 m^2 regular square and we evaluate 121 positions regularly separated by 3 cm and equally weighted. The Pareto front with NSGA-II has been obtained with a population of 600 individuals, where only individuals with the same number of sensors can perform crossover. We have run the algorithm for 2000 generations. The average time per iteration of the algorithm was 12 s. Figure 5.3 evidences the benefits and necessity of speciation.

The Pareto front has been split in six graphs according to the number of sensors. Each algorithm returns the same amount of Pareto solutions. As stated above, the solutions obtained with NSGA-II tend to the lowest amount of sensors, whereas the proposed algorithm can control the amount of solutions of each subpopulation. Hence, it converges to a Pareto front closed to that of Figure 5.1. Table 5.2 concludes this case study by providing a comparison of both algorithms.

5.4.2 Occluded sensors

This section shows the application of the algorithm for the same cases of [Domingo-Perez et al., 2014]. In that paper the standard NSGA-II did not converge to a smooth Pareto front. In addition, it can be seen that many solutions provide a high position error. The new algorithm provides a better convergence, as can be seen in the following results. We include a comparison with random deployment to show the benefits of using a deployment algorithm. The values of the objectives with random deployment have been obtained averaging 50 random sensor sets for each number of sensors. Instead of considering a coverage radius, we consider that a point is in the scope of a sensor if there is a straight line that joins them without crossing any obstacle. The degradation of the accuracy in points which are not near a sensor is taken into account in

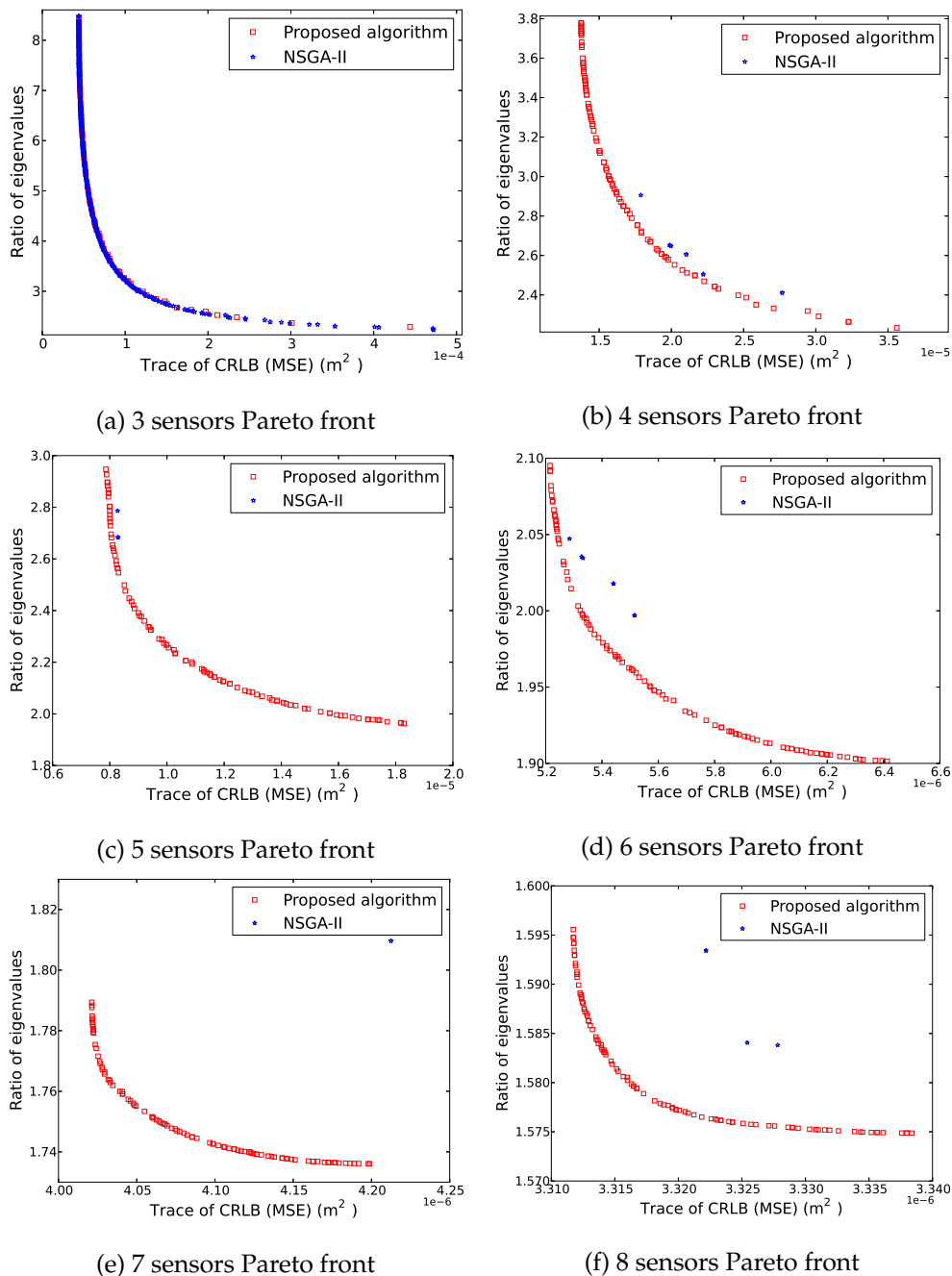


Figure 5.3: Comparison of Pareto fronts with NSGA-II and the proposed algorithm

the measurement error model, as was shown in Figure 4.2b.

Case 1: one obstacle

This case study focuses on the placement of 5 to 12 sensors in a 25 m^2 regular square with an obstacle in the center. The obstacle is a 1 m^2 square column. We evaluate a total of 112 grid points which are regularly separated by 0.5 m and equally weighted. The objectives to be optimized are the averaged trace of the CRLB and the percentage of the points which are at

Table 5.2: Extreme values of the Pareto fronts with NSGA-II and the proposed algorithm

Algorithm	Amount of Sensors	Amount of Solutions	Lowest CRLB Trace (m ²)	Lowest Ratio of Eigenvalues
NSGA-II	3	573	4.4085e-5	2.0723
	4	9	1.7882e-5	2.4111
	5	3	8.2704e-6	2.6833
	6	7	5.2845e-6	1.997
	7	4	4.117e-6	1.8098
	8	4	3.3222e-6	1.5838
Proposed algorithm	3	100	4.4083e-5	2.0397
	4	100	1.3753e-6	2.2331
	5	100	7.8631e-6	1.9624
	6	100	5.2156e-6	1.9014
	7	100	4.0213e-6	1.7361
	8	100	3.3117e-6	1.5749

least 3-covered. Each subpopulation contains 100 individuals and the algorithm was run for 2000 generations. Each iteration of the algorithm took 55 s on average. Figure 5.4 shows some Pareto optimal solutions, and a comparison of our algorithm with random deployment can be seen in Table 5.3.

Our algorithm outperforms random deployment considerably, and the lower the number of sensors the higher the evidence. The higher coverage is achieved with any amount of sensors. With a low number of sensors and the presence of occlusions it may easily happen that some points of the ROI are only in the scope of collinear sensors. In case this happens, the accuracy of the target localization in these points will be very poor — see Table 5.3, five sensors with random deployment. As shown in Figure 5.4, the symmetry of the solutions is also a good indicator of the algorithm's performance.

Case 2: two obstacles

In this example we place 5 to 15 sensors in a room with the same shape considering the presence of two obstacles. The obstacles are again 1 m² square columns, their center points are [1.25, 2.5] and [3.75, 2.5]. The subpopulations can contain 20 individuals. The algorithm has been run for 1000 generations and each iteration took 30 s on average. Figure 5.5 shows some Pareto

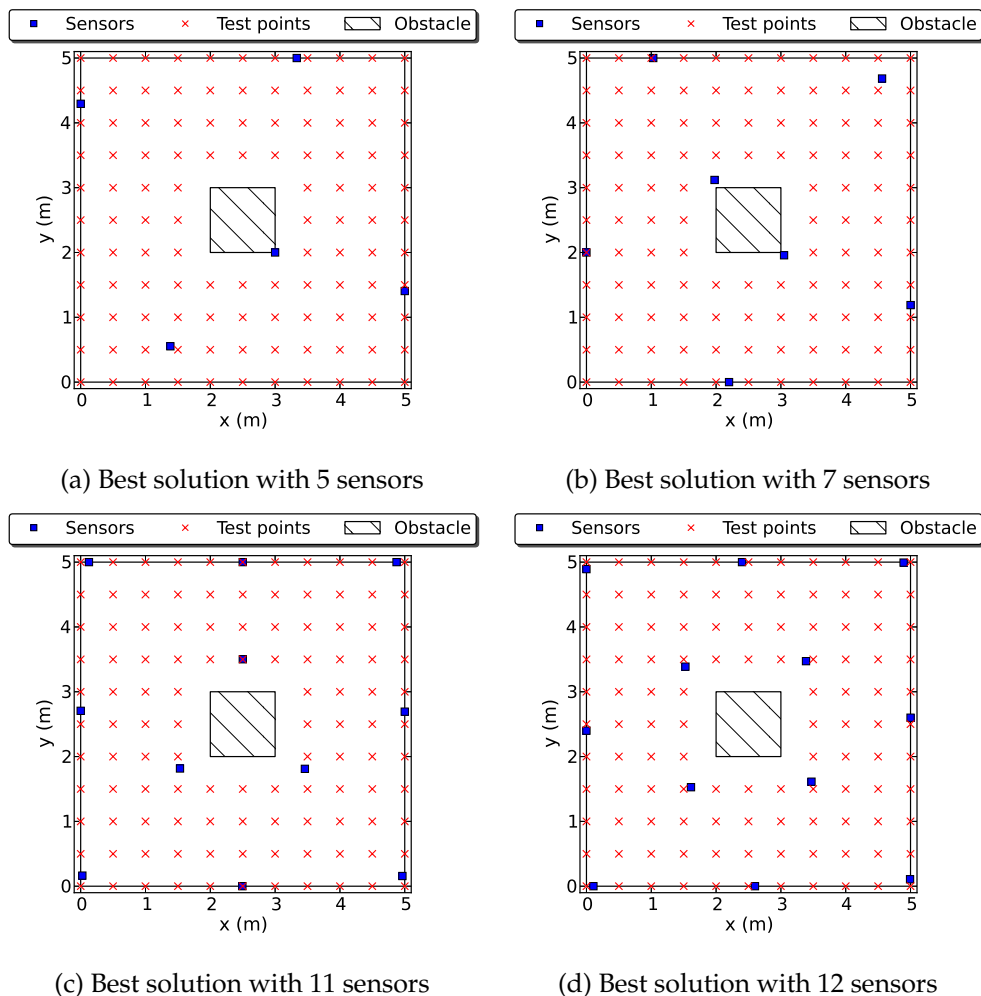


Figure 5.4: Some optimal configurations found by the proposed algorithm when deploying 5 to 12 sensors with an obstacle in the center. The whole ROI is at least 3-covered in all cases.

optimal solutions. The full coverage is not always achieved with the best accuracy and we show the extreme solutions of the Pareto front in these cases. When the solution with the best accuracy provides full coverage the Pareto front is made of a single solution and there is no actual trade-off. The configurations show a certain degree of symmetry, some basic shapes can also be recognized. Table 5.4 provides a comparison with random deployment. We only show the worst values of the Pareto front for each objective, the improvement is evident.

Finally, after analyzing these solutions, it can be seen that sensors are usually placed near the boundaries of the 5×5 m square and the obstacles. We can consider an intuitive approach that places sensors in these boundaries regularly. However, this solution has probably the highest target-sensor distance; hence, it would be a good solution when the error due to distance between sensor and target is low or negligible. We must also take into account the fact that the area covered by a sensor decreases when the sensors are placed in the boundaries of obstacles.

Table 5.3: Comparison of the Pareto optimal solutions obtained by the proposed algorithm and random deployment for the case with one obstacle. The values for random deployment have been obtained averaging 50 random placed sets of sensors for each amount of sensors.

Amount of Sensors	Proposed Algorithm		Random Deployment	
	CRLB Trace (m ²)	Coverage	CRLB Trace (m ²)	Coverage
5	9.5475e-5	1	2.1418	0.9116
6	4.1925e-5	1	0.5002	0.9552
7	2.1706e-5	1	0.5471	0.992
8	1.2324e-5	1	0.0382	0.9875
9	9.4244e-6	1	2.3467e-4	0.9989
10	6.9933e-6	1	1.5574e-4	0.9989
11	5.7051e-6	1	1.1498e-4	0.9996
12	4.7841e-6	1	6.4065e-4	0.9998

Nevertheless, we have evaluated this intuitive solution for the cases of one and two obstacles. We have placed sensors in the corners (internal and external squares, 8 sensors for the first case and 12 sensors for the second). Placing 8 sensors in the corners of the one obstacle case provides an average CRLB trace of $4.595e-5$ m². Comparing this value with Table 5.3 it can be seen that we obtain a better accuracy with 6 sensors. When we place 12 sensors in the corners of the case with 2 obstacles we get an accuracy of $1.533e-5$ m², which can be improved with 9 sensors according to Table 5.4. Anyway, this intuitive solution could also be a good starting point for generating the first population.

5.5 Conclusions

This chapter has presented a MOEA for deploying a variable number of sensors for RDOA localization. Our results have shown a great improvement over random deployment in some NLOS scenarios, which is singularity-prone in complex scenarios. We have used speciation and structural mutations on NSGA-II, which is included in most standard libraries. Using this approach we have avoided obtaining a solution which is biased towards the lowest number of sensors. The algorithm should therefore be easy to implement modifying these libraries. We have applied it on an infrared RDOA positioning system with a fairly complex measurement noise model. Additionally, using RDOA implies that the covariance matrix of the observations

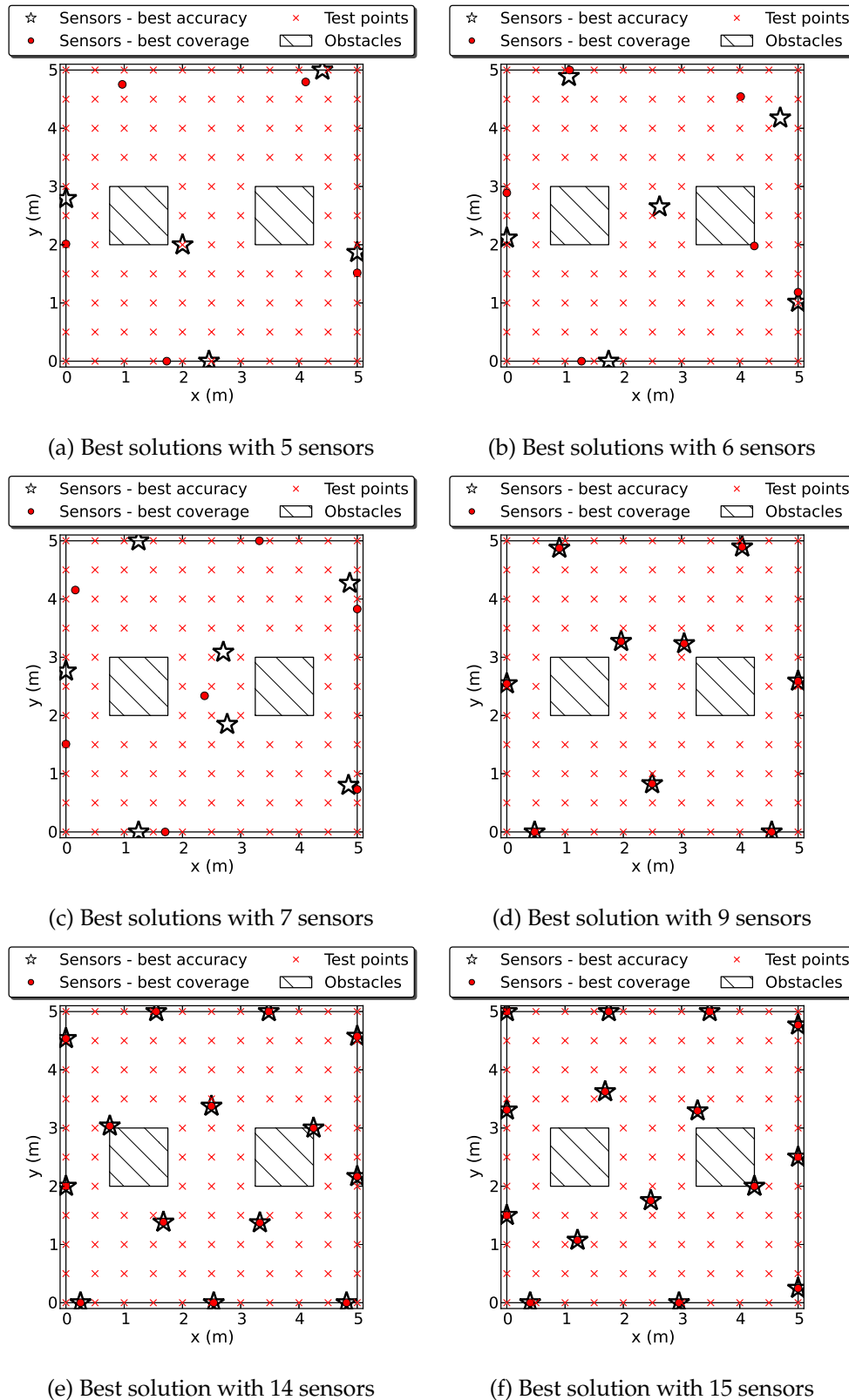


Figure 5.5: Some optimal configurations found by the proposed algorithm when deploying 5 to 15 sensors with two obstacles. The first three figures show optimum coverage and accuracy deployment, whereas the two objectives are simultaneously optimized in the other cases.

Table 5.4: Comparison of the worst Pareto values obtained by the proposed algorithm and random deployment for the case with two obstacles. The values for random deployment have been obtained averaging 50 random placed sets of sensors for each amount of sensors.

Amount of Sensors	Worst Pareto Values with Proposed Algorithm		Random Deployment	
	CRLB Trace (m ²)	Coverage	CRLB Trace (m ²)	Coverage
5	2.0486e-4	0.7523	0.2175	0.7593
6	9.2725e-5	0.9817	0.5072	0.8930
7	3.2163e-5	0.9817	0.0178	0.9349
8	1.5879e-5	1	0.0123	0.9624
9	1.2524e-5	1	0.009	0.9679
10	9.4426e-6	1	2.9721	0.9811
11	7.0657e-6	1	0.3861	0.9868
12	5.8686e-6	1	8.2985e-4	0.9910
13	5.1978e-6	1	6.883e-3	0.9901
14	4.4578e-6	1	0.4218	0.9936
15	4.0501e-6	1	1.508e-4	0.9963

is not diagonal. Dealing with algebraic methods in such a system is quite hard or even unfeasible. However, with an evolutionary algorithm we only need to evaluate the objectives without resorting to the computation of complicated derivatives. The structural mutations should improve the performance and speed of the algorithm. This can intuitively be seen with the shapes of some placement patterns. Deploying four sensors, we find the optimum configuration to be a square; whereas the configuration that optimizes the placement of five sensors is a square with a sensor in the center. It is evident that once we have obtained one of those solutions we can obtain the other one with a structural mutation in a single step. Other approaches that considered modifying the number of sensors are [Laguna et al., 2009] and [Leune et al., 2013]. The latter places or deletes the new sensor randomly. When deleting, there is only a $1/N$ chance of deleting the worst sensor; when adding a new sensor, it may be placed in a point where it does not provide much information. As for the former work, it deletes the sensor with the lowest contribution to the objective function. However, it goes only backward. This has two drawbacks, namely, the algorithm cannot be parallelized and the higher the amount of sensors the higher the computational cost.

Chapter 6

Conclusions and future work

Section 6.1 summarizes the contributions of this thesis. A list of publications of the work related to this thesis is shown in Section 6.2. Finally, we propose future research lines in Section 6.3.

6.1 Conclusions

The contributions of this thesis have already been stated in the respective sections of chapters 4 and 5. Here, we will only state the novel ideas explicitly to summarize and highlight our contribution to the state-of-the-art.

In Chapter 2 we have exposed the most usual localization techniques first. Even though our work focuses on RDOA, we have seen that the methods we use can be easily adapted to range-only, RSS, or AOA. Then, we have provided a thorough review of the current sensor deployment methods. We can see that there is a clear distinction among three approaches. Those methods that deal with sensor deployment to locate a single point usually provide an analytical treatment of the problem. Most of them optimize the determinant of the FIM or the DOP. They have theoretical importance, since they allow to mathematically express the relation between the relative position of the sensors and the localization error. However, they rely on oversimplifications of the problem so that they obtain mathematically tractable expressions. Hence, they cannot be used in real applications where we focus on a whole ROI or the measurement model is complex. To the second group belong those approaches that focus on covering whole areas or several targets, this thesis belongs to this group as well. Our main contribution is the consideration of several metrics of the covariance of the estimation and the proposal of a new algorithm based on NSGA-II to deploy sensors taking the presence of obstacles into account. Finally, the third group is made of methods that solve the combinatorial problem of selecting the best candidates out of a given set of possible positions. These methods need to a

priori decide the possible positions of the sensors. Additionally, they have only been applied to uncorrelated observations.

Chapter 4 has shown the first contribution of this thesis; that is, the MOO of several performance metrics of the covariance of the estimation. We optimize the CRLB as a limit on the attainable performance. The five proposed metrics are the trace of the CRLB, which is the MSE; the determinant of the CRLB; the maximum eigenvalue; the ratio of maximum and minimum eigenvalues, which is the condition number of the CRLB; and a measure of the variance in a given direction. The condition number is not usually taken into account. If we check those contributions that deal with optimal FIM for locating a single source, its optimal form is a diagonal matrix whose eigenvalues are equal. Hence, it is obvious that the FIM with minimum determinant provides the optimum condition number. However, as can be seen in Section. 4.4, when considering the grid points over a ROI there is a trade-off between the condition number of the CRLB and its trace or determinant. Exploiting this set of placements we have improved the performance of NLS searching the best configuration among the solutions of the PF. Additionally, we can provide more information in terms of error ellipsoids. Whereas other solutions provide just the DOP or a metric of the CRLB, we can say that the solution we choose will have a certain average MSE, a given isotropy of the error ellipsoids, and keep the maximum deviation below a threshold.

Finally, Chapter 5 proposes a new MOEA to solve the sensor placement problem. We have modified the probably most used MOO algorithm and obtained satisfactory results. As shown in the chapter, NSGA-II did not provide a full PF when we optimized the MSE, ratio of eigenvalues, and number of sensors. Additionally, we found the problem of performing crossover operations with set of sensors whose number is different. Dividing the whole population in subpopulations with the same number of sensors — speciation — allowed us to overcome those problems. In addition, we tested the algorithm including obstacles in the ROI that can cause occlusions due to NLOS conditions. The comparison with random placement highlights the importance of using a deployment algorithm.

6.2 Publications derived from the thesis

6.2.1 Peer-reviewed journals

- **Domingo-Perez, F.,** Lazaro-Galilea, J.L., Wieser, A., Martin-Gorostiza, E., Salido-Monzu, D., and Llana, A. (2016). Sensor placement determination for range-difference positioning using evolutionary multi-objective optimization. *Expert Systems with Applications*,

47:95–105.

Journal Citation Reports Impact Factor (2015): 2.981. Category: *Operations Research & Management Science* 6/82 Q1.

- **Domingo-Perez, F.**, Lazaro-Galilea, J.L., Bravo, I., Gardel, A., and Rodriguez, D. (2016). Optimization of the coverage and accuracy of an indoor positioning system with a variable number of sensors. *Sensors*, 16(6):934.
Journal Citation Reports Impact Factor (2015): 2.033. Category: *Instruments & Instrumentation* 12/56 Q1.

6.2.2 International conferences

- **Domingo-Perez, F.**, Lazaro-Galilea, J.L., Martin-Gorostiza, E., Salido-Monzu, D., and Wieser, A. (2013). Accuracy of an indoor IR positioning system with least squares and maximum likelihood approaches. In *International Conference on Indoor Positioning and Indoor Navigation (IPIN 2013)*, pages 22–23.
- **Domingo-Perez, F.**, Lazaro-Galilea, J.L., Martin-Gorostiza, E., Salido-Monzu, D., and Wieser, A. (2014). Evolutionary optimization of sensor deployment for an indoor positioning system with unknown number of anchors. In *Ubiquitous Positioning, Indoor Navigation, and Location Based Services (UPINLBS 2014)*, pages 195–202.
- **Domingo-Perez, F.**, Lazaro-Galilea, J.L., Bravo, I., Martin-Gorostiza, E., Salido-Monzu, D., Llana, A., and Govaers, F. (2015). Sensor deployment for motion trajectory tracking with a genetic algorithm. In *IEEE International Conference on Industrial Technology (ICIT 2015)*, pages 3435–3439.

6.2.3 Other contributions

Applications of the methods described in this dissertation to work of other researchers:

- Martin-Gorostiza, E., **Domingo-Perez, F.**, Lazaro-Galilea, J.L., Meca-Meca, F.J., Wieser, A., and Salido-Monzu, D. (2016). Specular multipath model for an optimal anchor placement evolutionary algorithm. In *International Conference on Indoor Positioning and Indoor Navigation (IPIN 2016)*.

- Macho-Pedroso, R., **Domingo-Perez, F.**, Velasco-Cerpa, J., Losada-Gutierrez, C., and Macias-Guarasa, J. (2016). Optimal microphone placement for indoor acoustic localization using evolutionary optimization. In *International Conference on Indoor Positioning and Indoor Navigation (IPIN 2016)*.

6.3 Future work

This section acknowledges some of the weaknesses and limitations of our proposed solutions. To summarize, we have chosen to use methods that have some drawbacks and a simple measurement model without considering extra sources of errors. There are limitations that are inherent to GAs, such as its convergence to optimal solutions, parameter setting, execution time, etc. Other limitations are the applicability of our approach to real situations due to the existence of other error sources.

We have not included any real experiment in the thesis to validate the results. If the reader checks most of the papers referenced in Chapter 2, it can be seen that none of those proposals contains tests using a real implemented system. Of course, testing all the positions of sensors that belong to the Pareto fronts obtained in Chapters 4 and 5 is completely unfeasible. Furthermore, testing other configurations to check if they outperform the Pareto optimal solutions is also a cumbersome task. However, there is no reason why the methods described in this thesis should not work in real situations unless what were described in Section 3.1 of Chapter 3 and Eq. (3.6) were not true. In Eq. (3.6), we assume that RDOA measurements are Gaussian variables whose mean is the true range-difference and variance is given by the model of Section 3.1. Any source of errors that can affect the RDOA measurement will affect the optimum sensor placement as well. One of the most common and highest errors is multipath. As a result of reflections in walls, ceiling, and floor, many reflected signals reach a sensor by different paths. This phenomenon is known as multipath interference. Multipath causes an offset in the distance measurement, which should be kept to a minimum. Our group is currently working on obtaining a model that determines the offset that reflected signals cause in the final measurement. The development and application of this model is an extremely difficult task since multipath effect is highly dependable on the ROI. We should model the distance measurement as a sum of the true distance between sensor and target, the noise of the LOS signal, and the contribution of the multipath (offset). The latter term will be another objective of the optimization problem. The transition from the measurement error due to multipath and the estimated position error should also be studied.

Another line for future work is the improvement of the execution time of the algorithm

exploiting the parallelization of modern multi-core processors and graphics processing unit (GPU). As can be seen in Fig. 5.2, the migration operator is the only part of the algorithm that cannot be parallelized, whereas evolution and trimming processes can happen concurrently. The different simulations shown in this paper took from three hours up to a full day running in a laptop, which is an affordable time for an offline process. Anyway, there are some application cases of GPU implementation of NSGA-II with a significant speedup [Wong, 2009; Shen et al., 2013; Padurariu and Marinescu, 2014].

We also need to select values for the parameters of the GA, i.e., rates of crossover and mutation, number of generations, size of population, etc. A recent work [Jameii et al., 2016] proposes combining NSGA-II with a learning automata that modifies the values of the mutation and crossover probabilities according to their contribution in previous generations. This approach could be applied to avoid the effect of the rate of the genetic operators.

The reliability of the algorithm is another weak aspect. Some researchers criticize genetic algorithms because we cannot say that the solutions are optimal solutions. It is known that every Pareto optimal solution must satisfy the Karush-Kuhn-Tucker (KKT) conditions. However, the computation of these conditions requires the calculation of gradients of the objectives. There are approaches that perform a post optimality check to verify that solutions obtained by a MOEA are close to KKT points [Deb et al., 2007] and also suggest to use this proximity measure as a stop condition even in non-differentiable problems [Abouhawwash and Deb, 2016]. We have chosen not to impose a stop condition but to run the algorithm for a high number of iterations. At this moment we were not interested in evaluating or optimizing the convergence speed of the algorithm. Hence, we preferred to leave enough room for the convergence to the best possible solution.

Bibliography

- [Abel, 1990] Abel, J. S. (1990). Optimal sensor placement for passive source localization. In *International Conference on Acoustics, Speech, and Signal Processing (ICASSP 1990)*, pages 2927–2930.
- [Abouhawwash and Deb, 2016] Abouhawwash, M. and Deb, K. (2016). Karush-Kuhn-Tucker proximity measure for multi-objective optimization based on numerical gradients. In *Genetic and Evolutionary Computation Conference (GECCO 2016)*, pages 525–532.
- [Adra and Fleming, 2011] Adra, S. F. and Fleming, P. J. (2011). Diversity management in evolutionary many-objective optimization. *IEEE Transactions on Evolutionary Computation*, 15(2):183–195.
- [Banks et al., 2010] Banks, H. T., Dediu, S., Ernstberger, S. L., and Kappel, F. (2010). Generalized sensitivities and optimal experimental design. *Journal of Inverse and Ill-posed Problems*, 18(1):25–83.
- [Bishop et al., 2007a] Bishop, A. N., Fidan, B., Anderson, B. D. O., Dogancay, K., and Pathirana, P. N. (2007a). Optimality analysis of sensor-target geometries in passive localization: Part 1-bearing-only localization. In *3rd International Conference on Intelligent Sensors, Sensor Networks and Information Processing (ISSNIP 2007)*, pages 7–12.
- [Bishop et al., 2010] Bishop, A. N., Fidan, B., Anderson, B. D. O., Doğançay, K., and Pathirana, P. N. (2010). Optimality analysis of sensor-target localization geometries. *Automatica*, 46(3):479–492.
- [Bishop et al., 2007b] Bishop, A. N., Fidan, B., Anderson, B. D. O., Pathirana, P. N., and Doğançay, K. (2007b). Optimality analysis of sensor-target geometries in passive localization: Part 2-time-of-arrival based localization. In *3rd International Conference on Intelligent Sensors, Sensor Networks and Information Processing (ISSNIP 2007)*, pages 13–18.

- [Bronk and Stefanski, 2007] Bronk, K. and Stefanski, J. (2007). Bad geometry influence on positioning accuracy in wireless networks. In *The International Conference on "Computer as a Tool" (EUROCON 2007)*, pages 1131–1135.
- [Burke and Bos, 2011] Burke, M. and Bos, N. (2011). Optimal placement of range-only beacons for mobile robot localisation. In *4th Robotics and Mechatronics Conference of South Africa (ROBMECH 2011)*.
- [Cao et al., 2013] Cao, N., Masazade, E., and Varshney, P. K. (2013). A multiobjective optimization based sensor selection method for target tracking in wireless sensor networks. In *16th International Conference on Information Fusion (FUSION 2013)*, pages 974–980.
- [Carter, 1977] Carter, G. C. (1977). Variance bounds for passively locating an acoustic source with a symmetric line array. *Journal of the Acoustical Society of America*, 62(4):922.
- [Chaffee and Abel, 1994] Chaffee, J. and Abel, J. (1994). GDOP and the Cramer-Rao bound. In *IEEE Position Location and Navigation Symposium (PLANS 1994)*, pages 663–668.
- [Chan et al., 2015] Chan, Y. T., Chan, F., Read, W., Inkol, R., Jackson, B., and Lee, B. H. (2015). Probable regions for emitter localization. In *IEEE Military Communications Conference (MILCOM 2015)*, pages 222–227.
- [Chan and Ho, 1994] Chan, Y. T. and Ho, K. C. (1994). A simple and efficient estimator for hyperbolic location. *IEEE Transactions on Signal Processing*, 42(8):1905–1915.
- [Chaudhry et al., 2011] Chaudhry, S. B., Hung, V. C., Guha, R. K., and Stanley, K. O. (2011). Pareto-based evolutionary computational approach for wireless sensor placement. *Engineering Applications of Artificial Intelligence*, 24(3):409–425.
- [Chen et al., 2006] Chen, Y., Francisco, J., Trappe, W., and Martin, R. P. (2006). A practical approach to landmark deployment for indoor localization. In *3rd Annual IEEE Communications Society on Sensor and Ad Hoc Communications and Networks (SECON 2006)*, pages 365–373.
- [Chepuri and Leus, 2015] Chepuri, S. P. and Leus, G. (2015). Sparsity-promoting sensor selection for non-linear measurement models. *IEEE Transactions on Signal Processing*, 63(3):684–698.
- [Chiu and Lin, 2011] Chiu, P.-L. and Lin, F. Y.-S. (2011). A lagrangean relaxation based sensor deployment algorithm to optimize quality of service for target positioning. *Expert Systems with Applications*, 38(4):3613–3625.

- [Coello Coello, 2006] Coello Coello, C. A. (2006). Evolutionary multi-objective optimization: a historical view of the field. *IEEE Computational Intelligence Magazine*, 1(1):28–36.
- [Deb, 2001] Deb, K. (2001). *Multi-objective optimization using evolutionary algorithms*. John Wiley & Sons, Chichester, UK.
- [Deb and Jain, 2014] Deb, K. and Jain, H. (2014). An evolutionary many-objective optimization algorithm using reference-point-based nondominated sorting approach, part I: solving problems with box constraints. *IEEE Transactions on Evolutionary Computation*, 18(4):577–601.
- [Deb et al., 2002] Deb, K., Pratap, A., Agarwal, S., and Meyarivan, T. (2002). A fast and elitist multiobjective genetic algorithm: NSGA-II. *IEEE Transactions on Evolutionary Computation*, 6(2):182–197.
- [Deb et al., 2007] Deb, K., Tewari, R., Dixit, M., and Dutta, J. (2007). Finding trade-off solutions close to KKT points using evolutionary multi-objective optimization. In *IEEE Congress on Evolutionary Computation (CEC 2007)*, pages 2109–2116.
- [Dogancay and Hmam, 2009] Dogancay, K. and Hmam, H. (2009). On optimal sensor placement for time-difference-of-arrival localization utilizing uncertainty minimization. In *17th European Signal Processing Conference (EUSIPCO 2009)*, pages 1136–1140.
- [Domingo-Perez et al., 2016a] Domingo-Perez, F., Lazaro-Galilea, J. L., Bravo, I., Gardel, A., and Rodriguez, D. (2016a). Optimization of the coverage and accuracy of an indoor positioning system with a variable number of sensors. *Sensors*, 16(6):934.
- [Domingo-Perez et al., 2015] Domingo-Perez, F., Lazaro-Galilea, J. L., Bravo, I., Martín-Gorostiza, E., Salido-Monzu, D., Llana, A., and Govaers, F. (2015). Sensor deployment for motion trajectory tracking with a genetic algorithm. In *IEEE International Conference on Industrial Technology (ICIT 2015)*, pages 3435–3439.
- [Domingo-Perez et al., 2013] Domingo-Perez, F., Lázaro-Galilea, J. L., Martín-Gorostiza, E., Salido-Monzú, D., and Wieser, A. (2013). Accuracy of an indoor IR positioning system with least squares and maximum likelihood approaches. In *International Conference on Indoor Positioning and Indoor Navigation (IPIN 2013)*, pages 22–23.
- [Domingo-Perez et al., 2014] Domingo-Perez, F., Lazaro-Galilea, J. L., Martín-Gorostiza, E., Salido-Monzu, D., and Wieser, A. (2014). Evolutionary optimization of sensor deploy-

- ment for an indoor positioning system with unknown number of anchors. In *Ubiquitous Positioning Indoor Navigation and Location Based Services (UPINLBS 2014)*, pages 195–202.
- [Domingo-Perez et al., 2016b] Domingo-Perez, F., Lazaro-Galilea, J. L., Wieser, A., Martin-Gorostiza, E., Salido-Monzu, D., and Llana, A. d. l. (2016b). Sensor placement determination for range-difference positioning using evolutionary multi-objective optimization. *Expert Systems with Applications*, 47:95–105.
- [Elkachouchi and Mofeed, 2005] Elkachouchi, H. and Mofeed, M. A. E. (2005). Direction-of-arrival methods (DOA) and time difference of arrival (TDOA) position location technique. In *Twenty-Second National Radio Science Conference (NRSC 2005)*, pages 173–182.
- [Eren et al., 2006] Eren, T., Whiteley, W., and Belhumeur, P. N. (2006). Using angle of arrival (bearing) information in network localization. In *45th IEEE Conference on Decision and Control (CDC 2006)*, pages 4676–4681.
- [Fang et al., 2016] Fang, X., Yan, W., and Chen, W. (2016). Sensor placement for underwater source localization with fixed distances. *IEEE Geoscience and Remote Sensing Letters*, 13(9):1379–1383.
- [Fortin et al., 2012] Fortin, F.-A., De Rainville, F.-M., Gardner, M.-A., Parizeau, M., and Gagné, C. (2012). DEAP: Evolutionary algorithms made easy. *Journal of Machine Learning Research*, 13(Jul):2171–2175.
- [Garza-Fabre et al., 2011] Garza-Fabre, M., Toscano-Pulido, G., Coello Coello, C., and Rodriguez-Tello, E. (2011). Effective ranking + speciation = many-objective optimization. In *IEEE Congress on Evolutionary Computation (CEC 2011)*, pages 2115–2122.
- [Gorostiza et al., 2011] Gorostiza, E. M., Lázaro Galilea, J. L., Meca Meca, F. J., Salido Monzú, D., Espinosa Zapata, F., and Pallarés Puerto, L. (2011). Infrared sensor system for mobile-robot positioning in intelligent spaces. *Sensors*, 11(5):5416–5438.
- [Grasso et al., 2013] Grasso, R., Cococcioni, M., Mourre, B., Osler, J., and Chiggiato, J. (2013). A decision support system for optimal deployment of sonobuoy networks based on sea current forecasts and multi-objective evolutionary optimization. *Expert Systems with Applications*, 40(10):3886–3899.
- [Han et al., 2015] Han, G., Zhang, C., Shu, L., and Rodrigues, J. J. P. C. (2015). Impacts of deployment strategies on localization performance in underwater acoustic sensor networks. *IEEE Transactions on Industrial Electronics*, 62(3):1725–1733.

- [Ho and Vicente, 2008] Ho, K. C. and Vicente, L. M. (2008). Sensor allocation for source localization with decoupled range and bearing estimation. *IEEE Transactions on Signal Processing*, 56(12):5773–5789.
- [Hu et al., 2013] Hu, X., Bao, M., Hu, Y.-H., and Xu, B. (2013). Energy balanced scheduling for target tracking with distance-dependent measurement noise in a WSN. *International Journal of Distributed Sensors Networks*, 9(12):1–12.
- [Iqbal et al., 2015] Iqbal, M., Naeem, M., Anpalagan, A., Ahmed, A., and Azam, M. (2015). Wireless sensor network optimization: Multi-objective paradigm. *Sensors*, 15(7):17572–17620.
- [Isaacs et al., 2009] Isaacs, J. T., Klein, D. J., and Hespanha, J. P. (2009). Optimal sensor placement for time difference of arrival localization. In *48th IEEE Conference on Decision and Control (CDC 2009)*, pages 7878–7884.
- [Jameii et al., 2016] Jameii, S. M., Faez, K., and Dehghan, M. (2016). AMOF: adaptive multi-objective optimization framework for coverage and topology control in heterogeneous wireless sensor networks. *Telecommunication Systems*, 61(3):515–530.
- [Jawaid and Smith, 2015] Jawaid, S. T. and Smith, S. L. (2015). Submodularity and greedy algorithms in sensor scheduling for linear dynamical systems. *Automatica*, 61:282–288.
- [Joshi and Boyd, 2009] Joshi, S. and Boyd, S. (2009). Sensor selection via convex optimization. *IEEE Transactions on Signal Processing*, 57(2):451–462.
- [Jourdan et al., 2008] Jourdan, D. B., Dardari, D., and Win, M. Z. (2008). Position error bound for UWB localization in dense cluttered environments. *IEEE Transactions on Aerospace and Electronic Systems*, 44(2):613–628.
- [Jourdan and Roy, 2008] Jourdan, D. B. and Roy, N. (2008). Optimal sensor placement for agent localization. *ACM Transactions on Sensor Networks*, 4(3):1–40.
- [Kammoun et al., 2014] Kammoun, S., Pothin, J.-B., and Cousin, J.-C. (2014). Beacon placement using simulated annealing for RSS-based localization systems. In *11th International Symposium on Wireless Communications Systems (ISWCS 2014)*, pages 537–541.
- [Kaune, 2012] Kaune, R. (2012). Accuracy studies for TDOA and TOA localization. In *15th International Conference on Information Fusion (FUSION 2012)*, pages 408–415.

- [Kay, 1993] Kay, S. M. (1993). *Fundamentals of statistical signal processing, volume I: estimation theory*. Prentice Hall.
- [Kirkpatrick et al., 1983] Kirkpatrick, S., Gelatt, C. D., and Vecchi, M. P. (1983). Optimization by simulated annealing. *Science*, 220(4598):671–680.
- [Kovacevic and Chebira, 2007a] Kovacevic, J. and Chebira, A. (2007a). Life beyond bases: The advent of frames (part I). *IEEE Signal Processing Magazine*, 24(4):86–104.
- [Kovacevic and Chebira, 2007b] Kovacevic, J. and Chebira, A. (2007b). Life beyond bases: The advent of frames (part II). *IEEE Signal Processing Magazine*, 24(5):115–125.
- [Krause et al., 2008] Krause, A., Singh, A., and Guestrin, C. (2008). Near-optimal sensor placements in gaussian processes: Theory, efficient algorithms and empirical studies. *Journal of Machine Learning Research*, 9(Feb):235–284.
- [Kumar, 2010] Kumar, R. (2010). System and method for the use of an adaptive mutation operator in genetic algorithms. *U. S. Patent*, 7,660,773.
- [Laguna et al., 2009] Laguna, M., Roa, J. O., Jiménez, A. R., and Seco, F. (2009). Diversified local search for the optimal layout of beacons in an indoor positioning system. *IIE Transactions*, 41(3):247–259.
- [Langley, 1999] Langley, R. B. (1999). Dilution of precision. *GPS World*, 10(5):52–59.
- [Leune et al., 2013] Leune, T., Wehs, T., Janssen, M., Koch, C., and von Cölln, G. (2013). Optimization of wireless locating in complex environments by placement of anchor nodes with evolutionary algorithms. In *IEEE 18th Conference on Emerging Technologies & Factory Automation (ETFA 2013)*, pages 416–421.
- [Levanon, 2000] Levanon, N. (2000). Lowest GDOP in 2-D scenarios. *IEE Proceedings - Radar, Sonar and Navigation*, 147(3):149–155.
- [Li and Kao, 2010] Li, J.-S. and Kao, H.-C. (2010). Distributed k-coverage self location estimation scheme based on Voronoi diagram. *IET Communications*, 4(2):167–177.
- [Liang and Jia, 2016] Liang, Y. and Jia, Y. (2016). Constrained optimal placements of heterogeneous range/bearing/RSS sensor networks for source localization with distance-dependent noise. *IEEE Geoscience and Remote Sensing Letters*, PP(99):1–5.

- [Liu et al., 2007] Liu, H., Darabi, H., Banerjee, P., and Liu, J. (2007). Survey of wireless indoor positioning techniques and systems. *IEEE Transactions on Systems, Man, and Cybernetics, Part C: Applications and Reviews*, 37(6):1067–1080.
- [Lui and So, 2009] Lui, K. W. K. and So, H. C. (2009). A study of two-dimensional sensor placement using time-difference-of-arrival measurements. *Digital Signal Processing*, 19(4):650–659.
- [Martin-Gorostiza, 2011] Martin-Gorostiza, E. (2011). *Sistema de posicionamiento local para localización absoluta de robots móviles en espacios inteligentes mediante infrarrojos*. PhD thesis, University of Alcalá.
- [Martin-Gorostiza et al., 2014] Martin-Gorostiza, E., Meca-Meca, F. J., Lázaro-Galilea, J. L., Salido-Monzú, D., Martos-Naya, E., and Wieser, A. (2014). Infrared local positioning system using phase differences. In *Ubiquitous Positioning Indoor Navigation and Location Based Service (UPINLBS 2014)*, pages 238–247.
- [Martínez and Bullo, 2006] Martínez, S. and Bullo, F. (2006). Optimal sensor placement and motion coordination for target tracking. *Automatica*, 42(4):661–668.
- [Mautz, 2012] Mautz, R. (2012). Indoor positioning technologies. Habilitation Thesis, ETH Zurich.
- [Meng et al., 2013] Meng, W., Xie, L., and Xiao, W. (2013). Optimality analysis of sensor-source geometries in heterogeneous sensor networks. *IEEE Transactions on Wireless Communications*, 12(4):1958–1967.
- [Meng et al., 2016] Meng, W., Xie, L., and Xiao, W. (2016). Optimal TDOA sensor-pair placement with uncertainty in source location. *IEEE Transactions on Vehicular Technology*, PP(99):1–1.
- [Moreno-Salinas et al., 2013] Moreno-Salinas, D., Pascoal, A., and Aranda, J. (2013). Optimal sensor placement for multiple target positioning with range-only measurements in two-dimensional scenarios. *Sensors*, 13(8):10674–10710.
- [Neering et al., 2007] Neering, J., Bordier, M., and Maizi, N. (2007). Optimal passive source localization. In *International Conference on Sensor Technologies and Applications (SensorComm 2007)*, pages 295–300.

- [Neering et al., 2008] Neering, J., Fischer, C., Bordier, M., and Maïzi, N. (2008). Optimal sensor configuration for passive position estimation. In *IEEE/ION Position, Location and Navigation Symposium (PLANS 2008)*, pages 951–960.
- [Nelder and Mead, 1965] Nelder, J. A. and Mead, R. (1965). A simplex method for function minimization. *The Computer Journal*, 7(4):308–313.
- [Padurariu and Marinescu, 2014] Padurariu, F. R. and Marinescu, C. (2014). NSGA-II: Implementation and performance metrics extraction for CPU and GPU. In *16th International Symposium on Symbolic and Numeric Algorithms for Scientific Computing (SYNASC 2014)*, pages 494–499.
- [Perez-Ramirez et al., 2013] Perez-Ramirez, J., Borah, D. K., and Voelz, D. G. (2013). Optimal 3-D landmark placement for vehicle localization using heterogeneous sensors. *IEEE Transactions on Vehicular Technology*, 62(7):2987–2999.
- [Povalac and Sebesta, 2010] Povalac, A. and Sebesta, J. (2010). Phase of arrival ranging method for UHF RFID tags using instantaneous frequency measurement. In *20th International Conference on Applied Electromagnetics and Communications (ICECom 2010)*, pages 187–190.
- [Povalac and Sebesta, 2011] Povalac, A. and Sebesta, J. (2011). Phase difference of arrival distance estimation for RFID tags in frequency domain. In *IEEE International Conference on RFID-Technologies and Applications (RFID-TA 2011)*, pages 188–193.
- [Ranieri et al., 2014] Ranieri, J., Chebira, A., and Vetterli, M. (2014). Near-optimal sensor placement for linear inverse problems. *IEEE Transactions on Signal Processing*, 62(5):1135–1146.
- [Rao et al., 2015] Rao, S., Chepuri, S. P., and Leus, G. (2015). Greedy sensor selection for non-linear models. In *IEEE 6th International Workshop on Computational Advances in Multi-Sensor Adaptive Processing (CAMSAP 2015)*, pages 241–244.
- [Ray and Mahajan, 2002] Ray, P. K. and Mahajan, A. (2002). A genetic algorithm-based approach to calculate the optimal configuration of ultrasonic sensors in a 3D position estimation system. *Robotics and Autonomous Systems*, 41(4):165–177.
- [Roa et al., 2005] Roa, J. O., Jiménez, A. R., Seco, F., Prieto, C., Ealo, J., and Ramos, F. (2005). Primeros resultados en la optimización de la ubicación de balizas para localización utilizando algoritmos genéticos. In *XXVI Jornadas de Automática*, pages 75–86.

- [Roa et al., 2006] Roa, J. O., Jiménez, A. R., Seco, F., Prieto, C., Ealo, J. L., Ramos, F., and Guevara, J. (2006). Un método heurístico mejorado basado en algoritmos genéticos para optimizar la ubicación de balizas en sistemas de localización. In *XXVII Jornadas de Automática*, pages 120–129.
- [Roa et al., 2007] Roa, J. O., Jiménez, A. R., Seco, F., Prieto, J. C., and Ealo, J. (2007). Optimal placement of sensors for trilateration: Regular lattices vs meta-heuristic solutions. In *11th International Conference on Computer Aided Systems Theory (EUROCAST 2007)*, pages 780–787.
- [Seco et al., 2009] Seco, F., Jimenez, A. R., Prieto, C., Roa, J., and Koutsou, K. (2009). A survey of mathematical methods for indoor localization. In *IEEE International Symposium on Intelligent Signal Processing (WISP 2009)*, pages 9–14.
- [Shamaiah et al., 2010] Shamaiah, M., Banerjee, S., and Vikalo, H. (2010). Greedy sensor selection: Leveraging submodularity. In *49th IEEE Conference on Decision and Control (CDC 2010)*, pages 2572–2577.
- [Shen et al., 2013] Shen, Z., Wang, K., and Wang, F.-Y. (2013). GPU based Non-dominated Sorting Genetic Algorithm-II for multi-objective traffic light signaling optimization with agent based modeling. In *16th International IEEE Conference on Intelligent Transportation Systems (ITSC 2013)*, pages 1840–1845.
- [Smith and Cheeseman, 1986] Smith, R. C. and Cheeseman, P. (1986). On the representation and estimation of spatial uncertainty. *The International Journal of Robotics Research*, 5(4):56–68.
- [So, 2012] So, H. C. (2012). *Handbook of position location: Theory, practice and advances*, chapter Source localization: Algorithms and analysis, pages 25–66. John Wiley & Sons.
- [Tichavský et al., 1998] Tichavský, P., Muravchik, C. H., and Nehorai, A. (1998). Posterior Cramér-Rao bounds for discrete-time nonlinear filtering. *IEEE Transactions on Signal Processing*, 46(5):1386–1396.
- [Torrieri, 1984] Torrieri, D. J. (1984). Statistical theory of passive location systems. *IEEE Transactions on Aerospace and Electronic Systems*, 20(2):183–198.
- [Trees et al., 2006] Trees, H. L. V., Bell, K. L., and Wang, Y. (2006). Bayesian Cramér-Rao bounds for multistatic radar. In *IEEE International Waveform Diversity Design Conference (IWDDC 2006)*.

- [Ucinski, 2004] Ucinski, D. (2004). *Optimal measurement methods for distributed parameter system identification*. CRC Press.
- [Van Diggelen, 1998] Van Diggelen, F. (1998). Innovation: GPS accuracy-lies, damn lies, and statistics. *GPS World*, 9:41–45.
- [Wieser, 2001] Wieser, A. (2001). *Robust and fuzzy techniques for parameter estimation and quality assessment in GPS*. PhD thesis, Technischen Universität Graz.
- [Wong, 2009] Wong, M. L. (2009). Parallel multi-objective evolutionary algorithms on graphics processing units. In *11th Annual Conference Companion on Genetic and Evolutionary Computation Conference: Late Breaking Papers (GECCO 2009)*, pages 2515–2522.
- [Yan et al., 2013] Yan, J., Tiberius, C. C. J. M., Janssen, G. J. M., Teunissen, P. J. G., and Bellusci, G. (2013). Review of range-based positioning algorithms. *IEEE Aerospace and Electronics Systems Magazine*, 28(8):2–27.
- [Yang and Scheuing, 2005] Yang, B. and Scheuing, J. (2005). Cramer-Rao bound and optimum sensor array for source localization from time differences of arrival. In *IEEE International Conference on Acoustics, Speech, and Signal Processing (ICASSP 2005)*, volume 4, pages 961–964.
- [Yang et al., 2012] Yang, C., Kaplan, L., and Blasch, E. (2012). Performance measures of covariance and information matrices in resource management for target state estimation. *IEEE Transactions on Aerospace and Electronic Systems*, 48(3):2594–2613.
- [Zekavat and Buehrer, 2012] Zekavat, R. and Buehrer, R. M. (2012). *Handbook of position location: Theory, practice and advances*. John Wiley & Sons.
- [Zhang, 1995] Zhang, H. (1995). Two-dimensional optimal sensor placement. *IEEE Transactions on Systems, Man, and Cybernetics*, 25(5):781–792.
- [Zhao et al., 2013] Zhao, S., Chen, B. M., and Lee, T. H. (2013). Optimal sensor placement for target localisation and tracking in 2D and 3D. *International Journal of Control*, 86(10):1687–1704.
- [Zuo et al., 2007] Zuo, L., Niu, R., and Varshney, P. K. (2007). Posterior CRLB based sensor selection for target tracking in sensor networks. In *IEEE International Conference on Acoustic, Speech and Signal Processing (ICASSP 2007)*, pages 1041–1044.